

**UNCLASSIFIED**

---

---

**AD 400 563**

*Reproduced  
by the*

**ARMED SERVICES TECHNICAL INFORMATION AGENCY  
ARLINGTON HALL STATION  
ARLINGTON 12, VIRGINIA**



---

---

**UNCLASSIFIED**

**NOTICE:** When government or other drawings, specifications or other data are used for any purpose other than in connection with a definitely related government procurement operation, the U. S. Government thereby incurs no responsibility, nor any obligation whatsoever; and the fact that the Government may have formulated, furnished, or in any way supplied the said drawings, specifications, or other data is not to be regarded by implication or otherwise as in any manner licensing the holder or any other person or corporation, or conveying any rights or permission to manufacture, use or sell any patented invention that may in any way be related thereto.

Unclassified

400 563

Technical Report No. 282

Radar Astronomy  
Measurement Techniques

P. E. Green, Jr.

12 December 1962

Lincoln Laboratory

MASSACHUSETTS INSTITUTE OF TECHNOLOGY



Unclassified

**Unclassified**

The work reported in this document was performed at Lincoln Laboratory, a center for research operated by Massachusetts Institute of Technology, with the joint support of the U.S. Army, Navy and Air Force under Air Force Contract AF 19(628)-500.

Non-Lincoln Recipients

**PLEASE DO NOT RETURN**

Permission is given to destroy this document  
when it is no longer needed.

**Unclassified**

When issued, this document had not been reviewed or released for public dissemination by the appropriate government agency. Reproduction or distribution for official government use is authorized. Other reproduction or distribution requires written authorization by Lincoln Laboratory Publications Office.

Upon notification of release, this page may be removed.

Unclassified

247

MASSACHUSETTS INSTITUTE OF TECHNOLOGY  
LINCOLN LABORATORY

RADAR ASTRONOMY MEASUREMENT TECHNIQUES

*P. E. GREEN, JR.*

*Group 34*

AFESD - 1DR - 62-279

TECHNICAL REPORT NO. 282

12 DECEMBER 1962

LEXINGTON

MASSACHUSETTS

Unclassified

## ABSTRACT

This report is a review of currently available techniques for studying the properties of objects of interest in radar astronomy, which are usually spread radar targets. The report is intended as a sequel to Lincoln Laboratory Technical Report 234, in which R. Price has presented a rather complete treatment of the theory and methodology of the detection of such spread targets.<sup>1</sup> Here we are interested in measurement (or estimation) rather than detection.

Spread targets are defined to be those that produce an observable smearing of the echo in range, or an observable rate of echo fluctuation, or both. (Spread targets may or may not be at the same time extended targets, i.e., ones that fill the antenna beamwidth.)

The approach taken here in presenting the available material on spread target measurements is to follow what happens to the various attributes (amplitude, delay, phase, frequency shift, polarization) of an incident signal upon reflection from such a target. Then the question is turned around by detailing the ways in which the study of these signal attributes by appropriate receiver processing can be used to infer target properties. In the case of such radar astronomy targets as rotating planets, these target properties might include range, velocity, shape, size, rotation vector, and surface characteristics. (The last of these may be studied either as average behavior over the target surface or as a function of location on the target surface.) The possible transmitted signals include simple (unity time-bandwidth product) signals, or complicated (large-TW) signals, including frequency-spaced sets of sinusoids. The receiver operations considered include processing of the echo signal received at spaced receivers (interferometry), and processing of separate components received at the same point (polarimetry), as well as the much more completely understood case of processing of the output of a single receiving antenna by various methods.

The concluding section is a summary of presently available information on the variance of the error in making such measurements (including some very recent results obtained by M. J. Levin and R. Price).

Much of this report consists of previous results that have not been placed in a connected story before. One topic that is new here is the extension of Manasse's study of radar interferometry to include the effect of target rotation, and the resulting motion of the diffraction pattern observed at the spaced radar receivers on earth.

# TABLE OF CONTENTS

	Abstract	iii
I.	Introduction	1
II.	Hard Targets	3
	A. The Angular Power Spectrum $\sigma_o$ of an Incremental Portion of the Target	3
	B. Power Reflected From the Target as a Whole	7
	C. Time Delay (Range)	9
	D. Frequency and Phase	10
	E. Polarization	18
III.	Soft Targets	21
	A. Reflected Power and Angular Power Spectrum	22
	B. Time Delay (Range)	23
	C. Frequency	23
	D. Polarization	24
IV.	Measurement Methodology	24
	A. The Target Scattering Function $\sigma(\tau, f)$	25
	B. Detection of a Point Nonfluctuating Target – the Matched Filter	27
	C. The Ambiguity Function $\psi^2$	28
	D. Interaction of the Signal and the Target in Terms of $\sigma$ and $\psi^2$	31
	E. Spaced-Time and Spaced-Frequency Measurements	37
	F. Some Equipment Problems	40
	G. Interferometry	42
	H. Polarimetry	43
V.	Measuring Quantities Of Astronomical Interest	45
	A. Ranging	45
	B. Velocity	46
	C. Planetary Radius	46
	D. Radar Angular Spectrum of a Uniform Hard Target	46
	E. Isolating Individual Surface Features	48
	F. Rotation Vector	51
	G. Ionospheres and Interplanetary Ionization	52
	H. Magnetic Field	53

VI. Measurement Errors	54
A. Statistical Estimation	54
B. Point Nonfluctuating Targets	56
C. Targets Spread only in Delay or Doppler	58
D. Deep Fluctuating Targets	62
VII. Summary and Conclusions	66
Appendix A – A Discussion of Correlation Functions and Angular Spectra of Interest in Radar Astronomy	73
Appendix B – Scattering Function for Uniform Rough Sphere	76

# RADAR ASTRONOMY MEASUREMENT TECHNIQUES

## I. INTRODUCTION

This report deals with the use of radar systems to measure quantities of astronomical interest. Radar astronomy targets, which may be rotating solid bodies, moving ionized regions, or clouds of particles, are examples of spread radar targets, i.e., objects that impose on the probing radar signal either or both of the following two effects: (a) an observable range smearing, and (b) an observable fluctuation rate. It is easy to imagine other examples of spread targets, for example aircraft, tumbling nose cones, missile wakes, and so forth, to which the ideas presented here may be more or less relevant, but we shall ignore these possibilities here and talk in terms of radar astronomy targets.

The theory and practice of optimizing the detectability of spread targets has been treated rather completely by Price<sup>1</sup> in Lincoln Laboratory Technical Report 234, to which this report is a sequel. The procedures developed there are applicable interchangeably to the detection of spread objects as radar targets or the use of them as communication channels. In this report we ignore the radar detection as well as the communication aspects of the spread target problem and deal solely with the use of the radar system for making measurements of the properties of the target.

The outgoing and returning electromagnetic signals are characterized by certain quantities, and we would like to investigate how the parameters of the outgoing signal are altered in the reflection process, and then how this alteration may be studied. If we regard the electrical signal as a scalar quantity, i.e., a narrow-band time function appearing at the two terminals of the antenna, then a description of the amplitude, frequency, and phase as a function of time completely specifies the signal. If in addition we are willing to take into account the vector direction of the electrical signals (that is, the instantaneous plane of polarization as a function of time), and the way in which all the quantities just listed vary from point to point in space, still more sensitive measurements on the target can be made. As we shall see, certain interesting things may be learned from such interferometric measurements (correlation between the waves observed at two different points) and polarimetric measurements (correlation between components observed at the same point).

A complete understanding of all these factors embraces a very large area indeed, and only parts of the subject are well understood. What we shall be doing in this report to systematize these scattered notions can be stated this way: The radar signal that is transmitted can be written

$$\vec{x}(t) = \vec{E}(t) \cos [2\pi f_1 t + \varphi(t)] \quad , \quad (1)$$

which is seen to be characterized by (a) scalar amplitude  $E$ , (b) origin of the time scale  $t$ , (c) phase  $\varphi$ , (d) average rate of change of phase, i.e., frequency  $2\pi f_1$ , and (e) instantaneous direction of polarization  $\vec{x}/x$ . (The arrow indicates a vector quantity.) Corresponding to the transmitted signal  $\vec{x}(t)$  there is received at a given point an echo signal

$$\vec{w}(t) = \vec{W}(t) \cos [2\pi f_0 t + \Theta(t)]$$

likewise characterized by five quantities. It is the fact that these five parameters can be controlled at will in the transmission (as well as measured in various ways on reception) that embodies any advantage that radar astronomy might have relative to radio astronomy.

It will be found most useful to employ the common representation of the real signal  $\vec{x}(t)$ , not in the trigonometric form [Eq. (1)], but rather as the real part of a complex signal  $\vec{\hat{x}}(t)$

$$\vec{x}(t) = \text{Re} \{ \vec{\hat{x}}(t) \} = \text{Re} \{ \vec{\mathcal{X}}(t) \exp [j2\pi f_0 t] \} \quad (2)$$

(in other words  $\text{Re} \{ \vec{\mathcal{X}}(t) \} = \vec{E}(t) \cos \varphi(t)$ ). The quantity  $\vec{\mathcal{X}}(t)$  is called the complex envelope. Manipulation of  $\mathcal{X}(t)$  is much less cumbersome than manipulation of  $x(t)$  since the usually irrelevant carrier frequency has been removed. By exercising reasonable care, the "real-part-of" operation can be reinserted at the conclusion of the manipulation to give the correct answer. The hypothetical imaginary part of  $\vec{\hat{x}}(t)$  is usually chosen to be the Hilbert transform of our real observable waveform  $\vec{x}(t)$ ; then for  $\vec{x}(t)$  a narrow-band function (center frequency much greater than bandwidth)  $\text{Im} \{ \vec{\hat{x}}(t) \}$  always represents the quadrature or out-of-phase component of the real signal  $\vec{x}(t)$ . Roman letters will be used to indicate the real-time function and script letters will denote the corresponding complex envelope.

In what follows we shall divide radar targets into two classes, hard and soft targets, and investigate one by one the influence of the target properties on each of our attributes:

- amplitude (or actually average power) (Secs. II-B and III-A),
- delay (II-C and III-B),
- phase and frequency (II-D and III-C), and
- polarization direction (II-E and III-D).

After a general discussion of the instrumentation of radar measurements (Sec. IV), we will proceed in Sec. V to turn things around and ask how various target properties of astronomical interest may be studied by studying the above attributes in the received signal  $\vec{w}(t)$ . Section VI discusses errors in such measurements.

It would be desirable to have a concise, and perfectly general notion of how optimally to measure the interesting target properties in the presence of the inevitable noise, finite observation bandwidth, finite observing time, and other factors causing errors. Using the statistical discipline known as hypothesis testing, the presence or absence of the radar astronomy target has been put on a sound enough theoretical basis.<sup>1</sup> Unfortunately the theory of measurement (or, in the language of the statistician, estimation of target parameters) has been placed on a similar strong foundation only for certain very simple types of measurements. What we shall attempt to do here in the case of most of the measurement procedures is to present them systematically as a collection of ad hoc ideas about reasonable ways to measure things about radar astronomy targets, and, whenever possible, to give an idea of the measurement accuracy.

## II. HARD TARGETS

By hard targets we mean bodies that, although they may be moving or changing their orientation, are nevertheless rigid and of fixed shape. The term soft targets will refer here to those that can change shape with time. The most interesting hard radar astronomy targets are obviously the moon, planets, and minor planets. These are all bodies whose size is much larger than any reasonable radar wavelength, and which have rough surfaces, in the sense that they possess surface irregularities having a scale size of the order of magnitude of a wavelength.

With the exception of some smaller minor planets, these hard targets may be safely assumed to have approximately spherical shapes with rough surfaces, and in our treatment of hard targets we will be most interested in the spherical case. Where the radar properties depend on a spherical target shape the fact will be pointed out.

### A. The Angular Power Spectrum $\sigma_0$ of an Incremental Portion of the Target

When an incident plane wave strikes a rough surface, energy is reflected in various directions (see Fig. 1). In adding up the individual contributions<sup>2</sup> one finds that across the wavefront of the reflection there are variations in delay, phase, amplitude, and direction of the polarization vector. The distant observer receives a plane wave which likewise contains irregularities as a function of position laterally on the advancing plane wavefront.

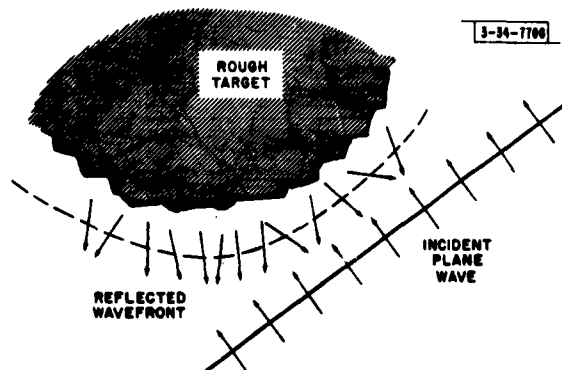


Fig. 1. The manner in which an irregular surface produces irregularities in the reflected wavefront.

As we shall see, it is possible to work backwards from the statistics of these irregularities at the distant observing point to get the statistics of the irregularities at some smooth quasi-planar boundary near but not on the target surfaces (dotted line of Fig. 1), but the question of how these wavefront irregularities relate to the surface irregularities themselves is a much more complicated one. The factors that enter include whether there is an undulating or jagged (discontinuous) surface, whether irregularities are smaller or greater than the wavelength in the lateral direction and in the up-down direction, whether the surface material is uniform in dielectric properties but of a rough shape or whether the body is smooth but of irregular dielectric composition, and so forth. It is safe to say that a large number of physical surface types could give rise to the same type of irregularities of delay, phase, amplitude, and direction across both the dotted boundary and the received wavefront. The reader is referred to Ref. 3 for a discussion of this question of the relation of terrain properties to properties of the reflected wavefront.

In this report we shall be content to start with the irregularities in the reflected field produced at the dotted boundary of Fig. 1 by terrain irregularities, and not with these latter irregularities themselves. In the rest of this report when we speak of the target surface we shall mean, strictly speaking, the wavefront of the reflected signal as examined over a quasi-planar region near to but not actually on the surface of the body.

The radar receiver at a great distance from the target is exposed to an electromagnetic signal formed by the propagation outward of the wavefront with all its irregularities. As we shall see in the next several sections, radar measurements on hard targets, whether performed by a single receiver or a set of spaced receivers (interferometer) often amount simply to the measurement of a quantity  $\sigma_0(\phi)$  called the radar angular power spectrum, which expresses the statistics of the wavefront irregularities in a particular way.

In the next several pages, we shall take the familiar Fourier transform relationship between field intensity across an aperture (at the target) and the remotely received signal, and derive an expression for  $\sigma_0(\phi)$  that shows just what statistical properties of the wavefront irregularities it measures. While we are at it, we shall define several other terms and draw several conclusions that will be useful later on.

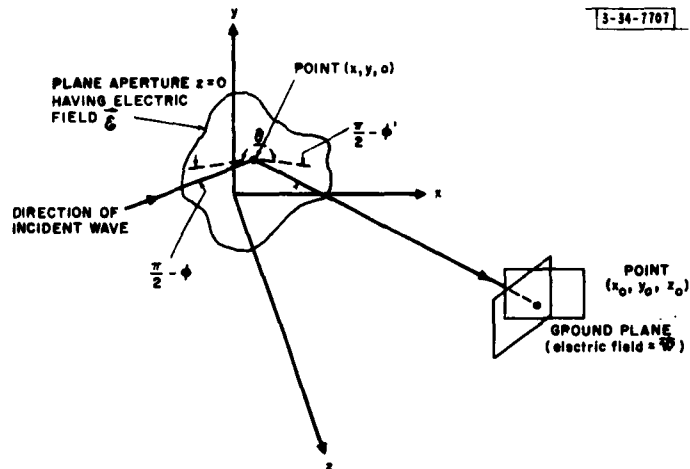


Fig. 2. Coordinate system for derivation of  $\sigma_0(\phi)$ , where  $\phi$  = the angle that an incident ray makes with the normal to a plane target region (aperture),  $\phi'$  = similar angle for ray to receiver,  $\theta$  = equatorial angle measured in the aperture plane between the projections of the two rays.

Figure 2 shows at  $z = 0$  a plane region of the target surface (in the sense just mentioned) with the irregular pattern of the electric field intensity of the echo being  $\vec{\mathcal{E}}(x, y, 0)$ . Denote the component of  $\vec{\mathcal{E}}$  that lines up with the receiving antenna on the ground as  $\mathcal{E}$ . The script letter indicates a complex envelope as before, and the distances  $x, y$ , and  $z$  are expressed in multiples of wavelengths. For the moment let us assume that  $\mathcal{E}$  is non-time-varying. The well-known relationship giving the electric field  $\mathcal{W}$  at the distant receiver point  $(x_0, y_0, z_0)$  on the ground plane as the Fourier transform of  $\mathcal{E}$  is<sup>4</sup>

$$\mathcal{W}(l, m) = \iint_{\text{Aperture}} \mathcal{E}(x, y, 0) \exp[-j2\pi(lx + my)] dx dy$$

or, more compactly,

$$\mathcal{W}(l, m) \longleftarrow \mathcal{E}(x, y) \quad , \quad (3)$$

where  $l, m,$  and  $n$  are the direction cosines

$$l = (x_0 - x) [z_0^2 + (x_0 - x)^2 + (y_0 - y)^2]^{-1/2}$$

$$m = (y_0 - y) [z_0^2 + (x_0 - x)^2 + (y_0 - y)^2]^{-1/2}$$

$$n = \sin \varphi' = z_0 [z_0^2 + (x_0 - x)^2 + (y_0 - y)^2]^{-1/2} \quad .$$

The equation represents the sum of contributions falling on an incremental portion of the ground plane having direction cosines in the range  $l$  to  $l + dl$  and  $m$  to  $m + dm$ . The Fourier inversion of Eq. (3) is, of course,

$$\mathcal{E}(x, y, 0) = \iint_{-\infty}^{\infty} \mathcal{W}(l, m) \exp [j2\pi(lx + my)] dl dm$$

or†

$$\mathcal{E}(x, y) \Longrightarrow \mathcal{W}(l, m) \quad . \quad (4)$$

Imagine now that at the target the aperture field distribution  $\mathcal{E}$  is actually a reflection caused by a plane wave incident along the ray path from the direction shown in the figure, and that this wave arrives on the target at a power level of one watt per square meter of the incident wavefront.  $\mathcal{W}$  is then seen to be the radar echo arriving at the receiving location. We want to determine the number of watts per steradian of time-averaged echo power per square meter of target when the power level of the incident signal is one watt per square meter of wavefront. This can be obtained by taking one-half the squared magnitude of the complex envelope  $\mathcal{W}$ , suitably corrected for the number of steradians subtended by each incremental area  $dl \times dm$ . This ratio is

$$\frac{1}{2Z_0} |\mathcal{W}(l, m)|^2 (1 - l^2 - m^2)^{1/2} \quad .$$

If the field  $\mathcal{E}$  on the aperture is randomly time-varying, then  $\mathcal{W}$  will likewise vary randomly with time and so will the power ratios just defined. We define the quantity  $\sigma_0$  to be  $4\pi$  times this average ratio:

$$\sigma_0 = \frac{4\pi}{2Z_0} \langle |\mathcal{W}(l, m)|^2 \rangle (1 - l^2 - m^2)^{1/2} \quad , \quad (5)$$

where  $\langle \rangle$  denotes the infinite time average and  $Z_0$  is the characteristic impedance of free space;  $\sigma_0$  is called the radar angular power spectrum of the target surface, and its dimensions are square meters of radar cross section per square meter of target surface. The factor of  $4\pi$  enters simply by an arbitrary convention whereby all radar cross sections are defined as a ratio of powers such as Eq. (5) multiplied by  $4\pi$ . As it stands,  $\sigma_0$  is a function of  $\varphi, \varphi', \Theta, l,$  and  $m$ .

† Note that Eqs. (3) and (4) constitute a Fourier transform pair all right, but in terms of direction cosines  $l$  and  $m$ , and not in either angles such as  $\varphi'$  or in distance on the ground plane ( $x_0$  and  $y_0$ ). Only near perpendicularity ( $x_0 \approx x$  or  $y_0 \approx y$ ) does one have ground distances as an argument.

If one rules out an anisotropic target material, then the dependence is only on  $\varphi$ ,  $\varphi'$ , and  $\Theta$ . If, further, a monostatic rather than bistatic radar situation is assumed (that is, the transmitter and receiver are collocated) then only one variable,  $\varphi = \varphi'$ , is left. In most of this report this assumption will be made and we shall be dealing with the radar angular spectrum  $\sigma_o(\varphi)$ .

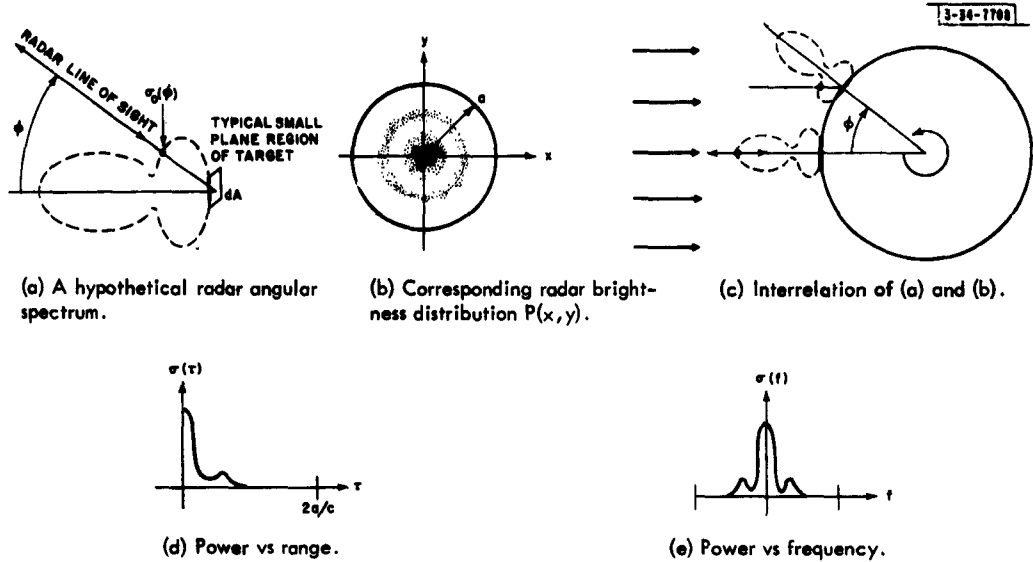


Fig. 3. The manner in which the radar angular spectrum  $\sigma_o(\varphi)$  influences the radar echo returned from a uniform spherical hard target.

An example of a radar angular spectrum is sketched in Fig. 3(a). Perhaps more familiar examples are the Lambert Law ( $\sigma_o \sim \cos^2 \varphi$ ) and Lommel-Seeliger or Euler Law ( $\sigma_o \sim \cos \varphi$ ).

That  $\sigma_o(\varphi)$  expresses certain statistics of the echo wavefront irregularities is now clear from the following reasoning. From Eq. (5), we see that  $\sigma_o(\varphi)$  is proportional to the time-averaged squared magnitude of the received electric field, but this electric field in turn is the Fourier transform of the aperture distribution [Eq. (3)]. Thus, since the squared magnitude of the function in one domain is the Fourier transform of the correlation function of the transformed function in the other domain, it follows that the power observed as a function of direction cosines is proportional to the Fourier transform of the spatial correlation function of the electric field across the aperture. Equations (3) and (4) are for non-time-varying fields. As shown in Appendix A [in particular, Eq. (A-9)], if we introduce the assumption that  $\mathcal{E}$  is time-varying, then the time-averaged received power as a function of direction cosines is proportional to the inverse transform of the spatial correlation function where the average is over time, that is,†

$$\sigma_o = \frac{4\pi}{2Z_o} \langle |W(t, m)|^2 \rangle \implies \text{Const} \times \frac{4\pi}{2Z_o} \int_{-\infty}^{\infty} \int_{-\infty}^{\infty} \langle \mathcal{E}(u, v) \mathcal{E}^*(u+x, v+y) \rangle du dv \quad (6)$$

† As discussed in Appendix A, this relation depends on the reasonable assumption of space stationarity of the aperture distribution  $\mathcal{E}$ . That is, the power level may vary across the aperture, but apart from this, the cross correlation of the random time variations occurring at two separate points on the aperture depends only on the separation of the points and not on their location.

So in measuring  $\sigma_0(\varphi)$ , we are really measuring the spatial correlation function of the wavefront irregularities at the target; this is as good a statistical description of the irregularities as has been considered to date.†

By similar reasoning we can show an equally important fact – that the spatial correlation function of the signal received on the ground (time average of the product of two receiver outputs) is the Fourier transform of the average power as a function of the coordinates  $x$  and  $y$  at the target. This fact is of obvious relevance to radar interferometry, and we shall investigate its consequences in Sec. II-D. The specific relationship [Eq. (A-10) of Appendix A] goes as follows:

$$\langle |F(x, y)|^2 \rangle \leftarrow \langle W(p, q)W^*(p + l, q + m) \rangle = Z(\vec{d}, 0) \quad , \quad (7)$$

where we define the (complex) number  $Z(\vec{d}, \Delta\tau)$  as the cross correlation obtained by time-averaging the product (taken with a relative delay  $\Delta\tau$ ) of the two voltages received at points spaced by a vector separation  $\vec{d}$  on the ground plane. The station separation  $\vec{d}$  is characterized by the direction cosine differences  $l$  and  $m$ .

### B. Power Reflected From the Target as a Whole

Radar astronomy targets are of course very large bodies, usually spherical. The received echo is made up of the superposition of individual echoes from a very large number of individual regions, each of which can be regarded as approximately planar, so that the development of the preceding section is valid for each region. Moreover, if the echoes from different regions fluctuate independently, superposition of power (rather than voltages) is permissible.

The received power (per steradian) per square meter of surface at a given point on the surface will be given, of course, by the radar angular power spectrum  $\sigma_0(\varphi)/4\pi$ , where  $\varphi$  is now the tilt of the radar line of sight from perpendicularity with the local horizontal. (Transmitter and receiver are assumed collocated and one watt per square meter is assumed incident on the target.) Figure 3(a) shows a hypothetical radar angular spectrum plotted in polar coordinates. An ocean area on the target could be expected to give a large narrow polar plot of  $\sigma_0(\varphi)$  concentrated near small values of  $\varphi$ , whereas the  $\sigma_0(\varphi)$  function of rough terrain would be lower in magnitude and extend out to greater values of  $\varphi$ .

There have been two basic approaches to radar study of lunar and planetary surfaces. The first is to assume that the body is uniform; that is, on the target surface  $\sigma_0(\varphi)$  is everywhere the same. Attention then centers on finding out what this  $\sigma_0(\varphi)$  function is, and then inferring average terrain characteristics by using the methods discussed in Ref. 3, based on Eq. (6). The second approach is somehow to isolate different regions of the target surface, presumably having different  $\sigma_0(\varphi)$  functions, and to study the power reflected from each region. The methods of Ref. 3 then re-enter the picture, but now as a tool in determining average features of just the local region. (We shall see shortly that it is not necessary to perform the isolation by using narrow antenna beams; other methods are available.)

---

† If the spatial wavefront undulations at the target are a gaussian random process, then statistical information of a higher order can be inferred from first-order and second-order data, and these data thus tell the whole story. If non-gaussian surface variations are suspected, it would be important to consider some form of experiment to develop higher-order statistical information, since in non-gaussian cases, first-order statistics and second-order statistics (such as  $\sigma_0(\varphi)$ ) do not specify the higher-order statistics.

We now introduce the assumption that the target is spherical and see what can be said about the total received echo power from such a target. If the spherical surface is uniform in the sense that all parts of the surface have the same angular power spectrum  $\sigma_0(\varphi)$ , say that shown in polar form in Fig. 3(a), then a head-on view of the body would appear as shown in Fig. 3(b), where the darkness of the shading is proportional to reflected power per square meter of incident wavefront. This function  $P(x, y)$ , representing echo power density across a hypothetical transverse plane in front of any target, is called its radar brightness distribution. The circular region on this plane projected by the spherical target is called the target's apparent disk.

At a point on the target where the normal to the spherical surface makes an angle  $\varphi$  with the line of sight from transmitter and receiver to the target, one square meter of the apparent disk will return toward the receiver  $[\sigma_0(\varphi) \sec \varphi]/4\pi$  watts per steradian for every watt per square meter of wavefront incident. The  $\sec \varphi$  factor is necessary because we have defined  $\sigma_0(\varphi)$  as cross section per unit area of surface rather than per unit area of wavefront; there will be  $\sec \varphi$  square meters of surface for every square meter of incident wavefront.

Figure 3(c) shows the way in which the polar plot of  $\sigma_0(\varphi)$  in Fig. 3(a) expresses the intensity of the reflection at various points on the surface like point P. Note carefully that this  $\sigma_0(\varphi)$  tells the story only for reflection back along the direction of the incident radiation;  $\sigma_0(\varphi)$  does not say anything about the power reflected off in other directions. [For this we would need the complete angular power spectrum  $\sigma_0(\varphi, \varphi', \Theta)$ .]

The brightness distribution  $P(x, y)$  for a uniform sphere is obtained trivially from the fact that there are  $\sigma_0(\varphi) \sec \varphi$  square meters of cross section per square meter of wavefront. Thus,  $P(x, y) d\Omega$  is defined as the number of watts per square meter received on the ground in a cone of unit solid angle  $d\Omega$  with its vertex on the ground; all this assuming still that the target is illuminated with a plane wave of power level one watt per square meter. Since a square meter of target subtends the same solid angle at the ground as vice versa, we have

$$P(x, y) = \sigma_0(\varphi) \sec \varphi = \sigma_0 \left[ \sin^{-1} \frac{\sqrt{x^2 + y^2}}{a} \right] \frac{a}{\sqrt{a^2 - x^2 - y^2}}, \quad x^2 + y^2 \leq a^2, \quad (8)$$

where  $a$  is the target radius.

The total effective cross section  $\sigma$  of the target can be obtained by adding up all the  $\sigma_0(\varphi)$  contributions over the entire surface illuminated by the incident signal. We have for  $\sigma$  in square meters

$$\sigma = \int_0^a 2\pi R dR \sigma_0(\varphi) \sec \varphi = 2\pi a^2 \int_0^{\pi/2} \sigma_0(\varphi) \sin \varphi d\varphi \quad (9)$$

since  $R = a \sin \varphi$ . ( $R$  is the radius of an annular strip of integration on the apparent disk of the body.) That is, if there is an incident transmitted wave at a power level of one watt per square meter of wavefront, then  $\sigma/4\pi$  watts per steradian will be reflected back toward the transmitter.

It is interesting to rewrite this expression for total cross section  $\sigma$  in terms of two parameters of the surface itself, called the reflectivity  $\rho$ , and the gain or directivity  $g$ . If the incident transmitted signal reaches the target at a power level of one watt per square meter, then obviously a total of  $\pi a^2$  watts is incident on the target. The total power reflected from the target in all directions is [by steps similar to those leading to Eq. (9)]

$$\frac{2\pi a^2}{4\pi} \int_0^{\pi/2} \sin \varphi \, d\varphi \int_0^{2\pi} \sigma_0(\varphi, \varphi', \Theta) \, d\Omega$$

2π steradians

$$= \frac{2\pi a^2}{4\pi} \int_0^{\pi/2} d\varphi \int_0^{\pi/2} d\varphi' \int_0^{2\pi} \sigma_0(\varphi, \varphi', \Theta) \sin \varphi \sin \varphi' \, d\Theta \quad (10)$$

The reflectivity  $\rho$  is defined as the ratio of total reflected power to total incident power, and is given from Eq. (10),

$$\rho = \frac{1}{2\pi} \int_0^{\pi/2} d\varphi \int_0^{\pi/2} d\varphi' \int_0^{2\pi} \tau_0(\varphi, \varphi', \Theta) \sin \varphi \sin \varphi' \, d\Theta \quad (11)$$

The directivity  $g$  is defined in just the same way as is the more familiar antenna gain or directivity, namely as the ratio:

$$g = \frac{\text{Total reflected power if reflection were as strong in all directions as it is toward the transmitter}}{\text{[Actual total reflected power]}}$$

$$= \frac{\text{Eq. (9)}}{\text{Eq. (10)}} = \frac{4\pi \int_0^{\pi/2} \sigma_0(\varphi) \sin \varphi \, d\varphi}{\int_0^{\pi/2} d\varphi \int_0^{\pi/2} d\varphi' \int_0^{2\pi} \sigma_0(\varphi, \varphi', \Theta) \sin \varphi \sin \varphi' \, d\Theta} \quad (12)$$

We see from Eqs. (9), (11), and (12) that the over-all cross section  $\sigma$  can be expressed as

$$\sigma = \pi a^2 \rho g$$

i.e., as the product of three factors,  $\pi a^2$  (the area of the apparent disk of the body), the quantity  $\rho$ , which depends only on the dielectric properties of the body, and  $g$ , which depends on the terrain geometry. Measurement of  $\sigma$  and its subsequent separation into these three factors is an important radar astronomical problem since knowledge of  $g$  gives considerable knowledge about terrain shape, and knowledge of  $\rho$  reveals much about the material of which the terrain is composed. However, as Eqs. (11) and (12) show, both  $\rho$  and  $g$  depend on  $\sigma_0(\varphi, \varphi', \Theta)$ , and the simpler  $\sigma_0(\varphi)$  does not give enough information to compute  $\rho$  and  $g$  separately. As Pettengill has pointed out,<sup>5</sup> in order to separate  $\rho$  and  $g$ , it is necessary to make bistatic measurements over a variety of angles  $\varphi$ ,  $\varphi'$ , and  $\Theta$ , which is not possible on radar astronomy targets from the earth alone, but instead requires some sort of radar space probe.

### C. Time Delay (Range)

We have just looked at one way of splitting up the echo power, saying that so much of the total radar cross section may be attributed to the projected area, so much to reflectivity and so much to directivity. There are other ways of dividing up the effect of the target on the echo produced, for example according to the time delay or frequency shift, and we shall find these to be much more important. We are particularly interested in any method that will allow resolution of portions of the echo coming from different places on the target.

Different portions of a deep target will return energy at different delays. Loci of all points having constant delay  $\tau$  will be concentric spheres of radius  $c\tau/2$  about the transmitter-receiver location, or if transmitter and receiver are not collocated, these loci will be ellipsoids of revolution with transmitter and receiver locations as foci, and a semimajor axis equal to  $c\tau/2$ . If

the target is remote enough these concentric spheres or ellipsoids can be approximated by parallel planes, and we shall assume that this is the case. Thus, at great distances for a body of any shape, an observer standing at a point perpendicular to the line of sight from radar to target center will see a scale of range reading linearly along the line of sight [the solid lines in Fig. 4(b)]. If the target is a sphere, these loci of constant range are circles as one views the target head-on from the radar [the solid lines of Fig. 4(a)].

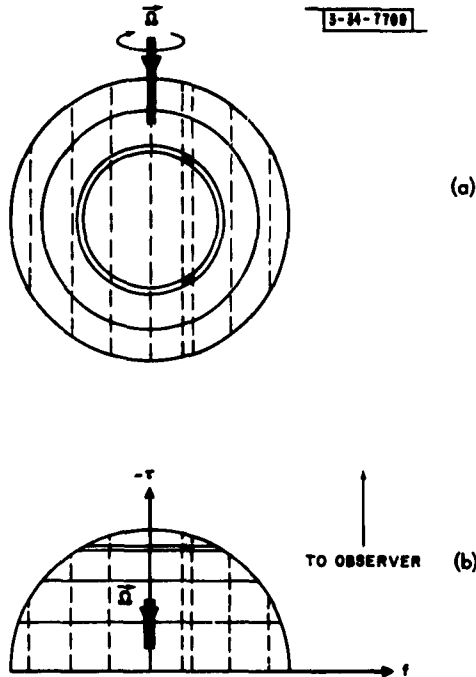


Fig. 4. Contours of equal range (solid lines) and equal doppler offset (dotted lines) for a spherical target.  $\vec{\Omega}$  is the rotation vector defining the polar axis of the body. A pair of regions (heavily shaded) can be associated with the echo returning with a given delay  $\tau$  and doppler offset  $f$ .

Clearly, one can isolate returns from regions lying at or near one of these loci of constant range by transmitting narrow pulses and observing the received return after an appropriately adjusted delay.

Going back to Fig. 3, the sketches (c) and (d) indicate how the average power response to narrow pulses would look if the target were uniform with a radar angular spectrum  $\sigma_0(\varphi)$  of the form shown in (a). In Appendix B it is shown that the distribution of power (actually cross section) as a function of time delay  $\tau$  for a uniform spherical target (expressed in square meters) is actually

$$\sigma(\tau) = \pi a c \sigma_0 \left( \cos^{-1} \frac{c\tau}{2a} \right) \quad (13)$$

where  $c$  is propagation velocity and  $a$  is the target radius.

#### D. Frequency and Phase

It has been mentioned several times that, because of the inhomogeneous nature of the target terrain, there will be irregularly different amplitude, phase, and polarization direction of the electromagnetic signal at different places on the wavefront of the reflected signal, even if these

quantities are constant across the transmitted wavefront. As long as the transmitter, receiver, and target are rigidly fixed relative to one another, there being no relative rotation of the target, then each transmitted Fourier component sinusoid arrives at the receiver as a sinusoid with a different but constant amplitude, phase and vector direction. However, at different receiver points these quantities will be randomly different constant values, if the target is rough.

If now the target rotates, these spatial irregularities in the wavefront will pass sideways over the receiving point at a certain speed in a certain direction and will give rise to fluctuations with time of the amplitude, phase, and polarization direction of the sinusoidal electromagnetic vector.† This means that what started out from the transmitter as a sinusoid will appear at the receiving antenna output to be a narrow-band noise of some type. The faster the rotation of the body, the wider the bandwidth of this narrow-band noise.

There is a second way of putting this: since some portions of the rotating and presumably rough target are moving toward the observer and some away from him there will be a spread or smearing of the frequency spectrum of any sinusoid incident on the target.

There are, then, these two ways of looking at the behavior of the phase and frequency [the trigonometric argument of Eq. (1)] in the received signal. Interferometer techniques, those involving more than one receiving point, are more conveniently analyzed by considering the motion sideways across the line of sight of the irregularities in amplitude, phase, and direction of polarization. What happens at a single radar receiver can be treated more readily by looking at the velocity of motion along the line of sight of various parts of the target producing echoes. These are just two different ways of looking at the same set of phenomena.

Let us look first at the velocity of radial motion of various points on the target. It can be shown fairly simply‡ that on a distant rotating body the locus of all points that have equal components of velocity along the line of sight to the target center is the line formed by the intersection of the surface of the body with a plane parallel to the plane of line of sight and polar axis. Moreover, the separation between this plane and the plane of line of sight and axis is proportional to the velocity. This means that a head-on view [such as that in Fig. 4(a)] of a body of any shape would show loci of target points producing equal doppler shift in an incident sinusoid as straight lines running parallel to the line formed by the polar axis. These lines are spaced proportionately with doppler shift.

Clearly, one can isolate returns from regions lying on or near one of these loci of constant doppler offset by transmitting a narrow-spectrum sinewave and observing the received return at an appropriately adjusted frequency offset. These loci are shown dotted in Figs. 4(a) and (b).

Looking at the target from a distant point on a line perpendicular to the radar line of sight and in the plane containing line of sight and polar axis [Fig. 4(b)], these same loci of equal velocity toward the radar are still straight lines spaced equally with doppler shift. It is now clear why we have investigated what the loci of constant range and constant frequency look like from this particular distant point at right angles to the radar line of sight; for this situation only, range and doppler frequency both read linearly along two perpendicular axes, irrespective of the

---

† The sinusoid is generated by motion at the propagation velocity of the electromagnetic field of wavelength  $\lambda$  along the line of sight. This motion should not be confused with the (much slower) sideways motion of the irregularities we have been discussing.

‡ For example from Eq. (B-6) of Appendix B.

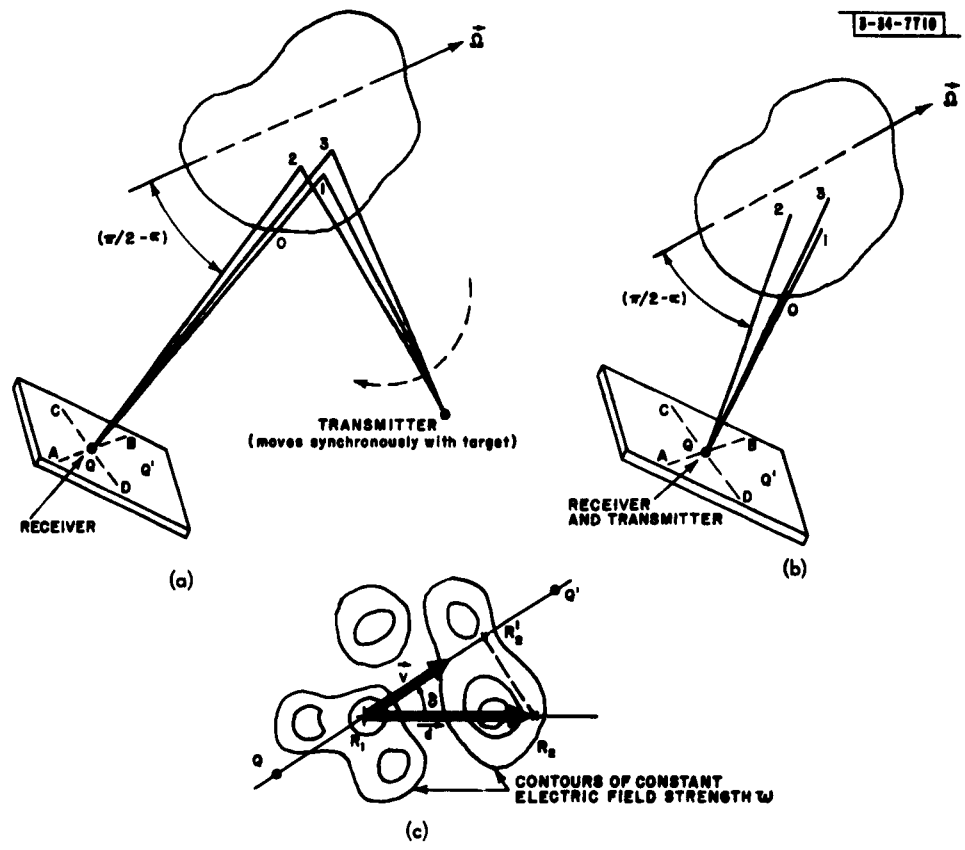


Fig. 5. Method of deducing direction of motion on the ground of corrugations in received wavefront: (a) hypothetical case of transmitter motion locked to target rotation; (b) actual case of transmitter and receiver stationary and approximately collocated; (c) view of ground plane showing diffraction pattern.

shape of the body. This distortionless mapping property<sup>6</sup> (of points on the body onto points in the range-vs-doppler plane) will prove to be a convenience later on.

If one looks head-on at the target, as in Fig. 4(a), contours of equal doppler shift intersect contours of equal range (which for a sphere are circles, as described in the preceding section) in at most two points as shown by the shaded regions. Thus we can isolate and study such a pair of points on the target surface simply by isolating that part of the echo having a given time delay and simultaneously a given frequency shift.

For a uniform spherical target, the distribution of power as a function of  $f$ , the frequency offset from a "zero doppler" represented by the radial velocity of the target center, is shown in Appendix B to be

$$\sigma(f) = \frac{c^2}{2f_0 \Omega \cos \alpha} \int_0^{\infty} \sigma_0(\cos^{-1} \frac{c\tau}{2a}) \times \left[ 1 - \left( \frac{c\tau}{2a} \right)^2 - \left( \frac{fc}{2f_0 a \Omega \cos \alpha} \right)^2 \right]^{1/2} d\tau \quad (14)$$

(expressed in square meters), where  $f_0$  is the carrier frequency,  $\Omega$  is the rotation speed in radians per second and  $\alpha$  is the tilt of the polar axis from perpendicularity with the line of sight. Figure 3(e) illustrates this quantity  $\sigma(f)$  for the particular  $\sigma_0(\varphi)$  sketched in Fig. 3(a).

Now let us look into the other method of visualizing the behavior of the phase and rate of change of phase of the received signal. We wish to examine the motion perpendicular to the line of sight of the corrugations in the wavefront reaching the radar receiver after reflection from a distant target, and we especially want to know the degree of correlation of the signals received at two points spaced by a (vector) separation  $\vec{d}$  as a function of relative delay  $\Delta\tau$  of one station behind the other one  $\vec{d}$  distant. This is expressed by the quantity  $Z$  introduced earlier in connection with Eq. (7).

The method we shall use to deduce the motion of the wavefront irregularities at the receiver is depicted in Figs. 5(a) and (b). We shall consider two situations, an "artificial" but easily analyzed case [Fig. 5(a)], in which the transmitter rotates with the target, and the "actual" real-life situation [Fig. 5(b)], in which only the target rotates and the transmitter and receiver are close together and are fixed relative to the target center.

Three arbitrary points forming a triangle are chosen on the target body itself. Consider points 1 and 2 of Fig. 5(a) or (b). Line AB is the locus of all points in a plane at the receiver (perpendicular to the line of sight) for which the phase angle of the composite sinusoidal signal reflected by points 1 and 2 is the same value as at the receiver. That is, it is the locus of all points having the same difference in time-of-flight from transmitter to receiver via the two points 1 and 2. Similarly, the line CD is the locus of all points satisfying a similar condition regarding propagation via points 1 and 3. Considering now that points 1, 2, and 3 are actually in motion in different directions due to target rotation, it is possible to find the direction and speed of motion of the wavefront irregularities at the receiver by finding the direction and speed of motion of point Q, the intersection of AB and CD.

Before getting to the desired case of transmitter and receiver collocated [Fig. 5(b)], let us analyze the artificial situation depicted in Fig. 5(a). Here the receiver is fixed, but the transmitter is imagined to swing around as the target rotates, always being at the same distance from

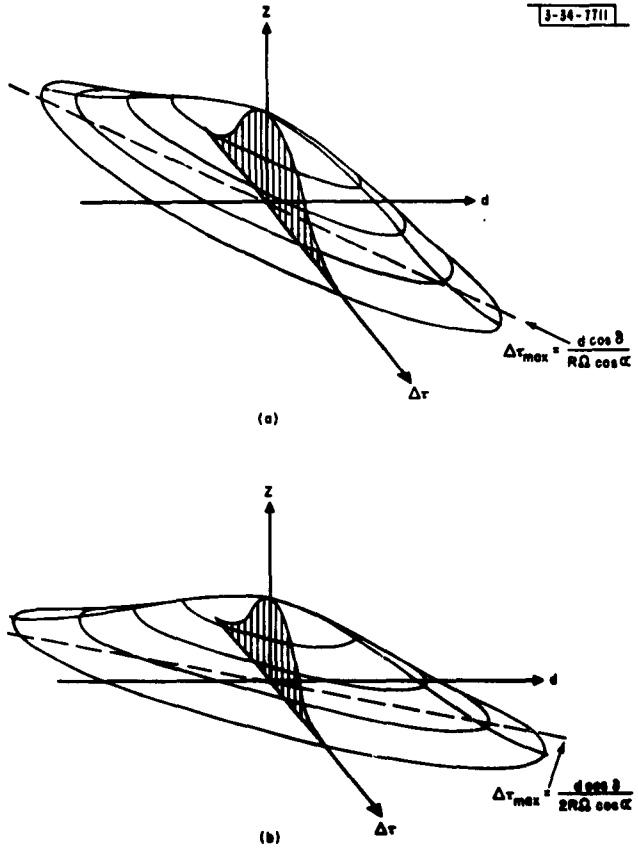


Fig. 6. The space-time correlation function  $Z(\vec{d}, \Delta\tau)$  for (a) the artificial case of a frozen echo pattern and (b) the actual case. (The quantity  $Z$  can be complex in general. For clarity it is drawn as a positive real quantity.)

the target and with the same orientation relative to it.<sup>†</sup> Thus, as the target rotates, the reflected wavefront at the target has its phase, amplitude and polarization corrugations "frozen"; that is, referring to Fig. 5(a), the times of flight from transmitter to points such as 1, 2, and 3 do not change. A moment's reflection convinces one that the direction of motion of the corrugations as observed on the ground must be in the direction in which the line OQ would swing if it, too, were frozen to the target at point O.

The important thing about this artificial example is that if we imagine two points Q and Q', equidistant from the target and mutually separated by a distance  $\overline{QQ'}$  lying parallel to the direction of pattern motion, then the following effect takes place. The pattern of irregularities that sweeps over the receiver point Q (and thus generates effectively a noise-like fluctuation in the receiver output at Q) is identical to the pattern at the point Q' at a later time equal to the time taken for the pattern to move the distance  $\overline{QQ'}$ . The velocity of pattern motion in the neighborhood of Q is clearly

$$v = \Omega R \cos \alpha \quad ,$$

where R is the range and  $\alpha$  is the polar angle, so that the time delay is

$$\Delta\tau_0 = \frac{\overline{QQ'}}{\Omega R \cos \alpha} \quad .$$

For radar astronomy targets, all the target points are essentially at the same range R. Figure 5(c) shows a plan view of the ground plane with the vector  $\vec{v}$  indicated by the arrow, and a snapshot of the variations of amplitude and phase across the wavefront schematized by the curved contours. Under certain conditions it may be assumed that, on the average, these contours are circles; that is, the pattern changes equally rapidly with distance in all directions on the ground plane. Among these conditions is the case of a spherical target with uniform surface properties, i.e., uniform  $\sigma_0(\varphi)$ .

Imagine now that we have two receivers  $R_1$  and  $R_2$  spaced by the vector distance  $\vec{d}$ , making an angle  $\delta$  with the pattern velocity  $\vec{v}$ , and that we wish to compute

$$\mathcal{Z}(\vec{d}, \Delta\tau) = \langle \mathcal{W}(t) \mathcal{W}^*(t + \Delta t) \rangle \quad ,$$

the cross correlation of the electric field  $\mathcal{W}_1$  and  $\mathcal{W}_2$  observed at the two receivers, as a function of the separation  $\vec{d}$  and a lag  $\Delta\tau$  of the first signal behind the second. The quantity  $\mathcal{Z}$  is complex in general; that is, it can be viewed as embodying the phase and amplitude of a sinusoid. (Just how this sinusoid can actually be generated in an interferometer experiment will be discussed in Sec. IV-F.) We will now describe heuristically how a  $\mathcal{Z}(\vec{d}, \Delta\tau)$ , such as is depicted in Fig. 6(a) expresses certain target properties. (This is an extension of Eq. (7) in which  $\mathcal{Z}(\vec{d}, 0)$  was related to the power across the target aperture.)

For  $\vec{d} = 0$ , this function  $\mathcal{Z}$  is the autocorrelation function of a single receiver output, and we already know the Fourier transform of this; it is just the power spectrum of the fluctuation  $\sigma(f)$  as expressed in Eq. (14) and depicted in Fig. 3(e), except that in this case this power spectrum is half as wide, because only the target-to-receiver distance is changing, the target-to-transmitter distance being constant. Denoting the transform of  $\sigma(f)$  by  $\mathcal{R}(\Delta\tau)$ , we have<sup>‡</sup>

<sup>†</sup> Equivalently, the transmitter could be fixed and the receiver move synchronously with target rotation.

<sup>‡</sup>  $\mathcal{R}(\Delta\tau)$  is a quantity to be discussed further in Sec. IV-E.

$$Z(0, \Delta\tau) = \mathcal{R}(\Delta\tau/2) .$$

It is almost equally simple to determine the zero-delay correlation  $Z(\vec{d}, 0)$ , still sticking to our "artificial" example of the synchronously rotating transmitter. The function  $Z(\vec{d}, 0)$  is derivable from Eq. (7), which states a Fourier transform relationship between ground space correlation function (with zero relative delay) and power across a plane aperture. If we imagine the aperture to be the apparent disk of the target, then the distribution of power across the aperture  $\langle |\mathcal{E}(x, y)|^2 \rangle$  in Eq. (7) is actually the brightness distribution  $P(x, y)$ , defined earlier. Thus

$$\iint_{\text{Aperture}} P(x, y) \exp [j2\pi(px + qy)] dx dy = \langle W(l, m) W^*(l + p, m + q) \rangle dldm = Z(\vec{d}, 0) .$$

Aperture

That is, the inverse transform of the brightness distribution is the ground correlation  $Z$  taken with time shift  $\Delta\tau = 0$ , and with station separation  $\vec{d}$  given by the two direction cosine arguments  $p$  and  $q$ . With no loss of generality, we can take  $\vec{d}$  parallel to one of the axes of the aperture in Fig. 2, say the  $x$  axis (so that  $q = 0$ ); then

$$\int_{\text{Aperture}} \exp [j2\pi px] dx \int_{\text{Aperture}} P(x, y) dy = Z(\vec{d}, 0) .$$

In other words, the right side is given by the single inverse transform (in  $x$ ) of the integral along  $y$  of the brightness distribution  $P(x, y)$ . Now notice that for a uniform spherical target the shape of  $Z(\vec{d}, 0)$  is the same (except for a scale factor) as  $Z(0, \Delta\tau)$ . This has to be so because the single Fourier transform with respect to  $\Delta\tau$  of the latter is just the echo power spectrum  $\sigma(f)$ , which in turn is simply the integral of the brightness distribution  $P(x, y)$  along one of the constant frequency strips in Fig. 4(a), i.e., the integral  $\int_{\text{Aperture}} P(x, y) dy$ .

About the only other thing we shall need to know about  $Z(\vec{d}, \Delta\tau)$  in order to discuss interference experiments later is the value of  $\Delta\tau$  that will maximize  $Z$  for a given station spacing  $\vec{d}$ . Referring to Fig. 5(c), in which the spacing  $\vec{d}$  lies between points  $R_1$  and  $R_2$ , we see that if the ground pattern has the generally isotropic character assumed earlier, maximum correlation will be achieved if, in performing the correlation, the first signal is delayed by a  $\Delta\tau$  equal to the time taken for the pattern to move the projected distance  $\overline{R_1 R_2}$ ; that is,

$$\Delta\tau_{\max} = \frac{d \cos \delta}{v} = \frac{d \cos \delta}{\Omega R \cos \alpha} .$$

We shall make use of such a relation later in deducing the planetary rotation vector  $\vec{\Omega}$  from  $\vec{v}$ , the ground pattern velocity. Note that the more nearly  $\vec{d}$  lies along  $\vec{v}$ , the larger the value of  $Z$  obtained by inserting the best delay  $\Delta\tau_{\max}$  in processing the two receiver outputs; indeed, when  $\delta = 0$ , the full correlation  $Z(\vec{d}, \Delta\tau_{\max}) = Z(0, 0)$  is obtained because, since the diffraction pattern is frozen, the two received voltages are identical apart from a time shift.

With this "artificial" example now disposed of, most of the groundwork has been laid for discussing the "actual" case. Figure 5(b) shows the transmitter, target, and ground plane for this situation, and now the transmitter is assumed fixed. To find the direction and speed of motion of the ground pattern we once again examine the motion of point  $Q$ , the intersection of equiphasic lines  $AB$  (due to reflection from target points 1 and 2), and  $CD$  (due to reflection from 1 and 3).

The actual rotation vector of the target is  $\vec{\Omega}$ . We can express this as the vector sum of two components  $\Omega_1$  and  $\Omega_2$  along the line of sight and perpendicular to it, respectively. We have  $\Omega_1 = \Omega \sin \alpha$ , and  $\Omega_2 = \Omega \cos \alpha$ . We can get the over-all behavior of lines AB and CD by considering these two rotation velocities separately,<sup>†</sup> knowing that the true motion of points 1, 2, and 3 is the vector sum of motions due to two rotations  $\Omega_1$  and  $\Omega_2$ . Now if we seek the motion of point Q, the intersection of AB and CD, it is clear that component  $\Omega_1$  has no effect on lines AB and CD except that they rotate at an angular rate  $\Omega_1$ , the point of intersection Q remaining fixed. This is true because the propagation path lengths are not changing. Therefore we need only consider the motion of point Q due to  $\Omega_2$ .<sup>‡</sup> Since  $\Omega_2$  is an angular velocity that the target would have if its polar axis were perpendicular to the line of sight and it rotated with a speed  $\Omega_2 = \Omega \cos \alpha$ , we can state that the motion of point Q is exactly the same in our "actual" example as it was in the "artificial" example of Fig. 5(a), except that the speed is twice what it was before, since both the propagation paths (up and back) to each target point are changing their length with time, so that point Q must move twice as fast toward Q' to equalize path length difference via points 1 and 2 and via 1 and 3.

Note that the contribution to the ground pattern produced by reflection from any point on the target has the same velocity of motion as that produced by a reflection from any other point, namely in direction QQ', and with twice the speed that a radius vector OQ from the target center would swing,

$$v = 2\Omega R \cos \alpha$$

This means, among other things, that there is no hope of distinguishing the echoes from different portions of the target on the basis of different velocities of their contributions to the ground pattern. We must go back to resolution according to range (Sec. II-B) or doppler (Sec. II-C) or the brute force method of using sharper antenna beams.

There is a second difference between the "artificial" and "actual" cases that must be pointed out besides the double velocity of the ground diffraction pattern motion. Since the propagation path lengths from transmitter to target are constantly changing as the target rotates in the "actual" case, the wavefront irregularities of amplitude, phase, and polarization direction at the target are not "frozen" as was true in the "artificial" case, but are constantly changing with time. Thus the contours of Fig. 5(c) are not only in motion, as before, but are changing with time. This means that there will be an additional diminution of the correlation  $Z(\vec{d}, \Delta\tau)$  from the maximum, over and above the factors discussed for the artificial case. (These factors were the failure of the direction of  $\vec{d}$  to coincide with that of  $\vec{v}$ , and then, of course, the nonzero values of variables  $d$  and  $\Delta\tau$ .) In particular, even if one inserts the  $\Delta\tau$  that maximizes  $Z$  for a given  $\vec{d}$ , namely  $\Delta\tau_{\max}$ , which is now given by

$$\Delta\tau_{\max} = \frac{d \cos \delta}{2\Omega R \cos \alpha} \quad (15)$$

he does not get the full correlation  $Z(0, 0)$  when  $\vec{d}$  lies along  $\vec{v}$  because the two received voltages are no longer exactly identical apart from a time shift.

<sup>†</sup> The author is indebted to J. V. Evans for pointing out this simple method of analyzing the motion of point Q in the "actual" case.

<sup>‡</sup> True except for the singular case of widely spaced transmitter and receiver points and the target axis appearing almost exactly end-on from the ground ( $\Omega_1 \gg \Omega_2$ ).

If the time rate of this pattern change were a sufficiently large fraction of the fading rate produced in a single antenna due to motion of the pattern, then we would know that Eq. (15) would not be valid. The best value of  $\Delta\tau$ ,  $\Delta\tau_{\max}$  would be shifted toward zero because, since the pattern is decomposing as it moves, a higher degree of correlation would be obtained by advancing  $\Delta\tau$  slightly to head off the decomposition. Thus, before we can be sure Eq. (15) is valid, we must be sure that the pattern decomposition can be neglected compared to pattern motion.

We can determine how big a part pattern fluctuation plays relative to pattern motion by inquiring how much of the signal fluctuation at a single receiver is due to motion and how much is due to pattern changes with time. It will now be shown (in the next paragraph) that all the fluctuation rate observed at a single receiver is due to pattern motion; it then being a safe assumption that for spacings  $d$  of the order of several multiples of the correlation distance, pattern decomposition is small. Equation (15) is then valid except for the case where one simultaneously has very small values of the angle  $\delta$  and large values of  $d$ .

Comparison of Figs. 6(a) and (b) shows that the profile of  $Z(0, \Delta\tau)$  for the "artificial" case of a frozen pattern of irregularities is twice as wide as the same profile for the "actual" case about which we are concerned. This is known from considering the radial motion relative to the observer of the different points on the target; a given such velocity [Fig. 4(a)] will produce one-half the doppler shift when the transmitter-to-target distance is not allowed to change [Fig. 5(a) -- the "artificial" case] as when the transmitter and receiver are collocated [Fig. 5(b)]. Yet we have already seen from different considerations that the sideways pattern velocity across the ground in the "actual" case is exactly twice that of the "artificial" case. But the physical size of the pattern corrugations is the same in both cases, as ensured by the fact that  $Z(d, 0)$  is the same for both cases. Thus, if the physical size of the irregularities is the same, and the velocity of motion along the ground is twice as large in the "actual" case, then this completely accounts for the fact that the echo power spectrum is twice as wide in the actual case. The pattern decomposition makes a negligible contribution to the fading rate, relative to the pattern motion.

It is instructive to compare these notions on rotating planets with equivalent ideas that have been applied for some years to the ionosphere. If one imagines a plane wave incident on a plane ionosphere overhead, then if the ionospheric irregularities are frozen, the horizontal motion of the ionosphere (an ionospheric wind) causes a motion along the ground of the frozen irregularities in the wavefront pattern. In actuality, however, since the ionosphere is a soft target in which there are turbulent effects, constant random alteration of the wavefront irregularities is present. With the ionosphere, the inability to recover complete correlation by readjusting  $\tau$  even when  $\vec{d}$  coincides with  $\vec{v}$  is due to the changing shape of the target; with a planet it is due to the fact that the transmitter is stationary instead of moving synchronously with target rotation. Briggs, et al.,<sup>7</sup> have made a lengthy analysis of the use of such interferometric methods to study ground pattern velocity and the way in which the moving ground pattern itself fluctuates with time. Their analysis goes a good deal further for the ionospheric case than the notions we have presented here for the rotating sphere case. The aim here has been simply to determine  $\Delta\tau_{\max}$  [Eq. (15)] without deriving the complete function  $Z(\vec{d}, \Delta\tau)$ .

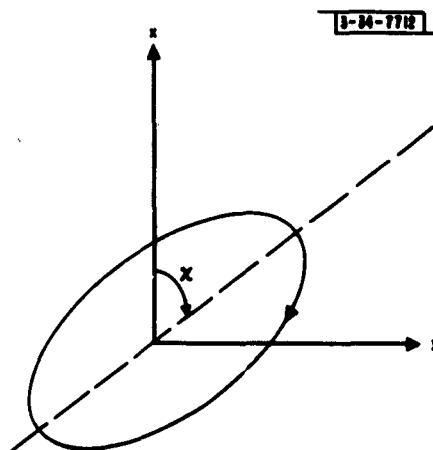
### E. Polarisation

Most of the radio and visible energy from cosmic sources is relatively unpolarized; that is, most of the energy in the arriving signal  $\vec{w}(t)$  not only has a randomly time-varying amplitude and

phase [ $W(t)$  a random complex variable], but also a random time-varying direction of polarization. By contrast, in making radar observations the character of the polarization is controlled on transmission for the dual purposes of conserving system efficiency (by not wasting power into unnecessary degrees of freedom of the signal) and of studying those target properties that affect the polarization. Since the target does not in general produce a complete randomization of the incident wave, it is often found that a large fraction of the received energy arrives systematically polarized (see, for example, Refs. 5, 8 and 9 for certain lunar results).

Such partly polarized radiation can be resolved uniquely into two parts, the "unpolarized" (i.e., randomly polarized) component, and the (systematically) "polarized" component. The unpolarized component will have a narrow-band noise spectrum (due, for example, to the doppler spreading discussed in Sec. II-D) and if resolved (for example into two linearly polarized components at right angles to one another) will exhibit zero correlation between the two. The polarized component, on the other hand, may or may not have a nonzero bandwidth. In either case the components at right angles are mutually coherent. That is, the electric vector traces out an ellipse (Fig. 7) which may be continually fluctuating in size (at the bandwidth rate), but maintains a constant orientation, ratio of axes and sense of rotation.

Fig. 7. Path traced by head of a vector representing received electric field strength as a function of time (complete polarization).



The polarized component is specified by its power  $P_e$ , orientation angle  $\chi$  and axial ratio  $r$ . The sense of rotation is contained in the sign of  $r$ ; that is,  $r > 0$  for left-hand circular polarization and  $r < 0$  for right-hand circular. In Fig. 7, the wave is propagating along the  $z$  axis into the paper; thus  $\chi$  is clockwise from the  $x$ -axis, and, as the arrow indicates,  $r$  is negative.

The unpolarized part is specified by a single parameter  $P_u$ , its power. The degree of polarization  $m$  is simply  $P_e/P$ , where  $P$  equals the total power  $P_e + P_u$ . Since in radar experiments the wave is transmitted completely polarized ( $m = 1$ ), the term depolarization ( $1 - m$ ) is perhaps more frequently encountered in radar usage than is the degree of polarization  $m$ . A monochromatic (i.e., single-frequency) signal is completely polarized, by definition. It should be noted that one sometimes encounters other definitions of depolarization in which a monochromatic wave can be said to be "depolarized." For example, if vertical polarization is transmitted, the horizontally polarized received component is sometimes called the "depolarized" component. Such a definition obviously is not equivalent to that employed here.

There are several different ways of rearranging the quantities  $P$ ,  $m$ ,  $\chi$  and  $r$  into a more usable form, and the preferred rearrangement depends on the particular properties of the radiation that are most interesting. For radio engineering purposes the most interesting choice is usually the four Stokes parameters<sup>10</sup>

$$\begin{aligned} I &= P \\ Q &= mI \cos 2(\tan^{-1} r) \cos 2\chi \\ U &= mI \cos 2(\tan^{-1} r) \sin 2\chi \\ V &= mI \sin 2(\tan^{-1} r) \end{aligned} \quad (16)$$

because of the ease with which the effect of various forms of targets and receiving antennas may be calculated. The parameters have the following physical interpretation:  $I$  is of course the total power,  $Q$  is the excess of  $\chi = 0$  linearly polarized power over that at right angles to it,  $U$  is the excess of  $\chi = 45^\circ$  linearly polarized power over that at right angles to it, and  $V$  is the excess of left-hand circular over right-hand circular power. The four quantities are often written as a column matrix or vector, and are then referred to as the Stokes vector  $\mathbf{S}$ . (Note that this is a vector in the mathematical sense and is not a vector property of the wave in physical space.)

The usefulness of the Stokes representation in deducing the effects of signals on specified antennas is clear from the above description of the parameters. The effect of a target on the incident signal turns out to be simply defined too. Specifically, the Stokes vector  $\mathbf{S}_r$  of the reflected wave is related to the Stokes vector  $\mathbf{S}_i$  of the incident wave by the set of simple linear equations given by

$$\mathbf{S}_r = \mathbf{M}\mathbf{S}_i \quad (17)$$

where  $\mathbf{M}$  is a four-by-four matrix called the Mueller matrix.<sup>†</sup>

The Mueller matrix representation has proved quite useful in studies of simple radar targets such as cones, corner reflectors, and so forth,<sup>11</sup> especially when the target is maintaining a fixed aspect, thus returning a monochromatic (completely polarized) signal.

Of central importance in the study of a hard rotating radar astronomy target is the degree of polarization

$$m = \frac{\sqrt{Q^2 + U^2 + V^2}}{I} \quad (18)$$

Only if the body is extremely simple in shape or not rotating at all relative to the line of sight does one expect  $m$  to be unity. The more realistic situation involves complicated diffractive and multiple reflection effects giving rise to the wavefront irregularities we have spoken of earlier. The way in which  $m$  drops from the unity value it would have for an ideally smooth shape (for example a sphere) as the surface roughness increases appears not to have been studied

<sup>†</sup>A matter of terminology is worth mentioning here. The elements of the Mueller matrix (which, like those of the Stokes vector, deal with powers) are sums of products of the elements of a matrix of voltages that characterizes the target also. This two-by-two matrix of voltages is called the scattering matrix of the target and is something entirely different from the target scattering function to be defined in Sec. IV. The reader may already be familiar with the scattering matrix; it should not be confused with the scattering function.

in the literature. Indeed it is not entirely clear that  $m$  should drop completely to zero as surface roughness increases.<sup>†</sup>

The theory of depolarization of electromagnetic waves by reflection from rough surfaces seems to have been given very little attention,<sup>‡</sup> although a great deal of experimental data exists. P. Beckmann and his coworkers have made an encouraging start on the theory. Beckman<sup>12</sup> has treated the case of random surfaces with radii of curvature much larger than the wavelength, and Chytil<sup>13</sup> has examined a variety of target shapes (such as disks, strips, cylinders, spheres and prisms) in the region  $\lambda \sim a$  to  $\lambda = a/10$  (where  $a$  is the target size). Chytil finds that with linearly polarized radiation incident, as  $\lambda \rightarrow a$  the echo power becomes about equally divided between components parallel with and perpendicular to the incident polarization direction for all shapes.

### III. SOFT TARGETS

According to the definition adopted earlier in this chapter, soft targets include those that are changing shape, such as turbulent clouds of one sort or another. The soft targets of greatest radar interest are the ionized regions (sun's corona, planetary ionospheres, and the interplanetary medium), and this part of the present chapter will focus on the influence of such regions on the transmitted signal.

On the other hand, clouds of material particles, such as the zodiacal particles, terrestrial raindrops, etc., are of only minor radar astronomical interest and it is not necessary to say very much about them here. They are usually so rarified that multiple reflections can be neglected, and a computation of radar cross section of a cloud or portions of it consists simply of multiplying the cross section of a single typical particle by the number of particles in the region. If the particles are perfectly conducting spheres,<sup>14</sup> for example, the cross section per particle is that given by Fig. 8, in which it is seen that when the radius  $a$  is much smaller than the wavelength  $\lambda$ , the cross section falls off as the fourth power of  $a/\lambda$  (the "Rayleigh scattering law").<sup>§</sup> This  $a/\lambda \ll 1$  condition holds with such soft targets as the zodiacal regions and terrestrial rain clouds, and it also holds in a rough quantitative way with ionospheric free-electron scattering.<sup>15</sup> (The cross section per free electron is obtained by substituting the classical electron diameter in the Rayleigh law.) It is interesting to observe in Fig. 8 that in the spherical case as one passes from the  $a/\lambda \ll 1$  situation (relevant to some of the soft radar astronomy targets) over into the  $a/\lambda \gg 1$  case (to which our discussion of hard targets has been directed), the cross section approaches  $\pi a^2$ , the projected area of the sphere, as would be expected from the discussion in Sec. II-B.<sup>¶</sup>

<sup>†</sup> In reflection from random media where there are no multiple reflections and the individual scatterers have a strong anisotropy, the depolarization may not be complete. This is suggested by a study of the reflection of RF signals from clouds of randomly oriented dipoles<sup>16</sup> for which it was found that  $m = 1/2$ .

<sup>‡</sup> The Stokes vector-Mueller matrix formalism might have some application to hard radar astronomical targets. (Parke<sup>17</sup> gives a very complete survey of this formalism.) This is suggested by the following interesting properties. In the case of multiple reflections, the  $M$  describing the over-all process is the product of the  $M$ 's describing the individual reflections, and when a number of wavelets add to give a composite signal, although the over-all  $M$  is not the sum of the individual  $M$ 's, the summation can be handled in terms of the scattering matrices of the reflections. Conceptually at least, this sort of formalism then provides the possibility of theoretically studying the polarization properties ( $S_r$ ) of an echo made up of a sum of multiple reflections.

<sup>§</sup> It is not necessary that the body be spherical for the fourth-power law to hold.

<sup>¶</sup> Notice here that the peculiar method of defining all radar cross sections as a power ratio times an arbitrary  $4\pi$  [referred to in connection with Eq. (5)] does have the advantage that the cross section of a perfectly conducting sphere equals its projected area. It is difficult to imagine a single other advantage of this curious convention.

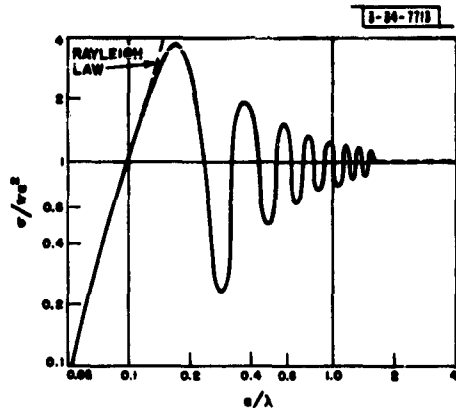


Fig. 8. Wavelength dependence of the radar cross section of a perfectly conducting sphere of radius  $a$ .

As we have just indicated, soft targets of radar astronomy interest are limited for the most part to ionized media, since clouds of material particles (such as the zodiacal particles) suffer the  $(a/\lambda)^4$  dependence and are at prohibitively large ranges; and those effects in our own atmosphere not associated with its ionized condition are minor.

In discussing the reflection of electromagnetic signals from ionized media it will be necessary here only to review one or two points and to emphasize the dissimilarities of soft targets and hard targets.

#### A. Reflected Power and Angular Power Spectrum

The effective radar cross section of a given volume of plasma can vary over the enormous range from simply the sum of the cross sections of individual free electrons (free electron scatter) to the unity reflectivity obtained in the case of reflection below the critical frequency (in the absence of collision losses). Exactly where in this range the effective cross section of a unit volume of plasma will lie thus depends on many factors, principally the operating frequency, electron and ion densities, collision frequency, magnitude and direction of the magnetic field and the temperature.

When the target presented to the probing radar signal is a large and inhomogeneous body of plasma, such as the sun's corona, then matters become quite complicated. Unlike the hard targets discussed earlier, the target material is in constant relative motion so that it is impossible to use most of the neat properties one can attribute to rotating hard targets (such as the location of loci of constant range or doppler offset).<sup>†</sup>

However, under certain conditions it may still be useful to retain some of these ideas, particularly the notion of radar angular spectrum. For example, although our own ionosphere is a soft target, there are some reasonable constraints on shape (particularly the common assumption that it has a general horizontal stratification, on which are superimposed statistical irregularities), and the notion of angular spectrum of reflection from the irregularities has proved quite meaningful

<sup>†</sup> And even if the ionized plasma target were rigid, its geometrical properties would be more difficult to evaluate, since we are not always dealing here with reflection from objects but more often with penetration of the wave to points where certain conditions on refractive index are fulfilled (these conditions being dependent on the direction of arrival). Thus it is even more difficult to associate the angular power spectrum with detailed structure of the medium than it is with a hard target. (This association for the hard target case is discussed in Ref. 3.)

(see the last paragraph of Sec. II-D). A first-order approximation<sup>18</sup> to the true, highly irregular state of affairs in the sun's corona has been to assume that it is spherically symmetric with a general radial decrease of electron density, on which, as with the ionosphere, local spatial irregularities are superimposed, giving rise to a uniform roughness in the reflected wavefront; i.e., a definite radar angular spectrum  $\sigma_0(\varphi)$ , uniform throughout the corona.

### B. Time Delay (Range)

For soft targets, contours of equal time delay will no longer necessarily be contours of equal range because the group propagation velocity in the plasma may be less than the free space value. In particular, the total group time delay  $T$  will be twice the reciprocal of the integrated product of group velocity and distance: i.e.,

$$\frac{2}{T} = \int_0^R w(s) ds \quad ,$$

where  $w$  is the group velocity and  $R$  is the range of the point of reflection. In general, the medium will be dispersive; that is,  $w$  will depend on frequency. In the important case for which both collision frequency and gyro frequency are negligible compared to the operating frequency  $f$ ,

$$w(s) = nc = c \sqrt{1 - [f_p(s)/f]^2} \quad ,$$

where  $n$  is the index of refraction and  $f_p$  is the local plasma frequency in cps;

$$f_p(s) = 9.0 \sqrt{N(s)} \quad ,$$

$N$  being in electrons per cubic meter. If  $f_p \ll f$  also, then we have the useful formula

$$\frac{2}{T} = \frac{c}{R} - \frac{81c}{2Rf^2} \int_0^R N(s) ds \quad , \quad (19)$$

which expresses the excess of time of flight over that in vacuo in terms of integrated electron density along the propagation path (number of electrons in a one-square-meter column traversing the radar-to-target path).

### C. Frequency

We have just referred to the fact that for a soft target, both the reflected power and the propagation velocity can be frequency-dependent, and as is well known, the behavior of these quantities (and polarization too) can under certain conditions change violently with frequency. This makes it possible, in principle, to deduce certain parameters in the corona, or in planetary ionospheres, by means of measurements at different frequencies. This sort of technique has been richly cultivated for years in the study of our own ionosphere (see, for example, Ref. 19) whose various layers are studied by noting the frequency below which a test signal no longer passes through but is refracted back.

It is clear that gross shifts in the frequency of the radar echo are to be associated with radial components of motion in the soft target. For example, parts of the solar corona having the same range but different velocities relative to the radar line-of-sight may thereby be distinguished one from the other much as with various portions of hard targets (Secs. II-C and II-D). However, the lack of target rigidity destroys much of the usefulness of range-doppler echo resolution.

#### D. Polarization

The way in which the polarization characteristics of the incident radar signal are altered by passage through a plasma in the presence of a magnetic field is quite complicated in the general case. If there is no magnetic field, or if it is the incoherent scatter mode that is being employed, then the polarization is unaffected; it is as though the reflection were from a smooth hard target.

When a magnetic field is present in the ionized medium, and for the common case of operating frequency considerably larger than both gyro and plasma frequencies, then propagation takes place via two independent modes having opposite senses of circular polarization and slightly different phase velocities (neglecting collisions). When present simultaneously, these two waves, the "ordinary" and "extraordinary," form an elliptically polarized wave whose ratio of axes and sense of rotation do not change along the ray path, but whose plane of polarization does, because of the different phase velocities. The rotation is cumulative in the sense that it continues on the return trip from the target rather than undoing itself. The total number of radians  $\Delta\chi$  of this Faraday rotation is<sup>20</sup>

$$\Delta\chi = \frac{4.72}{r^2} \int_0^R N(s) B_s(s) ds \quad , \quad (20)$$

where  $B_s(s)$  is the longitudinal component of magnetic field (in gauss). Note that there is a dispersion (strong frequency dependence) of the total amount of rotation. In the special case in which the incident radiation is linearly (plane-) polarized, it can be considered the sum of equal-strength right-hand and left-hand circularly polarized components. One propagates by the ordinary mode only, and the other by the extraordinary mode only, so that the composite signal arriving is still linearly polarized – if not depolarized on reflection (see Sec. II-E) – but with the polarization axis twisted by  $\Delta\chi$  radians.

An ideally smooth target converts linear polarization into linear, and right circular into left circular, and vice versa.† In preference to linear polarization, one often uses circular transmitted polarization in conjunction with a receiving antenna adjusted for the opposite direction of circular polarization so that the signal power received from a smooth hard target can be maximized independently of the Faraday rotation angle  $\Delta\chi$ .

#### IV. MEASUREMENT METHODOLOGY

In the next few sections of this report, the way in which radar systems perform measurements on radar targets will be systematized. In Sec. V we shall collect all the preceding notions and list the way in which quantities of astronomical interest can be deduced from these radar measurements.

The targets dealt with in radar astronomy differ from those discussed in much of the standard radar literature by their sheer physical size and large differential velocities. Very rarely will these targets be extended targets, meaning that they more than fill the antenna beam because they are usually at extreme ranges; but, they will be what we shall call spread targets

† The (normalized) Mueller matrix of Eq. (17) is

$$M = \begin{bmatrix} 1 & 0 & 0 & 0 \\ 0 & 1 & 0 & 0 \\ 0 & 0 & 1 & 0 \\ 0 & 0 & 0 & -1 \end{bmatrix} .$$

in both delay and frequency. That is, since they are so deep and since different portions are apt to be moving differently relative to the observer, the returns are spread significantly in both range and doppler.

If neither the range spread nor the doppler spread is discernible to the radar system in use, we call the target a point nonfluctuating target. If the bandwidth of the signal is insufficient to resolve the target in range, and yet there is a discernible doppler spread of the received signal, we shall call the target a point fluctuating target. If the signal resolves the target in range but with no observable doppler spreading we can treat the target as a deep nonfluctuating target. In the general case in which observable range spreading and doppler spreading are present simultaneously we speak of a deep fluctuating target.

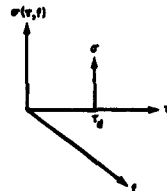
#### A. The Target Scattering Function $\sigma(\tau, f)$

It has proved convenient to describe the average reflecting properties of a spread radar target in terms of its scattering function  $\sigma(\tau, f)$ , the average reflectivity as a function of the two variables delay and doppler shift. The scattering function can thus be depicted as a surface in three dimensions, as in Fig. 9. The two independent variables are delay  $\tau$  (seconds) and doppler shift  $f$  (cycles per second). The dependent variable  $\sigma(\tau, f) d\tau df$  is defined as that part of the total target cross section  $\sigma$  (in square meters) that belongs to target regions that both reflect a signal with delays of  $\tau$  to  $\tau + d\tau$  and at the same time subject the signal to doppler shifts from  $f$  to  $f + df$ . A more concise discussion of the scattering function follows in Sec. IV-D.

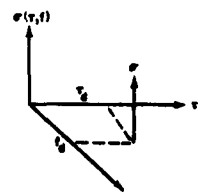
The concept of a scattering function has proved useful in unifying various techniques of measurement (this report) and detection.<sup>4</sup> Many of the measurement techniques we shall describe shortly are nothing more than measurements (i.e., estimates) of the scattering function or something derivable from it. In Ref. 1 it is found that, under certain reasonable assumptions, all one needs to know about the target in order to discuss its detectability completely is its scattering function.

Several cases are shown in Fig. 9. For example, a stationary point target at delay  $\tau_d$  would have the scattering function depicted in Fig. 9(a), namely an impulse of value  $\sigma$  at  $\tau = \tau_d$  and  $f = 0$ . If the point target were moving toward the observer at a velocity  $v = c f_d / 2f_0$  ( $f_0$  being the carrier frequency) the scattering function would appear as shown in Fig. 9(b). If the target (at delay  $\tau_d$  and moving at velocity  $c f_d / 2f_0$ ) could be regarded as having negligible depth in delay, but as producing rapid random fluctuations in the returned echo, the scattering function  $\sigma(\tau, f)$  would have the character shown in Fig. 9(c) — there would be a spread only along the  $f$ -axis. The width  $B$  along the  $f$ -coordinate is proportional to the fluctuation rate. Similarly, if the fluctuation rate were negligible, but the target were still quite deep and thus had a wide range spread, the scattering function would appear as in Fig. 9(d). The duration of delays or "multipath spread" is labeled  $L$ .

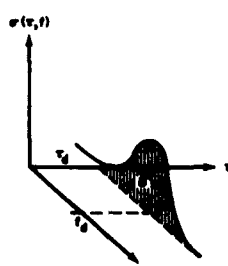
Figure 9(e) shows the scattering function of a hypothetical target having a significant spread along both axes. Figure 9(f) shows a typical such scattering function for the important special case of a uniform rotating rough sphere. As mentioned earlier, a uniform sphere is one having the same radar angular spectrum  $\sigma_0(\varphi)$  everywhere on its surface. Appendix B presents a derivation of the following equation for  $\sigma(\tau, f)$  of the uniform sphere of radius  $a$ , rotation speed  $\Omega$  and angle  $\alpha$  between polar axis and perpendicularity to the line of sight:



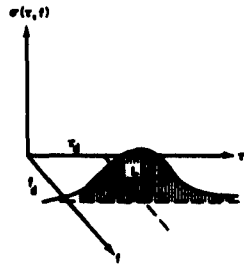
(a) Stationary point target at delay  $\tau_d$ .



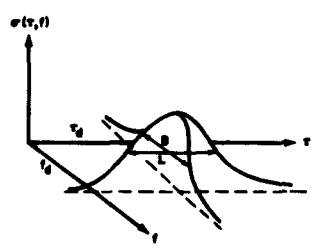
(b) Point target at delay  $\tau_d$  moving with velocity  $f_d/2f_0$ .



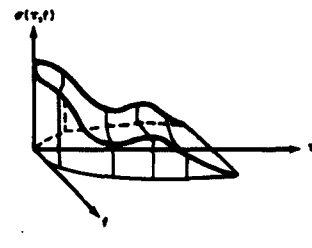
(c) Point fluctuating target of fluctuation rate  $B$ .



(d) Deep nonfluctuating target of depth  $L$ .



(e) Deep fluctuating target.



(f) Uniform rotating sphere.

Fig. 9. Scattering function of various forms of targets (the total volume under the function is equal to  $\sigma$ , the over-all radar cross section).

$$\sigma_o(\tau, f) = \frac{c^2 \sigma_o \left( \cos^{-1} \frac{c\tau}{2a} \right)}{2f_o \Omega \cos \alpha} \left[ 1 - \left( \frac{c\tau}{2a} \right)^2 - \left( \frac{fc}{2f_o a \Omega \cos \alpha} \right)^2 \right]^{-1/2} \quad (\text{real values only}) \quad (24)$$

where  $f_o$  is the carrier frequency and  $c$  is propagation velocity. The  $\tau$ -origin is at the target center.

It will be recalled from Sec. II-D that, because of the mapping property of rotating hard targets, points in the  $\tau, f$  plane correspond to locations on the surface of the target. Therefore a measurement of the scattering function  $\sigma(\tau, f)$  represents a map of reflected power from various regions of the target with the correspondence being that given in Fig. 4. [Note the occurrence in Fig. 9(f) of the same semicircular or semielliptical region in the  $\tau, f$  plane as is shown in Fig. 4(b).]

The scattering functions shown in Fig. 9 have been labeled to indicate roughly the two parameters  $B$  and  $L$ , the doppler spread and the delay spread, respectively [for 9(c) we have  $L = 0$  and for 9(d),  $B = 0$ ]. An important attribute of spread radar targets is the spread factor, the product  $BL$ . If  $BL < 1$  the target is termed underspread, and if  $BL > 1$ , overspread. As pointed out in Ref. 1, the radar detectability of a target of given total cross section

$$\sigma = \iint_{-\infty}^{\infty} \sigma(\tau, f) d\tau df$$

(the volume under the surface depicted in Fig. 9) decreases steadily with  $BL$  if  $BL$  becomes greater than roughly unity. In the neighborhood of  $BL = 1$ , even when the over-all system sensitivity is enough to overcome this loss in detectability, we shall see in Sec. VI-D of this report that it may become difficult to perform an estimation of the scattering function or derived parameters, a necessity for studying target properties in detail.

In order to discuss processes of estimating the scattering function, or derived properties, we must make a short digression to introduce the notions of a matched filter and the associated ambiguity function. (For a more detailed discussion see the paper by Turin.<sup>24</sup>)

### B. Detection of a Point Nonfluctuating Target - the Matched Filter

The simplest form of target is one whose scattering function is an impulse, i.e., a point nonfluctuating target. As is well known, the form of receiver that will develop maximum signal-to-noise ratio from such a target is a matched filter. (Most conventional radar receivers employ matched filtering in the IF.) That is, denoting the transmitted waveform as  $x(t)$ , if the noise spectrum is uniform, the optimum receiver consists of a filter having an impulse response  $m(t) = x(t_o - t)$  followed by a sampling device that observes the filter output at time  $t_o$  (where  $t_o$  is an irrelevant time delay introduced to make the filter physically realizable, i.e., no response before excitation). The matched filter has an impulse response that is a time-reversed version of the signal. Since its complex frequency function is thus the complex conjugate of the frequency function of the signal, a matched filter is often referred to as a conjugate filter.

It will be relatively simple and quite instructive to prove that this matched condition maximizes the signal-to-noise ratio as follows. Let  $X(f)$  be the Fourier transform of the signal  $x(t)$  (i.e., its complex spectrum), and  $M(f)$  be the complex frequency function of the filter. We want to adjust  $M(f)$  so as to maximize the output signal-to-noise ratio, defined as the ratio of  $S_{out}$ , the square of the output voltage at time  $t_o$  due to signal alone, divided by  $N_{out}$ , the output noise power. The latter is

$$N_{\text{out}} = \frac{N_0}{2} \int_{-\infty}^{\infty} |M(f)|^2 df \quad (22)$$

for input noise of uniform spectral density  $N_0/2$  watts per cycle per second ( $N_0$  watts per cps for a single-sided spectrum). The signal output is

$$S_{\text{out}} = \left[ \int_{-\infty}^{\infty} X(f) M(f) \exp[j2\pi ft_0] df \right]^2 \leq \int_{-\infty}^{\infty} |X(u) \exp[j2\pi ut_0]|^2 du \int_{-\infty}^{\infty} |M(v)|^2 dv \quad (23)$$

from the Schwarz inequality for two complex quantities A and B:

$$\left[ \int_{-\infty}^{\infty} A(x) B(x) dx \right]^2 \leq \int_{-\infty}^{\infty} |A(y)|^2 dy \int_{-\infty}^{\infty} |B(z)|^2 dz$$

Clearly, in order for the inequality (23) to be an equality, we must have

$$M(f) = \{X(f) \exp[j2\pi ft_0]\}^* = X^*(f) \exp[-j2\pi ft_0]$$

or in terms of the impulse response  $m(t)$ ,

$$m(t) = x(t_0 - t) \quad (24)$$

which was to be proved. When this matched condition exists, Eqs. (22) and (23) combine to give for the signal-to-noise ratio

$$\frac{S_{\text{out}}}{N_{\text{out}}} = \frac{2E_s}{N_0} \quad (25)$$

where  $E_s$  is the total signal energy  $\int_{-\infty}^{\infty} |X(f)|^2 df$ . This ratio  $2E_s/N_0$  is an important factor in the detectability of any signal.

The output voltage at time  $t_1$  produced from any filter of impulse response  $m(t)$  due to an input  $w(t)$  is given by the convolution

$$f_o(t_1) = \int_{-\infty}^{\infty} w(\tau) m(t_1 - \tau) d\tau$$

which for the matched condition is, by Eq. (24),

$$f_o(t_1) = \int_{-\infty}^{\infty} w(\tau) x(\tau - t_1 + t_0) d\tau \quad (26)$$

From this last equation, we see that the operation of observing the matched filter output at a given instant is mathematically equivalent to correlation detection, i.e., a multiplication of the incoming signal-plus-noise mixture  $w(t)$  with a reference copy of the transmitted signal  $x(t)$  followed by integration over the duration of the product signal. We have already met correlation operations in connection with Eq. (7), which deals with a complex correlation function. We will return to the question of correlation operations shortly.

### C. The Ambiguity Function $\neq^2$

This matched filtering or correlation detection operation is optimum if the scattering function has the form of an impulse located at the origin. If the impulse-like scattering function is

not at the origin but at the point  $(\tau, f)$ , the output is in general diminished, and the filter must be readjusted by the appropriate frequency offset  $f$  and its output observed  $\tau$  seconds later to restore the condition of optimality.

Suppose we plot the signal output power from a matched filter set for such a point non-fluctuating target at  $\tau = 0$  and  $f = 0$  as a function of delay and doppler misalignments  $\tau$  and  $f$ . The result is the quantity  $\psi^2(\tau, f)$  called the ambiguity function<sup>22,23</sup> (or the uncertainty function, resolution function, or two-dimensional autocorrelation function). More explicitly, the ambiguity function  $\psi^2(\tau, f)$  is defined as simply  $|\mathcal{F}_0(t_0)|^2$ , the square of the envelope of the output  $f_0(t)$  of a matched filter at  $t = t_0$  to an input waveform  $x(t)$  that has been misaligned by a lag of  $\tau$  seconds and an upward shift in frequency  $f$  cycles per second:

$$\psi^2(\tau, f) = |\mathcal{F}_0(t_0)|^2 = \left| \int_{-\infty}^{\infty} x^*(t) x(t + \tau) \exp[j2\pi ft] dt \right|^2 \quad (27)$$

or, alternatively,

$$\psi^2(\tau, f) = \left| \int_{-\infty}^{\infty} G(\varphi) G^*(\varphi + f) \exp[-j2\pi\varphi\tau] d\varphi \right|^2, \quad (28)$$

where  $G(f)$  is the Fourier transform of  $x(t)$ , (i.e.,  $G(f) \leftarrow x(t)$ ). As before,  $t_0$  is the time at which one optimally samples the matched filter output if  $\tau = 0$  and  $f = 0$ . The ambiguity function expresses the ability of a given combination of waveform  $x(t)$  and filter matched to it to discriminate targets in range and doppler. Ambiguity functions for some common sorts of waveforms are shown in Fig. 10.

The ambiguity function has a number of interesting properties. The width in  $\tau$  at  $f = 0$  is roughly the reciprocal of  $W$ , the bandwidth of the signal; and the width in  $f$  at  $\tau = 0$  is roughly the reciprocal of the signal duration  $T$ . If the energy in the signal and the gain of the matched filter are normalized so that

$$\int_{-\infty}^{\infty} |X(f)|^2 df = \int_{-\infty}^{\infty} |M(f)|^2 df = 1,$$

then not only do we find readily from Eq. (27) that the height of the ambiguity surface at the origin is unity

$$\psi^2(0, 0) = 1, \quad (29)$$

but also that the total volume under the surface is invariant to the form of signal,

$$\int_{-\infty}^{\infty} \int_{-\infty}^{\infty} \psi^2(\tau, f) df d\tau = 1. \quad (30)$$

The "invariance" relation [Eq. (30)] is highly significant. The diagrams in Fig. 10 show the ambiguity functions of several types of waveforms. In all cases the height at the origin is unity [Eq. (29)], and the volume is also unity [Eq. (30)]; the difference lies in how this volume is distributed. The first three examples shown concentrate substantially all of the volume in one central peak. Thus, lengthening a simple pulse produces a broadening in delay which would be irrelevant if only the doppler were being measured [Fig. 10(a)]; or narrowing a simple pulse in time [Fig. 10(b)] produces a broadening in frequency which would be irrelevant if one were measuring range only.

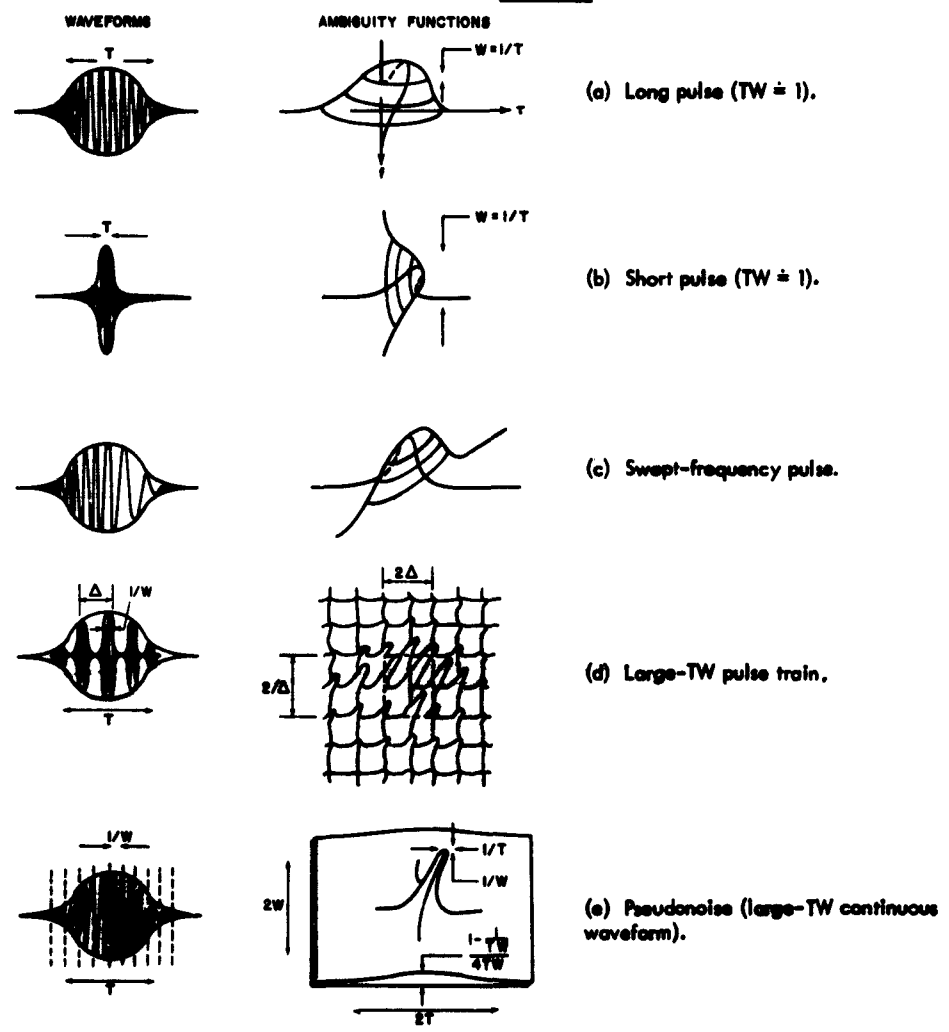


Fig. 10. Ambiguity functions of typical gaussian-shaped pulse waveforms.

The last two examples in the figure represent deliberate efforts to make both dimensions of the central peak small. This allows range and doppler resolution to be obtained simultaneously. In the case of the "large-TW pulse train" [Fig. 10(d)], the rest of the volume goes into subsidiary peaks. For the continuous large-TW waveform or "pseudonoise" waveform [Fig. 10(e)], the volume is mostly in the "skirts" away from the central peak. A great deal of study has been given to ways of making these skirts even, so that there are no large subsidiary peaks (e.g., Ref. 24).

Signals of the type shown in Figs. 10(c) through (e) are useful for another reason besides the availability of simultaneous doppler and range resolution. For a given peak power limitation on the transmitter, these waveforms allow an increase in signal energy  $E_s$  by leaving the transmitter on longer, without a sacrifice in range resolution as would be the case with the waveform in Figs. 9(a) and (b).

In estimating the performance of the various waveforms of Fig. 10 it will be convenient later on to use the crude approximations given in the right-hand diagrams of Fig. 10. There the volume in a given peak is assumed to be concentrated uniformly within the half-power contours, and in the case of the pseudonoise waveform the skirt level is assumed uniform.

#### D. Interaction of the Signal and the Target in Terms of $\sigma$ and $\psi^2$

We have now introduced two functions of delay  $\tau$  and doppler  $f$ , one being the target scattering function  $\sigma(\tau, f)$ , a property of the target only, and the other being the ambiguity function  $\psi^2(\tau, f)$  which describes the transmitted signal independently of target properties. These have been illustrated in Figs. 9 and 10, respectively. We shall now obtain an expression involving these two quantities that shows how a simple matched filter radar system responds to a spread target. This expression<sup>25</sup> is a convolution of  $\sigma$  and  $\psi^2$ . For the more complicated radar systems that provide optimum detectability on spread targets<sup>1</sup> other expressions are obtained, but they, too, are found to take into account the target properties only through the ambiguity function, and to involve the same convolution of  $\tau$  and  $\psi^2$ , as we shall see.

Imagine that we have an ensemble of statistically identical targets. With a transmitted signal of complex envelope  $X(t)$  emerging from the transmitter, a signal  $s(\tau', f') X(t)$  represents the random complex echo signal returning from the elementary region having a span of delays lying between  $\tau'$  and  $\tau' + d\tau'$  seconds, and at the same time having a range of doppler frequency shifts lying between  $f'$  and  $f' + df'$  cycles per second. The target scattering function  $\sigma(\tau', f')$  is defined as

$$\sigma(\tau', f') = \overline{|s(\tau', f')|^2},$$

where the bar represents the ensemble average, and parameters such as range, antenna gain, etc., are normalized out so that  $\sigma(\tau', f')$  is in terms of the number of effective square meters of cross section per second of range increment per cps of doppler increment. That is, one watt per square meter of incident power flux will scatter toward the receiver  $[\sigma(\tau', f') d\tau' df']/4\pi$  watts per steradian of solid angle subtended at the target.<sup>†</sup>

<sup>†</sup> In determining the scattering function of soft targets such as clouds of scatterers, it is useful<sup>26</sup> to consider  $\sigma(\tau', f')$  to be the average cross section of a typical particle times the probability that such a particle will fulfill the condition that the range is in the interval  $\tau'$  to  $\tau' + d\tau'$  and the velocity lies in  $f'$  to  $f' + df'$ .

The easiest way to deduce the effect of the spread target on the radar signal is first to divide the target up into zones having different delays. Suppose we have isolated such a region of the target containing all points lying within a range of path delays  $\tau'$  to  $\tau' + d\tau'$ . We next imagine that the rest of the target is absent and we compute the contribution of this zone to the output of the matched filter. If those regions within the zone that introduce a frequency offset<sup>†</sup> lying in the range  $f'$  to  $f' + df'$  return an echo  $s(\tau', f') \mathcal{X}(t)$ , then the envelope of the output from a filter that is matched to the transmitted waveform (except that the filter is misaligned upward by  $f$  in frequency and the output is observed at  $t = t_0 + \tau$  instead of at  $t = t_0$ ) will be

$$|\mathcal{f}_0(t_0)| = |s(\tau', f')| \left| \int_{-\infty}^{\infty} \mathcal{X}^*(t) \mathcal{X}(t + \tau' - \tau) \exp[j2\pi(f - f')t] dt \right| = \psi(\tau' - \tau, f - f') |s(\tau', f')|$$

since the signal arrives with a total time offset  $(\tau' - \tau)$  and total frequency offset  $(f' - f)$  relative to the values giving maximum filter output. Use has been made of the relation  $|AB| = |A| |B|$  for two complex quantities A and B. The average power  $[P(\tau, f)]_{\tau'}$ , appearing in the output of the filter offset by  $\tau$  and  $f$  due to the entire zone having delay near  $\tau'$  will then be gotten by integrating the average of the square of this quantity over all frequency (contributions at different frequencies always adding as powers, not as voltages):

$$\begin{aligned} [P(\tau, f)]_{\tau'} &= \overline{|\mathcal{f}_0(t_0)|^2} = \int_{-\infty}^{\infty} \psi^2(\tau' - \tau, f - f') |s(\tau', f')|^2 df' \\ &= \int_{-\infty}^{\infty} \psi^2(\tau' - \tau, f - f') \sigma(\tau', f) df' \end{aligned}$$

As a final step, we add up the contributions due to all range zones of the target. If we assume that the echoes from different range elements are uncorrelated;<sup>‡</sup> i.e.,  $|s(\tau'_1, f'_1) s(\tau'_2, f'_2)| = 0$  for all  $\tau'_1 \neq \tau'_2$ , then we can add together the powers returned in the different range intervals to get

$$P(\tau, f) = \int_{-\infty}^{\infty} [P(\tau, f)]_{\tau'} d\tau' = \iint_{-\infty}^{\infty} \psi^2(\tau' - \tau, f - f') \sigma(\tau', f) d\tau' df' \quad (31)$$

Thus the power out of the matched filter as a function of the time and frequency offsets is proportional to the (two-dimensional) convolution of the scattering function with the ambiguity function.<sup>§</sup> Equation (31) says that the process of matched filter reception isolates certain areas

<sup>†</sup> The frequency offset might occur because at the given range there are regions in motion with the appropriate velocity. On the other hand, a frequency spread of the energy returning from a given range could just as easily occur as a result of other physical mechanisms. For example, at a given range there might be a single fixed scatterer whose reflectivity is fluctuating rapidly enough to cause the assumed doppler broadening.

<sup>‡</sup> As noted later at the close of Sec. V-E, it is conceivable that the signal returning from the target in one cell of the  $\tau', f'$  plane might be partially coherent with that appearing in a nearby cell at a later time. In such cases this step cannot strictly be taken. The whole question of such cell-to-cell coherences remains to be studied in the radar astronomy context.

<sup>§</sup> In order to avoid a weighting proportional to the antenna gain pattern, we have implicitly assumed that the antenna beamwidth is much greater than the angle subtended by the target (or equivalently, for targets broader than the beamwidth, extended targets, that the antenna radiates uniformly throughout a certain solid angle, and zero elsewhere). Also, it should be added that whenever the filter and transmission are not matched,  $\psi^2$  is simply replaced by the slightly more general "cross ambiguity function."<sup>27</sup>

of the scattering function. The process can be visualized as a process of overlaying the three-dimensional surface  $\phi^2(\tau, f)$ , the ambiguity function of Fig. 10, onto a similar representation of the scattering function  $\sigma(\tau, f)$  of Fig. 9 (after providing the appropriate  $\tau$  and  $f$  offsets) and then reading off the total volume under the product of these two functions.

Let us now investigate the various forms of receivers that are actually used in radar astronomy work where adequate signal-to-noise ratio is always a problem. As detailed by R. Price in the companion report,<sup>1</sup> in order to build up the signal-to-noise ratio, one usually builds a receiver structure that goes beyond simple matched filtering or simple correlation detection as just discussed in Sec. IV-B.

The matched filter with a sampling of the output voltage at  $t_0$  is appropriate only for a nonfluctuating point target for which one knows target delay  $\tau$  to within a fraction of an RF cycle. Since this means a fraction of a wavelength, in practice, carrier phase is almost always unknown, and so one samples instead the envelope at  $t_0$ . Figure 11(a) shows two alternate versions of the matched filter for known RF phase, the matched filter operation itself (as we have described it in Sec. IV-B), and the correlation detection equivalent (Eq. 26). The matched filter and equivalent correlation detector of Fig. 11(b) are the receivers of Fig. 11(a) suitably modified for optimality when RF phase is unknown. In the case of the matched filter shown on the left, the envelope of the output is sampled, and in the correlation detector shown at the right, the envelope of the (complex) cross correlation of arriving signal  $w(t)$  and transmission  $x(t)$  is observed, rather than only the real part as in Eq. (26). The distinction will be discussed further in the next section.

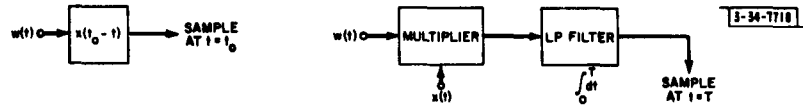
For uniformity with the other more complicated detectors which we are about to discuss, Fig. 11(b) shows the square of the envelope being sampled, not the envelope itself. For a point nonfluctuating target, the output power signal-to-noise ratio is  $(E_s/N_0)^2$  as compared with  $2(E_s/N_0)^2$  available when carrier phase is known exactly. In terms of required signal energy  $E_s$ , the lack of phase knowledge costs 3 db. For a more general form of target, the output power signal-to-noise is

$$\rho_{MF}(\tau, f) = \text{Const} \times \left[ \frac{E_s}{N_0} \iint_{-\infty}^{\infty} \phi^2(\tau' - \tau, f - f') \sigma(\tau', f') d\tau' df' \right]^2 \quad (32)$$

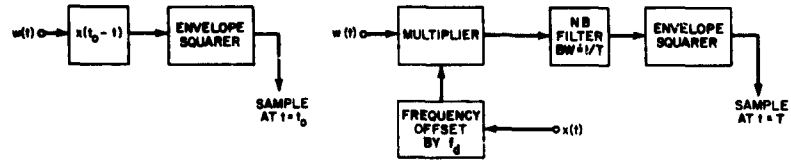
In radar astronomy experiments the duration  $T$  of the transmission is usually very long compared to the received signal fluctuation period  $1/B$ , so that one must regard the target as being a point fluctuating target (spread in frequency  $f$ ), so that its scattering function is

$$\sigma(\tau, f) = \sigma(f) \delta(\tau - \tau')$$

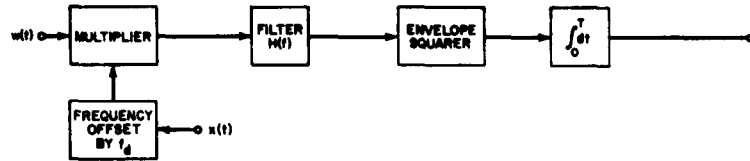
where  $\delta$  is the unit impulse. (The condition  $T \gg 1/B$  is often unavoidable irrespective of the target properties simply because of limits on the achievable frequency stability of the transmitting and receiving conversion stages.) The usual form of receiver is then the one shown in Fig. 11(c), where the received signal  $w(t)$  is premultiplied or "weighted" by a replica of the transmission  $x(t)$  to undo any phase modulation imposed at the transmitter and to accentuate those portions of the received signal  $w(t)$  during which one expects greater amplitude; the weighting is followed by the familiar predetection filtering, rectification, and postdetection integration operations. In the general theory of signal-to-noise ratio optimization developed by Price<sup>1</sup> and summarized here, such a receiver is called a weighted radiometer because the three operations



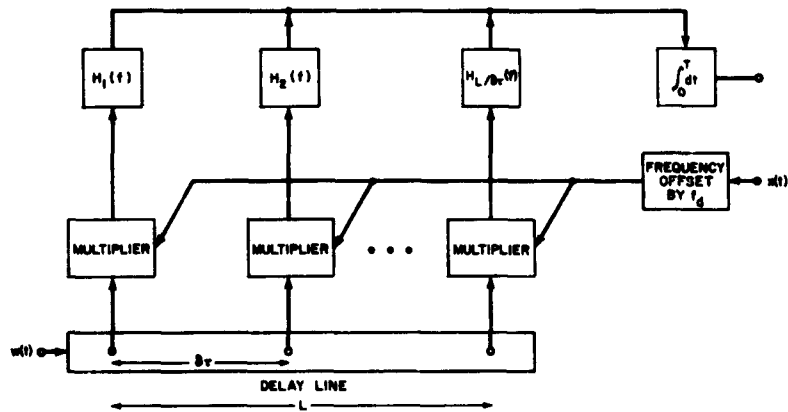
(a) Matched filter (left) and correlation detector (right) for case of known RF phase.



(b) Matched filter (left) and correlation detector (right) for RF phase unknown.



(c) Weighted radiometer, for point fluctuating targets.



(d) Rake receiver, for deep fluctuating targets.

Fig. II. Various signal-to-noise ratio maximizing receivers.

following the weighting are precisely those used in a radiometer such as is employed in radio astronomy to develop maximum signal-to-noise ratio from an incoherent narrow-band source such as the hydrogen line. For maximum signal-to-noise ratio,<sup>†</sup> it turns out that the predetection filter characteristic  $H(f)$  must be chosen to match the power profile of the line, or in our context,

$$|H(f)|^2 = \text{Const} \times \sigma(f) \quad (33)$$

For the general case of a target that may or may not be spread in both  $\tau$  and  $f$ , and for an arbitrary  $H(f)$ , the following expression gives the output signal-to-noise ratio for the weighted radiometer

$$\rho_{WR}(\tau, f) = \text{Const} \times \left\{ \frac{E}{N_0} \int_{-\infty}^{\infty} |H(f' - f)|^2 df' \iint_{-\infty}^{\infty} \psi^2(\tau' - \tau, f' - f'') \sigma(\tau', f'') d\tau' df'' \right\}^2 \quad (34)$$

(As before,  $\tau$  and  $f$  are the offsets inserted in the receiver processing, usually in the timing and frequency shift of the weighting operation.) That is, the convolution appearing in Eqs. (31) and (32) is itself smoothed in turn frequency-wise by the squared magnitude of the predetection filter frequency characteristic  $H$ .

The theory developed in Ref. 1 goes on to say that if the target is significantly spread not only in frequency  $f$  but also in delay  $\tau$  (deep fluctuating target), then the optimum receiver is the rake radiometer of Fig. 11(d), which is obtained, plausibly enough, by iterating the weighted radiometer of Fig. 11(c) at a number of delays successively spaced by a small  $\delta\tau$ , the total range of delays being large enough to at least span  $L$ , the duration in  $\tau$  of the target scattering function. For signal-to-noise ratio maximization, it will turn out that the frequency functions of the predetection filters  $H_i(f) = H(\tau_i, f)$  (where  $\tau_i = \text{some } \tau_0 + i\delta\tau$ ) must obey the condition

$$|H(\tau, f)|^2 = \text{Const} \times \sigma(\tau, f) \quad (35)$$

That is, the filter squared magnitudes, when read off along the succession of delay-line taps (and according to frequency at a given tap) must reproduce the target scattering function. For the more general case of arbitrary  $H(\tau, f)$ , the following expression gives the output signal-to-noise ratio for the rake radiometer:

$$\rho_{RR}(\tau, f) = \text{Const} \times \left\{ \frac{E}{N_0} \iint_{-\infty}^{\infty} |H(\tau' - \tau, f' - f)|^2 d\tau' df' \iint_{-\infty}^{\infty} \psi^2(\tau'' - \tau', f' - f'') \sigma(\tau'', f'') d\tau'' df'' \right\}^2 \quad (36)$$

That is, the original convolution of Eq. (31) undergoes a two-dimensional convolution with the predetection filter power-vs-frequency functions read off in  $\tau$ .

Thus we see that for the entire class of receivers considered to be of value from the signal-to-noise ratio point of view, the convolution Eq. (31) is the central relationship. To see how the two-dimensional convolution operation works out in practice, consider convolving the scattering functions of Fig. 9 with the ambiguity functions of Fig. 10. In probing a target spread in both

<sup>†</sup>As is pointed out in Ref. 1, the results quoted here on the form of receiver that is optimum are strictly true only for the reasonable condition that the receiver input signal-to-noise ratio is smaller than unity in a certain sense.

range and doppler (deep fluctuating target), such as Fig. 9(e) or 9(f), one can resolve the detailed structure of the  $\sigma(\tau, f)$  surface only by using an ambiguity function whose central peak (with lateral dimensions of  $1/W$  by  $1/T$ ) is sufficiently narrow. As we have seen earlier, such studies of hard targets are very interesting because of the simple correspondence between places on the target and places in the  $\tau, f$  plane for the received signal.

However, we are often not interested in measuring the whole scattering function itself but rather certain simpler quantities derivable from it. Two such quantities are the power impulse response  $\sigma(\tau)$  and the echo power spectrum  $\sigma(f)$ . These quantities were briefly alluded to in Secs. II-C and II-D, respectively. (Two further quantities, the echo correlation function and the spaced-frequency correlation function, are described in the next section.) If we are observing a spherical body with uniform surface properties, any one of these four quantities is sufficient to specify the angular spectrum  $\sigma_o(\varphi)$  of the surface (given the diameter and rotation vector), so a measurement of the entire scattering function is not very interesting for such uniform targets. For targets with nonuniform surfaces, measurement of the scattering function is important. Moreover, it is clear that the design of the optimum detectors of Ref. 1 demands as complete a knowledge of the scattering function as can be had.

The quantity  $\sigma(\tau)$ , the power impulse response of the target, is a plot of power as a function of range only, and could be obtained in practice by using simple  $TW \approx 1$  pulses [Fig. 9(b)] of such a wide bandwidth as to resolve all the interesting variations with  $\tau$  of the function  $\sigma(\tau, f)$  and also exceed greatly its frequency width  $B$ . Thus  $\sigma(\tau)$  is defined as follows:

$$\sigma(\tau) = \int_{-\infty}^{\infty} \sigma(\tau, f) df \quad ; \quad (37)$$

and the average power as a function of range for a short pulse<sup>†</sup> will be

$$P(\tau) = \int_{-\infty}^{\infty} \psi^2(\tau - \tau', 0) \sigma(\tau') d\tau' \quad , \quad (38)$$

the  $\tau$ -convolution of  $\sigma(\tau)$  with the  $f = 0$  profile of the pulse ambiguity function. According to Eq. (27), this profile, in turn, is the magnitude of the time autocorrelation of the pulse complex envelope. For a uniform sphere, the power impulse response is given by Eq. (13), discussed earlier.

Similarly, the echo power spectrum  $\sigma(f)$ , defined as

$$\sigma(f) = \int_{-\infty}^{\infty} \sigma(\tau, f) d\tau \quad , \quad (39)$$

can be obtained by using a simple  $TW = 1$  waveform of such a long duration  $T$  [Fig. 9(a)] as to resolve all interesting variations with  $f$  of the function  $\sigma(\tau, f)$ . The average power as a function of frequency offset for a long transmitted pulse is thus

$$P(f) = \int_{-\infty}^{\infty} \psi^2(0, f - f') \sigma(f') df' \quad , \quad (40)$$

<sup>†</sup>One occasionally encounters the term "modulation loss" in the literature on lunar communications techniques (e.g., Ref. 28). This term refers simply to the average received power obtained with the nonzero pulsewidth in use, relative to that which would result if an indefinitely long pulse of the same energy were used, and observed on reception at the most favorable delay value.

the  $f$ -convolution of  $\sigma(f)$  with the  $\tau = 0$  profile of the pulse ambiguity function. Equation (28) says that this profile is the frequency autocorrelation of the spectrum corresponding to the pulse complex envelope. The echo power spectrum of a uniform rough rotating sphere was presented earlier as Eq. (14).

### E. Spaced-Time and Spaced-Frequency Measurements

There is another important way of measuring the distribution of echo power with range and doppler (scattering function) besides that of sending a signal whose ambiguity function probes the scattering function itself. This method involves sending two sinusoids spaced by  $\Delta f$  in frequency and then cross-correlating (as a function of delay  $\Delta\tau$ ) the corresponding received sinusoids. That is, one of the two received randomly varying sinusoids is delayed by  $\Delta\tau$  seconds, readjusted in frequency by the original  $\Delta f$ , and then the two are multiplied together and integrated. (Variations at the carrier rate are ignored, as was done with the ambiguity function.) As an engineering matter the measurement would probably be done most conveniently by passing the two received functions (with one delayed by  $\Delta\tau$ ) into a multiplying device and then measuring the amplitude and phase of the difference-frequency sinusoid produced at frequency  $\Delta f$ , as will be discussed in the next section.

The complex quantity derived in this way,  $\mathcal{R}(\Delta f, \Delta\tau)$ , the two-frequency correlation function, can be shown to be the inverse Fourier transform of  $\sigma(\tau, f)$ , the target scattering function<sup>29</sup>

$$\mathcal{R}(\Delta f, \Delta\tau) = \int_{-\infty}^{\infty} \int_{-\infty}^{\infty} \sigma(\tau, f) \exp[j2\pi(\Delta f\tau + \Delta\tau f)] d\tau df \quad (41)$$

or, using the notation introduced in Sec. II-A,  $\mathcal{R}(\Delta f, \Delta\tau) \implies \sigma(\tau, f)$ .

Setting  $\Delta f = 0$  we find as the echo correlation function  $\mathcal{R}(0, \Delta\tau)$ , which we abbreviate  $\mathcal{R}(\Delta\tau)$ ,

$$\mathcal{R}(\Delta\tau) \implies \sigma(f) \quad , \quad (42)$$

the inverse Fourier transform of the received frequency spectrum  $\sigma(f)$  obtained when a sinusoid is transmitted [Eq. (39)], just as one would expect. Similarly, setting  $\Delta\tau = 0$  we find that the spaced-frequency correlation function  $\mathcal{R}(\Delta f, 0) \equiv \mathcal{R}(\Delta f)$  is

$$\mathcal{R}(\Delta f) \implies \sigma(\tau) \quad , \quad (43)$$

where  $\sigma(\tau)$  is given by Eq. (37). So, referring back to Fig. 9, we expect the maximum  $\Delta\tau$  value for which correlation of the fluctuations is still preserved to be roughly  $1/B$ , the reciprocal of the doppler smear. Also, the maximum frequency separation  $\Delta f$  for which the fluctuations are still correlated is roughly  $1/L$ , the reciprocal of the multipath delay smear.

The three quantities  $\sigma(\tau)$ ,  $\sigma(f)$ , and  $\sigma(\tau, f)$  are all real and positive (since they are powers), but are not, in general, even functions. Therefore, their inverse transforms,  $\mathcal{R}(\Delta f)$ ,  $\mathcal{R}(\Delta\tau)$  and  $\mathcal{R}(\Delta f, \Delta\tau)$ , respectively, will be even functions, but will not, in general, be real. However, if one of the  $\sigma$ 's happens to be even [as would be the case for  $\sigma(f)$  of a rotating uniform sphere] then the corresponding transform  $\mathcal{R}$  will be real.

Figure 12 presents a summary of the interrelations between the scattering function  $\sigma(\tau, f)$ , the two-frequency correlation function  $\mathcal{R}(\Delta f, \Delta\tau)$ , and the four derived quantities  $\sigma(\tau)$ ,  $\sigma(f)$ ,  $\mathcal{R}(\Delta f)$  and  $\mathcal{R}(\Delta\tau)$ . The method of measuring each of these will be summarized presently (in Table I).

The reader may wonder at this point why the scattering function has been singled out as the basic quantity and all the others (including the two-frequency correlation function) spoken of as

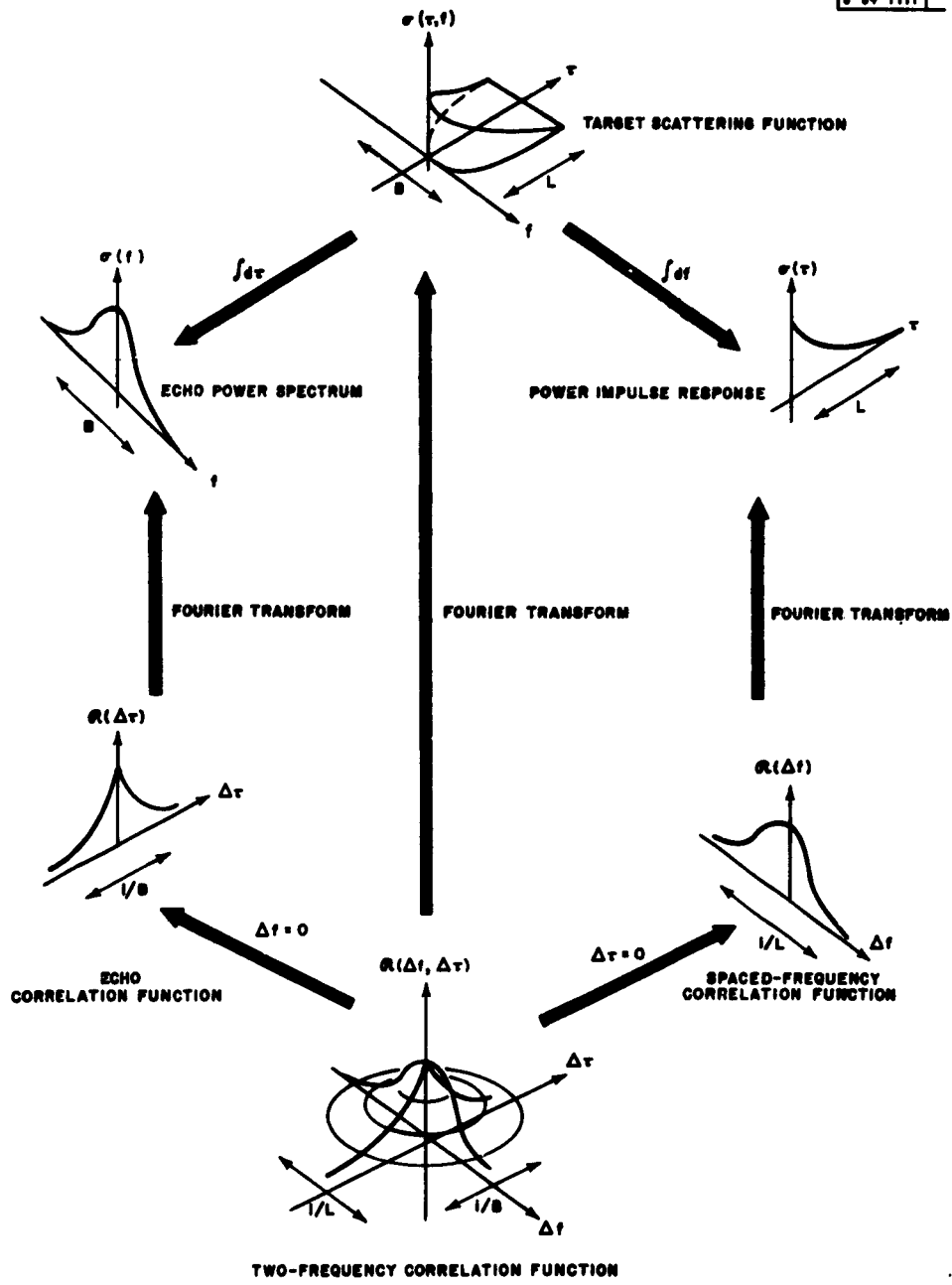


Fig. 12. Summary of the interrelationship of the target scattering function and related quantities. (The quantities  $\mathcal{R}$  can all be complex in general. For clarity they are drawn as positive real quantities.)

TABLE I

Function	Method of Measurement
Power impulse response $\sigma(\tau)$	Average the power vs range ( $\tau$ ) of a large number of short pulses.
Echo power spectrum $\sigma(f)$	Spectral analysis of a long record of the signal received when a sinusoid is transmitted.
Scattering function $\sigma(\tau, f)$	Transmit repeatedly a waveform $x(t)$ with duration $T$ equal to the reciprocal of the desired frequency resolution, and with a bandwidth $W$ equal to the reciprocal of the desired range resolution. At the receiver, either (1) build a filter matched to $x(t)$ and observe average envelope squared of the output at desired values of delay and frequency offsets $f$ and $\tau$ , or (2) use the correlation detection equivalent; i.e., multiply the incoming signal by a replica of the transmission $x(t)$ , except that the replica is offset by $\tau$ in delay and $f + f_d$ in frequency. The product is integrated (in a bandpass filter tuned to $f_d$ ) over the arriving signal duration ( $=T$ ), and the mean square of the envelope of all such integrations is determined. Repeat for other $\tau$ and $f$ settings over the range of $\tau$ and $f$ values covered by the target.
Two-frequency correlation function $\mathcal{R}(\Delta f, \Delta\tau)$ (a complex quantity)	Transmit two sine waves of known spacing $\Delta f$ . Arrange to receive the two sinusoids separately; insert a delay $\Delta\tau$ in one, and measure average amplitude and phase of the difference-frequency tone (at frequency $\Delta f$ ) generated by passing the two into a mixer (multiplier). Repeat for other values of $\Delta f$ and $\Delta\tau$ . (Phase is measured relative to that which would result from a point target observed with the $\Delta f$ in use.) The averaging of phase and amplitude of the difference-frequency tone is done by passing the mixer output into a narrow-band filter tuned to $\Delta f$ .
Spaced frequency correlation function $\mathcal{R}(\Delta f)$ (complex)	Same as above except use zero relative delay $\Delta\tau$ .
Echo correlation function $\mathcal{R}(\Delta\tau)$ (complex)	Transmit a single sinusoid. Pass received signal into one input of mixer and also into the other mixer input, but with a delay of $\Delta\tau$ and a frequency offset of some $f_d$ . Examine average amplitude and phase of mixer output at $f_d$ .

being derivative from it. Measurement of the entire target scattering function  $\sigma(\tau, f)$  itself [or equivalently,  $\mathcal{G}(\Delta f, \Delta\tau)$ ] may not be very interesting in some circumstances (notably where the target is uniform). However, by starting our presentation with this basic quantity and then discussing the five derived functions, a more unified presentation has been possible. And more important, as we have seen from our earlier discussion of hard targets, features in the scattering function  $\sigma$  may be associated directly with physical features on the object; this direct connection is not available with the correlation function  $\mathcal{G}$ .

However, in certain circumstances, the two-frequency method leading to  $\mathcal{G}$  might be preferable; the scattering function can then be obtained by Fourier transformation. The choice of method of observation depends on the characteristics of the transmitter (e.g., how it is limited in power and amplitude form factor of the exciting signal) and receiver signal processing equipment (e.g., how many variables of what fluctuation rate can be operated upon simultaneously).

#### F. Some Equipment Problems

It is now time to deal in more explicit detail with methods of implementing some of the operations we have discussed. In radar astronomy practice, the choice between matched filtering and the equivalent correlation detection is usually decided in favor of the latter. For certain simple waveforms like a single square pulse it often pays to synthesize a filter having approximately the desired response.<sup>30</sup> However, for waveforms with large time-bandwidth products, only rarely<sup>31,32</sup> does it pay to synthesize a filter with such a response in preference to simply generating the waveform and using it in a correlation device.

So at this point we will focus our attention on the practical problems of doing the cross-correlation operation, with particular attention to the implications of the statement that the desired cross-correlation function is sometimes a complex quantity. We have met the complex correlation function of signals at spaced antennas ( $\mathcal{Z}$ ) and at spaced frequencies ( $\mathcal{G}$ ); we shall presently discuss a similar correlation function in connection with polarimetric observations.

First we must explain the operation depicted in Fig. 11(b). It is well known that when the target is a point nonfluctuating target and carrier phase is unknown, detectability is maximized by observing the envelope of the (complex) cross correlation of  $w(t)$ , the incoming signal, and the transmission  $x(t)$ . A straight multiplication of  $w(t)$  and  $x(t)$  followed by integration will produce a number  $f_0(t_1)$  of Eq. (26) which is the real part of the correlation, and so will the matched filtering-plus-sampling operation. But the desired envelope  $|\mathcal{F}_0(t_1)| = |\hat{f}_0(t_1)|$  is the square root of the sum of squares of this quantity  $f_0(t_1) = \text{Re} \{ \mathcal{F}_0(t_1) \}$  and its Hilbert transform,  $\text{Im} \{ \mathcal{F}_0(t_1) \}$ , and we have no way of observing anything but the former for the schemes described in Fig. 11(a). However, as the reader may recall from a statement made in the introduction to this report, if we can somehow contrive to make the correlator output  $f_0(t_1)$  a bandpass function, then  $\text{Im} \{ \mathcal{F}_0(t_1) \}$  is observable as the quadrature component of this output. And this is easily done by frequency-offsetting either  $w(t)$  or  $x(t)$  by an amount  $f_d$ , doing the integration in a narrow bandpass filter tuned to  $f_d$ , instead of the low-pass filter implied by the integral sign, and finally examining the in-phase and quadrature components of the  $f_d$  tone appearing at filter output at time  $t_1$ . The in-phase and quadrature components are  $\text{Re} \{ \mathcal{F}_0(t_1) \}$  and  $\text{Im} \{ \mathcal{F}_0(t_1) \}$ , respectively, and the desired  $|\mathcal{F}_0(t_1)|$  is of course the envelope of the tone observed at  $t_1$ .

Such a device is called a bandpass correlator,<sup>33</sup> and is not only capable of providing the correlation function, its Hilbert transform and its envelope, but is also much simpler to build than the straight correlator indicated at the right in Fig. 11(a), for which the integrator is a

low-pass rather than bandpass filter. The true correlator requires an accurate multiplier of wide dynamic range and low zero-drift, and the integrator (low-pass filter) must be built with small DC zero drift. With the bandpass correlator the multiplier can be such a simple element as a mixer tube biased to minimize undesired intermodulation products at frequency  $f_d$ , and the integrator can be any form of narrow-band element, for example, a quartz crystal filter.

As for the matched filter equivalent shown at the left in Fig. 11(b), the observation of the envelope at  $t_1$  is done by building the filter at bandpass (and without a frequency offset), and observing the envelope of the output time function in the neighborhood of  $t_1$ .

The envelope detection that follows either the bandpass correlator or matched filter can be performed by using the usual combination of diode and RC circuit to follow the crests of the sinusoidal tone. At high output signal-to-noise ratios this registers the envelope exactly.

The correlation function expressions presented in this report have involved infinite time averages, an obviously academic restriction. In actual practice, not only is the duration of the experiment finite, but the phenomenon being observed may not persist for very long. Moreover, lack of complete equipment phase stability over a long period may make it difficult to separate the real and imaginary parts of the correlator output by in-phase and quadrature-phase detection over more than just a local portion of the experiment. That is, the integrating filter can be no narrower than the reciprocal of the stability time of the conversion equipment.

The effect of noninfinite integration time is to introduce noise of two kinds into the correlator output. The additive noise that is picked up by the receiving antenna and also generated in the receiver front end will not be integrated out completely. Also, since the processes being cross-correlated are noise-like fluctuations (usually gaussian), the output resulting from a noninfinite integration time will not converge to the true value. The fluctuation about the true value due to finite integration time is classed as self-noise, a term describing any fluctuation components in the output that do not go to zero as the additive noise is removed. The effect of finite-time integration in bandpass correlators using filters of arbitrary shape has been discussed in Ref. 33.

Often the integration time provided by the methodology just outlined is not enough to produce an adequately high output signal-to-noise ratio. One must then resort to postdetection integration; i. e., integration of the output of the bandpass correlator after envelope detection (which of course destroys the resolution into in-phase and quadrature components). Figure 11(c) shows how in the weighted radiometer the detectability of a point fluctuating target is maximized by in effect following a bandpass correlator (with integration time equal to the fluctuation period  $1/B$  of the target) with a postdetection integration of the squared envelope.

Often it is desirable to use a linear envelope detector rather than a square-law envelope detector in systems like the weighted radiometer. The only effect of this is a small reduction of about 0.2 db in the postdetection output signal-to-noise ratio.<sup>34</sup>

Another artifice that is sometimes resorted to in practice, and one that has more serious consequences, is the cross correlation of the envelopes of two signals instead of the signals themselves. This has been done, for example, with interferometry because of the difficulty of transmitting the two signals to the multiplier point with the phase relations still preserved. If the two signals are gaussian and  $S(\tau)$  is the complex cross-correlation function (normalized to the product of the two powers), then the (real) cross-correlation function of the two envelopes  $\varphi_{ENV}$  is a function of the envelope of  $S$  only<sup>35</sup>

$$\varphi_{\text{ENV}}(\tau) = \text{Const} \times [2E(|S|) - (1 - |S|^2) K(|S|)] = \text{Const} \times \left[ |S|^2 + \frac{|S|^4}{16} + \frac{|S|^6}{64} + \dots \right],$$

where E and K are elliptic integrals. Since  $|S| \ll 1$ ,  $\varphi_{\text{ENV}}$  always differs from  $|S(\tau)|^2$  by less than 6 percent. However, only the magnitude of the complex correlation function is preserved, and also there is clearly a serious loss in signal-to-noise ratio whenever such a nonlinear operation as envelope detection is carried out on a weak signal mixed with noise. Specifically, if the signal-to-noise ratio  $\rho$  of one member of the pair is less than unity, then after the envelope detection the signal-to-noise ratio of that member will be  $\rho^2$ . This is the well-known weak-signal-suppression effect (see, e.g., Davenport and Root<sup>36</sup>).

The methods of instrumenting measurements of  $\sigma(\tau, f)$  and related quantities are summarized in Table I, which supplements Fig. 12 by giving a short recipe for the measurement of the target scattering function  $\sigma(\tau, f)$  and the five derived quantities  $\mathcal{R}(\Delta f, \Delta\tau)$ ,  $\mathcal{R}(\Delta f)$ ,  $\mathcal{R}(\Delta\tau)$ ,  $\sigma(f)$  and  $\sigma(\tau)$ .

### G. Interferometry

In Sec. II-D it was pointed out that by computing  $Z(\vec{d}, \Delta\tau)$ , the cross correlation of spaced antenna outputs, it was possible to determine the strip-integrated brightness distribution, or what is equivalent to it for a uniform sphere, the echo power spectrum. Moreover, it was shown that measurements on ground pattern velocity could be made by determining the value of  $\Delta\tau$  giving maximum cross correlation for a given spacing  $\vec{d}$ . The ground plane was assumed to be perpendicular to the line of sight.

We now touch briefly on some of the methodology involved in using radio interferometers to study the received signal. The value of radar interferometric measurements for radar astronomy was first pointed out by Manasse,<sup>37</sup> who suggested interferometric methods of studying surface roughness and rotation vector. Here we will mention a few of the characteristics of interferometers and defer until Sec. V-D and V-F a discussion of the specific experiments proposed by Manasse.

In actually carrying out interferometer measurements the stations will not, in general, lie on the plane perpendicular to the line of sight; therefore, an obvious projective correction is necessary. As long as the station separation as projected along the line of sight is not an appreciable fraction of the wavelength in space of the modulation bandwidth, the results of Sec. II-D still apply. (That is, the attempted range resolution of the modulation must not exceed the range difference of the two stations.) This condition will be fulfilled until radar range resolution of, say, several tens of miles or less is attempted. Let us then refer to  $\vec{d}$  as the actual physical baseline as projected on this perpendicular plane.

The fact that the baseline orientation changes as the earth rotates can be used to advantage. In Sec. II-D it was pointed out that the behavior of the correlation  $Z$  is interestingly different when the baseline  $\vec{d}$  is chosen to lie in different directions. In practice, provided opportunities to observe are sufficiently frequent, it may not be necessary to build more than a two-station interferometer since different directions and magnitudes of  $\vec{d}$  become available as the earth presents different aspects.

The directivity pattern of any antenna system is, of course, the Fourier transform of its aperture distribution (as we have seen in regarding the distant target as a transmitting antenna). By reciprocity, the same thing holds true for the interferometer, as for any receiving antenna the outputs of whose elements are combined coherently. Thus, it is easy to visualize why the interferometer output  $|Z|$  drops as the spacing in wavelengths increases by more than  $R/D$ ,

where R is the target range and D is the diameter of the central patch of the brightness distribution in which most of the reflected power is concentrated. The power will drop as the width of the antenna lobe becomes narrower than D because of phase cancellation (contributions from alternate lobes combine in antiphase).

Another fact that can be easily visualized using this Fourier transform way of looking at the directivity pattern is that for planetary radar astronomy experiments we can neglect the finite size of the individual antennas and regard them as point receivers, a condition we have been assuming throughout Secs. II-A and II-D. The planets subtend angles of about one minute of arc at most, and until the individual elements making up the interferometer attain this order of beamwidth the nonzero size can be neglected. The sun and moon, with their one-half degree angular widths, do require antenna widths to be taken into account.

A unified discussion, using the Fourier transform picture, of the effects of nonzero element size is given in papers by Bracewell,<sup>38,39</sup> whose treatment also allows for such variations in realization as multielement interferometers and "crosses," phase-switching techniques, and the fact that one may not be measuring  $Z$  (both in-phase and quadrature components) but only  $\text{Re}(Z)$ .

In practice, the complex quantity  $Z$  would appear as a difference-frequency sinusoid (of frequency  $f_d$ ) generated by offsetting the local oscillator injections of one of the two receivers by  $f_d$ ; the in-phase and quadrature components of this sine wave then correspond to  $\text{Re}(Z)$  and  $\text{Im}(Z)$ . Gehrels and Parsons<sup>40</sup> have described the construction and use of an interferometer which is associated with the Millstone Hill radar and which has a sufficiently long baseline for planetary studies. The necessary phase identity of the two local oscillator injections is obtained by using a special line-of-sight radio link between stations.

## H. Polarimetry

The object of a radar experiment using polarimetry will usually be to measure total Faraday rotation  $\chi = \chi_0 + \Delta\chi$  of a soft ionized target [ $\chi_0$  is the polarization orientation in the absence of the ionization and  $\Delta\chi$  is given by Eq. (20)] or the degree of polarization  $m$  of the echo from a hard target, or perhaps both for a hard target echo passing through an ionized region. As mentioned in Sec. II-E, there are several schemes in use for specifying the polarization of an electromagnetic signal, for example the Stokes vector, Eq. (46). For radar astronomy the problem of measuring any or all of the four parameters of the Stokes vector does not differ appreciably from the radio astronomy case, and there is a fairly large literature available on such radio polarimetry instrumentation. The reader is therefore referred to the survey paper by Cohen,<sup>10</sup> which discusses both theory and technique in some detail.

For example, if the receiving antenna structure consists of two elements responding to left-circular and right-circular polarization, the four Stokes parameters are given by

$$\begin{aligned}
 I &= \langle |V_L|^2 \rangle + \langle |V_R|^2 \rangle = P_L + P_R \quad , \\
 Q &= 2 \text{Re} \langle V_L V_R^* \rangle = 2A \cos \gamma \quad , \\
 U &= 2 \text{Im} \langle V_L V_R^* \rangle = 2A \sin \gamma \quad , \\
 V &= \langle |V_L|^2 \rangle - \langle |V_R|^2 \rangle = P_L - P_R \quad .
 \end{aligned}
 \tag{44}$$

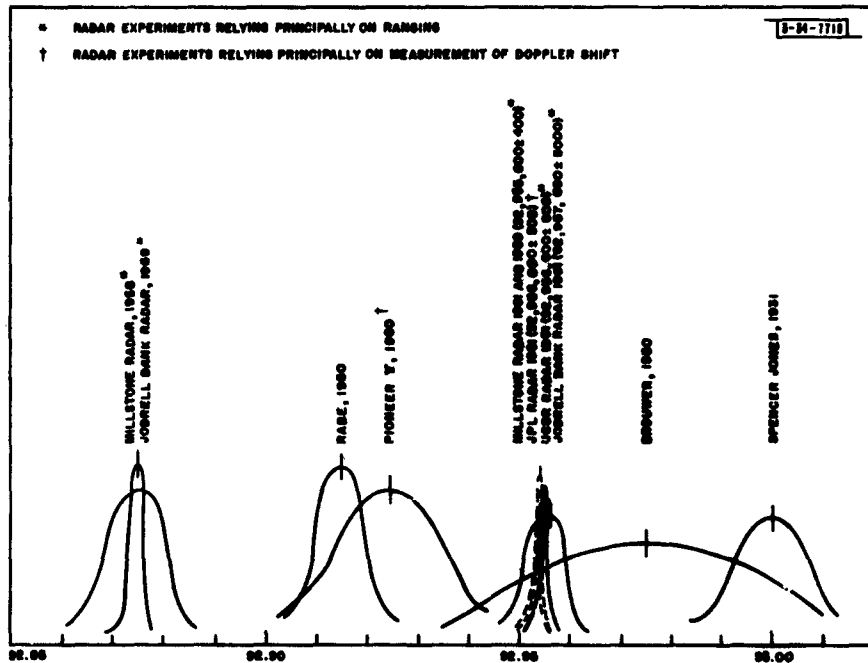


Fig. 13. Various proposed values of the Astronomical Unit in millions of statute miles (as of October 1962).

The two quantities appearing in the equations for I and V are the average powers of the two antenna outputs. The quantity  $\langle V_L V_R^* \rangle$  is the cross correlation of the two outputs, and can be obtained in practice by passing the two antenna outputs into the two inputs of a mixer after first frequency-offsetting one of the two by  $f_d$ ; the output tone at frequency  $f_d$  is then averaged. This tone will have an average amplitude and phase denoted above by A and  $\gamma$ , respectively. In practice the averaging interval would not be infinite as implied by the abbreviation  $\langle \rangle$ , partly because it may be desirable to study the slow time variations in the Stokes vector, in particular the quantities Q and U which place in evidence the angle  $\chi$ . If the degree of polarization m is the only interesting quantity and one is not trying in addition to follow slow variations of  $\chi$  in Fig. 7, then the averaging interval can be extended.

Note from Eq. (18) that the degree of polarization m is not given simply by  $(P_L - P_R)/(P_L + P_R)$  unless one can be sure that the right- and left-hand received signals are uncorrelated so that  $Q = U = 0$ . In practical terms this means that in order to determine the depolarization introduced by a target, one must use a true polarimeter which preserves the relative phases of the two received signals, rather than working only with the powers of the two received component signals. The expression  $(P_L - P_R)/(P_L + P_R)$  gives a lower bound on m.

## V. MEASURING QUANTITIES OF ASTRONOMICAL INTEREST

It is time now to take the material on the effects of target properties on the electromagnetic signal (Secs. II and III) and turn the question around to inquire what astronomically interesting target properties can be deduced from the received echo.

### A. Ranging

The measurement of interplanetary distances and their various order time derivatives is, of course, a central astronomical problem. The basic yardstick of the solar system is the Astronomical Unit (a. u.) — the mean radius of the earth's orbit — whose accuracy has been subject to steady refinement by optical means over a period of several centuries. Knowledge of the position of bodies in the solar system to one part in at least  $10^6$  is presently possible, so long as the results are expressed in terms of the a. u. (At present  $10^{-6}$  represents the accuracy with which free-space light velocity is known.) However, for some years various attempted measurements of this distance spread over a range of about a part in  $10^3$ . The extent of this disagreement is evident from Fig. 13, which lists various suggested values of the a. u. The difficulty lies partly in the fact that all previous nonradar methods of fixing the size of the a. u. depended on measurements of angle, and thus, by virtue of the short baseline obtainable on the earth and because of atmospheric refraction, were likely to be permanently limited to about this order of precision. Recently, measurement of the orbit of a deep space probe with a radar repeater aboard has been employed<sup>41</sup> (see the value labeled "Pioneer V" in Fig. 13). Figure 13 also shows the results of several Venus radar experiments. The experiments labeled with an asterisk used the time of flight to deduce the a. u.; those labeled with a dagger employed doppler shift (next section). Recent radar range measurements<sup>42,43,44,45</sup> of the a. u. agree within several parts in  $10^5$ .

As radar sensitivity improves, more subtle things are being sought in interplanetary distance measurements. In addition to providing refinement of the single quantity embodied in the a. u., it is possible to use radar data to refine the orbital elements of various bodies<sup>46,47,48</sup> so that previously undiscernible effects may be measured, for example the effect of higher order

perturbations due to other planets. Among the interesting things to look for in the future are the relativistic perihelion motion of an eccentric-orbit planet such as Mars, the depth below the cloud cover of Venus' reflecting surface, and other quantities. If a given planet has an appreciably dense ionosphere, then the retardation effects discussed in Sec. III-B will impair the accurate measurement of range, unless one has some knowledge of the target ionosphere density.

From the discussion in Sec. IV-D, it is clear that to measure the range, one uses a waveform with as great a bandwidth  $W$  as possible. The accuracy of the measurement depends on  $W$  and the signal-to-noise ratio as will be discussed quantitatively in Sec. VI-B.

### B. Velocity

Precise measurements of the velocity of a planet can also serve to provide a determination of the a. u. and this technique was recently employed on Venus.<sup>45</sup> The accuracy goes up with the ratio of total relative velocity between earth and target and the frequency resolution of the system. A slight disadvantage of this method over direct ranging is that the required velocity accuracy increases when the body is closest to the earth (since the total relative velocity is a minimum at this time) and yet this may be the only time when the object is detectable.

Clearly, to measure the velocity most accurately one uses a waveform with as great a duration  $T$  as possible. The accuracy of the measurement depends on  $T$  and signal-to-noise ratio, as will be discussed in Sec. VI-B.

### C. Planetary Radius

Radar measurement of the radius of a target planet or satellite is not of pressing interest, since usually this quantity is already known optically. To measure target radius from the total extent of  $\sigma(r)$  or  $\sigma(f)$  is unpromising, since the energy returned from the limb will be very small because of a grazing incidence of the line of sight from the radar, and will thus usually be buried in noise.

It is worthwhile to recall, however, that a measurement of the target scattering function of a hard target gives information on shape and size. As Fig. 4(b) shows, with proper normalization of the frequency axis, nonzero values of the scattering function in the  $r, f$  plane occupy a region that reproduces the shape of the target body, as viewed from the side. Therefore the radius of a spherical planet can be determined from the high signal-to-noise ratio portions of the observed scattering function (independently of knowledge of rotation vector and thus doppler width) by fitting an ellipse to the perimeter of observed nonzero values of received power in the  $r, f$  plane and reading off the length of the  $r$  semiaxis.

In what follows, we shall assume that the planetary radius  $a$  is one of the known quantities.

### D. Radar Angular Spectrum of a Uniform Hard Target

The link between the detailed character of a portion of the rough surface of the target and the received signal is the radar angular power spectrum  $\sigma_\theta$  of that portion. As we saw in Sec. II-A, the angular power spectrum expresses the statistical character of the corrugations of phase, amplitude and vector direction of the electromagnetic signal returning from a plane region near to the surface of the target on which a plane wave is incident. One of the most useful types of observation of hard targets to be made by radar is the determination of the angular power spectrum for different surface regions.

The astronomical significance of radar information on the target surface is obvious. Indeed, it is interesting to note how significant the radar observations on the moon have turned out to be considering the moon's accessibility to optical observation.

If the spherical surface can be assumed uniform [i.e.,  $\sigma_0(\varphi)$  the same everywhere], then determination of  $\sigma_0$  is straightforward. A narrow-pulse experiment to determine the power impulse response  $\sigma(\tau)$  [Eq. (37)] gives  $\sigma_0(\varphi)$  directly by the inverse of Eq. (13),

$$\sigma_0(\varphi) = \frac{1}{\pi a c} \sigma\left(\frac{2a}{c} \cos \varphi\right) \quad (45)$$

In practice, as a result of nonzero pulse width one will actually observe not  $\sigma(\tau)$  but  $P(\tau)$  of Eq. (38).

This short-pulse method of determining  $\sigma(\tau)$  is probably the simplest method of all. A mathematically almost equivalent method is to measure the correlation between sinusoids spaced by  $\Delta f$  as a function of  $\Delta f$ . This gives  $\mathcal{R}(\Delta f)$ , which then can be Fourier transformed to give  $\sigma(\tau)$ , provided one has been able to measure the complex  $\mathcal{R}$  and not simply the magnitude.

Obviously  $\sigma_0(\varphi)$  can also be obtained from a measurement of the echo power spectrum  $\sigma(f)$  [Eq. (39)], since the two are uniquely related by the integral equation (14) (where the projected rotation speed  $\Omega \cos \alpha$  is known). Determination of  $\sigma(f)$  is accomplished by determining  $P(f)$  [Eq. (40)] from the received version of a long pulse of sine wave either by direct spectral analysis or by determination of  $\mathcal{R}(\Delta\tau)$ , the echo correlation function, followed by Fourier transformation. Taking this data on  $\sigma(f)$  is simple enough, but the inversion of (14) is more tedious than solving Eq. (45) for the short-pulse method. The inversion to Eq. (14) is<sup>49</sup>

$$\begin{aligned} \sigma_0(\varphi) \propto \frac{1}{2\pi} \cos \varphi \int_{\sqrt{a^2 - (c\tau/2)^2}}^{\infty} & \left[ \left( \frac{fc}{2f_0 \Omega \cos \alpha} \right)^2 - a^2 + \left( \frac{c\tau}{2} \right)^2 \right]^{-1/2} \\ & \times \frac{\partial}{\partial f} \left[ \sigma \left( \frac{fc}{2f_0 \Omega \cos \alpha} \right) \right] df \quad (46) \end{aligned}$$

It is worth pointing out that if the target is a uniform sphere, all four of these measurements [ $\sigma(\tau)$ ,  $\sigma(f)$ ,  $\mathcal{R}(\Delta f)$  and  $\mathcal{R}(\Delta\tau)$ ] are mutually redundant. That is, any one of them suffices (if  $a$  and  $\Omega \cos \alpha$  are known) to uniquely specify the scattering function  $\sigma(\tau, f)$  or, equivalently, the correlation function  $\mathcal{R}(\Delta f, \Delta\tau)$ . This is clear from the development of Appendix B in which it is shown that the angular power spectrum, target radius and projected rotation speed completely define the target scattering function if the sphere is uniform.

A fifth method of measuring  $\sigma_0(\varphi)$  is the interferometer method<sup>37</sup> of correlating the output of spaced receivers separated by distance  $\vec{d}$  and with relative delay  $\Delta\tau = 0$  to give  $Z(\vec{d}, 0)$  as in Sec. II-D and Fig. 6(b). If the target is uniform, then the brightness distribution  $P(x, y)$  of Fig. 3(b), will be circularly symmetric and  $Z$  becomes independent of the orientation of  $\vec{d}$ . That is,  $Z(\vec{d}, 0) = Z(d, 0)$ . Repeating the measurement at a number of spacings to get  $Z(d, 0)$  will give the brightness distribution  $|E|^2 = P(x, y)$  of Eq. (7) and thence  $\sigma_0(\varphi)$  from Eq. (8). However, one does not need to go to all the trouble of using variable spacing, because the variable  $\Delta\tau$  is available. The echo power spectrum  $\sigma(f)$  at a single station is the inverse Fourier transform of the echo correlation function  $\mathcal{R}(\Delta\tau)$ , which is recognized to be none other than  $Z(0, \Delta\tau)$ . Thus, Manasse suggests that measurement of the power spectrum of the signal received at a single

station gives the desired radar angular spectrum  $\sigma_0(\varphi)$  through Eq. (46) unless perchance one does not know the projected rotation rate  $\Omega \cos \alpha$ , which is a scale factor on the bandwidth of  $\sigma(\Omega)$ , in which case determination of  $Z(d, \Delta r)$  for a single value of  $d$  resolves this scale factor. That is, both  $\sigma_0(\varphi)$  and  $\Omega \cos \alpha$  can be determined by a cross correlation between outputs of two stations plus an autocorrelation at one of them. The experiment gives, then, information about surface roughness and rotation vector. We shall say more about measurement of the rotation vector  $\vec{\Omega}$  in Sec. V-F.

The surface roughness of a hard target can also be inferred grossly from measurement of the degree of polarization  $m$  of the returning echo signal, as was mentioned in Sec. II-E. This type of measurement has been made on Venus.<sup>50</sup>

In case the body can be regarded as composed partly of an ideally smooth and specularly reflecting material and partly of rough material, the amplitude probability density distribution affords a crude method of deducing the ratio of powers due to the two components.<sup>51</sup> For a completely specular smooth surface, the received signal would not fade at all but would maintain a constant value. A rough surface will produce a gaussian distribution of voltages about a zero mean (i.e., a Rayleigh distribution of the envelope). In-between cases give an intermediate density distribution.<sup>52</sup> This first-order statistic is relatively useless compared to the second-order quantities we have been discussing, since it is relatively insensitive to the ratio of specular and scattered power and this ratio would thus be quite difficult to measure accurately with noise present.

#### E. Isolating Individual Surface Features

A more realistic model of the surfaces of planets and the moon is achieved by assuming that they are not uniform in surface properties. Ideally one would like to resolve individual surface regions and, by studying them at different aspect angles  $\varphi$ , learn something about their specific nature through determination of their angular spectra  $\sigma_0(\varphi)$ ; thence, using the theories discussed in Ref. 3, one could decide on reasonable physical models for the terrain features. One might also study the polarization properties and the amplitude probability distribution of returns from isolated regions.

The most obvious approach is to point a sufficiently narrow antenna beam at the region in question, but this requires such enormous antenna gains as to appear unpromising at the moment, except in the case of the moon or sun, where it is only now becoming possible to resolve to several tenths of a target diameter.

Interferometry next suggests itself, but if the interferometer consists of only a pair of antennas with fixed spacing to give the desired resolution, the echoes picked up in the undesired lobes render the received data too noisy to isolate a given target feature. Two measures are then possible: (1) the original element spacing  $d$  is filled with  $n - 1$  other equispaced antennas, whereupon there is only one major lobe every  $n\lambda/2d$  radians instead of every  $\lambda/2d$ , as would be the case with only two elements; or (2) many interferometer records are made, using many different spacings, so that the results may be combined to give a Fourier synthesis of the distribution of power over the target ("aperture synthesis"). The two schemes are roughly equivalent.

However, it is really not necessary to go to all this trouble, at least for hard targets, because the variables time delay and doppler offset provide isolation of various surface regions, as was discussed in Secs. II-C and II-D. This mapping property gives a simple geometrical

correspondence between points on the target and regions in the  $\tau, f$  plane of the target scattering function  $\sigma(\tau, f)$ . That is, energy returning with a certain doppler shift and time delay imposed on it could only have come from certain places on the target surface. To isolate the pair of points heavily shaded on the surface of Fig. 4(a), one uses a transmitted waveform  $x(t)$  of duration  $T$  and bandwidth  $W$  such that the ambiguity function  $\phi^2$  has the desired frequency width  $1/T$  and range width  $1/W$ ; observation of the power received at the appropriate value of delay  $\tau$  and with the proper doppler offset  $f$  then ensures the desired isolation.<sup>†</sup> In order to be able to average a number of readings of power in the  $\tau$ - $f$  cell  $1/T \times 1/W$  in size, the transmission should be repeated many times (see Sec. VI-D).

It remains to resolve the twofold ambiguity between the pair of points in Fig. 4(a). This can be done by repeating the measurement at a time when the apparent rotation axis orients differently relative to the observer. Or, spaced receivers will allow an interferometer null to be laid onto one of the two regions unless, fortuitously, the baseline lies perpendicular to the ground projection of the polar axis.<sup>‡</sup>

The range-doppler mapping technique has been used by Pettengill in investigating the character of the lunar surface,<sup>8,9</sup> and a preliminary such observation on Venus has been reported by Smith.<sup>48</sup>

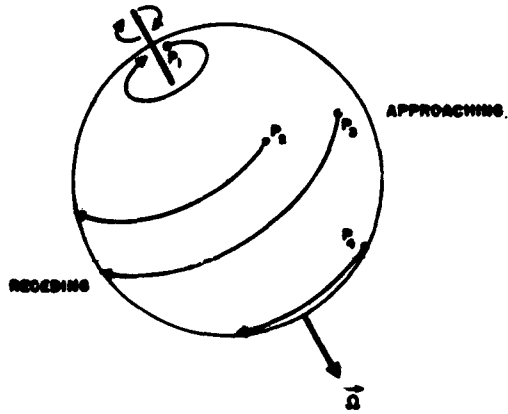
So far we have discussed isolation of a fixed region on the body by examining that part of the return arriving in the neighborhood of fixed values of range  $\tau$  and doppler  $f$ . Actually, as the body rotates, the return associated with a given target feature lies at different places in the range-doppler plane as time progresses. That is, there will be a characteristic trajectory or range-doppler history through the  $\tau$ - $f$  plane which will be followed by the echoes from each point on the target as time progresses. In the spherical case, these trajectories are unambiguous with one another, unless the polar axis happens to lie perpendicular to the radar line of sight, whereupon there is still the twofold ambiguity just referred to. In Fig. 14 are sketched the trajectories of several points on a typical spherical surface.

Knowing the range-doppler history of a given point on the target, one can process returns taken at different times during a rotation period and build up at least a partial picture of  $\sigma_0(\theta)$ , the radar reflectivity as a function of incidence angle. It should be possible also to use this correspondence to build up the signal-to-noise ratio and also the degree of range-doppler resolution (i.e., the fineness of the "resolution cells" of the range-doppler map). Roughly speaking, both these quantities increase with increased observing time on a given return. An ingenious ground-mapping radar using just these range-doppler histories has been built by Cutrona, et al.<sup>53</sup> Because there is one trajectory for each of many thousands of observed target points, techniques of parallel processing of thousands of hypotheses were necessary in this equipment. Two-dimensional optical methods were chosen and developed to a high degree. This sort of parallel processing warrants much further investigation for radar astronomical mapping and also for some of the other less elaborate signal processing procedures we have discussed.

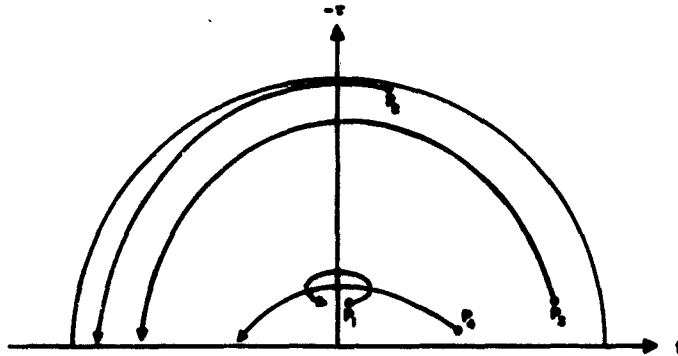
The possibility that the echo in one range-doppler cell will be correlated with that in another cell after a suitable time delay (and possibly a frequency shift) means that certain previous

<sup>†</sup> Provided the target is not overspread, as will be discussed in Sec. VI-D.

<sup>‡</sup> Expressed in terms of voltage, the nulls are narrower than the peaks because the pattern has the character of the magnitude of a sinusoid. Complete suppression would result then only for very small resolution cells. But this requires large bandwidths, which itself causes a filling-in of the null, unless the center frequency is sufficiently high.



(a) Head-on view.



(b) Range-doppler plane.

Fig. 14. Trajectories through the  $r$ - $f$  plane (range-doppler histories) of the echoes from four points,  $P_1$  through  $P_4$ , on a spherical surface.

assumptions may ultimately have to be re-examined. As pointed out in the footnote preceding Eq. (31), the scattering function  $\sigma(\tau, f)$  then no longer suffices to completely specify the echo behavior and one must extend the definition of this function to take into account these "cell-to-cell coherences." Measurement techniques of astronomical interest that take these coherences into account (as does the ground-mapping radar just referred to) await a systematic investigation. Likewise, not much is known about the effect on signal detectability of cell-to-cell coherences, although Kailath<sup>54</sup> has given the problem some attention. It is clear that known systematic coherences in the echo signal should make possible an increase in detectability.

#### F. Rotation Vector

The quantity  $\vec{\Omega}$ , indicating the rotation velocity in radians per second, has appeared in several of the expressions developed in Sec. IV of this report. We shall now inquire how one might measure the speed  $\Omega$  and the axial direction. In the case of several planets, notably Venus,  $\vec{\Omega}$  is at present largely unknown.

The width of the doppler spectrum constitutes a measure of the projected rotation rate  $\Omega \cos \alpha$ , where  $\alpha$  is the tilt of the axis from perpendicularity with the line of sight. The total overall width of the echo power spectrum  $\sigma(f)$  gives  $\Omega \cos \alpha$  immediately, since this width is equal to  $(4a/cf_0) \Omega \cos \alpha$ . ( $a$  is the target radius,  $f_0$  the carrier frequency, and  $c$  is propagation velocity.) However, the outer limits of the echo spectrum are usually buried in noise and it is necessary to infer the spectrum width from the width of the central high-energy portions. But if this is so, one clearly requires more information than data on the spectrum  $\sigma(f)$  alone, since a given width of the center of the spectral peak could have been caused by either a smooth target rotating rapidly or a rougher target rotating more slowly.

Information on surface roughness is clearly necessary and there are several ways of getting it. Manasse<sup>37</sup> suggested that a single reading of  $Z(\vec{d}, 0)$  (the correlation of spaced receiver signals as a function of spacing at zero delay) would suffice, since for a uniform spherical target, the shape of  $Z$  is determined once  $\sigma(f)$  is known, except for a scale factor on width (see Sec. II-D and Fig. 6). A simpler method<sup>55</sup> that does not involve a separate receiving facility is to determine the roughness, i.e., the angular power spectrum  $\sigma_0(\varphi)$ , from the power impulse response  $\sigma(\tau)$  by Eq. (45); Eq. (14) then gives the value of the projected rotation rate  $\Omega \cos \alpha$  that corresponds to the observed  $\sigma_0(\varphi)$  and the observed doppler spectrum  $\sigma(f)$ .

If the target is nonuniform, the magnitude  $\Omega$  of the rotation velocity can also be deduced from periodicities observed in long-term records of echo power.

Cohen<sup>56</sup> has pointed out that one should observe a systematic change of the width of the echo spectrum  $\sigma(f)$  as observed over many months because the rotation vector  $\vec{\Omega}$  remains fixed in inertial space as the aspect from which the planet is viewed changes. Cohen shows how, by observing the "phase angle" and "amplitude" of this quasi-periodic oscillation of spectrum width, it is possible to infer not only the rotation speed but also to establish the tilt of the axis. The ambiguity in axis direction that remains is that the direction of rotation might be clockwise or counterclockwise and the axis might be tipped at some angle  $q$  or  $-q$  to the plane of the orbit.

In his discussion of radar interferometry, Manasse<sup>37</sup> suggested a way of resolving the first of these two ambiguities, namely whether it is the left or the right side of the apparent disk of the target that is approaching the observer. One simply narrows the input filters of the two spaced receivers so that they both pass only the energy arriving from a strip of the apparent disk

of the target, detunes both input filters together so that this strip lies either in the approaching side or the receding side, and then steers the interferometer lobe to maximize received power. The direction of movement of the best position of the lobe can be compared with the direction of frequency offset to get the sense of rotation.

The sense of rotation can also be obtained from interferometer experiments in which time delays  $\Delta\tau$  are allowed, using the effects described in Sec. II-D. As Fig. 6(b) indicates, for a given receiver spacing  $\vec{d}$ , there is a value of  $\Delta\tau$  that maximizes the correlation  $Z$ , namely  $\Delta\tau_{\max}$  of Eq. (15). The true velocity vector  $\vec{v}$  of the ground pattern expresses the projected target rotation velocity  $\vec{\Omega} \cos \alpha$ , and can be found by making two observations of  $\tau_{\max}$  using crossed baselines, and solving two equations like Eq. (15)

As a practical example of the application of this technique, suppose we have a radar transmitter at point A, and receivers at points A and B (A and B might be Millstone Hill and Lexington, respectively, 20 km apart). Suppose the transmission  $x(t)$  is a train of phase-coherent pulses 2 msec in duration occurring every 30 msec, and suppose the planetary target, Venus, is overhead. We desire to determine the ground diffraction pattern velocity as projected along the baseline  $\overline{AB} = \vec{d}$ . First, the outputs of the two receivers would be gated into the two inputs of a correlator for 2 msec every 30 msec (with the range of the planet known) to give  $Z(\vec{d}, 0)$ . Then, to try different values of  $\Delta\tau$  to find  $\Delta\tau_{\max}$ , the one for which  $Z(\vec{d}, \Delta\tau)$  is greatest, one would delay one of the correlator inputs by various integral multiples of 30 msec. If Venus' rotation period were 225 days ( $\Omega \sim 4 \times 10^{-7}$  radians/sec), then the ground pattern speed would be some 15 km/sec, and one would find that for the Lexington-Millstone baseline lying along the direction of pattern motion, maximum correlation would be obtained for values of  $\Delta\tau$  around 1.3 seconds.

In summary, it appears that by the combined use of several types of radar experiments, it is possible to determine rotation speed  $\Omega$  and resolve all the ambiguities in the direction of the polar axis except whether it is tipped toward the observer or away from him ( $\alpha$  positive or negative).

### G. Ionospheres and Interplanetary Ionization

It is reasonable to suppose that above certain levels in planetary atmospheres, recombination rates are low enough and the incident solar flux strong enough that a significant density of free electrons exists. As discussed in Sec. III, if losses are not excessive, such regions interposed between the earth and a reflecting hard target can be studied in terms of the time delay suffered by the echo components, or in terms of the critical frequencies at which the attenuation changes abruptly, or (if a magnetic field is present) in terms of the accumulated Faraday rotation.

Equation (19) gives an expression for the round-trip time of flight of a signal reflected from an object at range  $R$ . The second term, the excess of time of flight over that in vacuo, is seen to be a measure of electron density integrated along the path, and this quantity appears weighted by the inverse square of the frequency. This strong frequency dependence suggests several methods of measuring integrated electron density. The most sensitive would be a pair of separate radar experiments spaced as widely in frequency as possible, and with the lowest frequency as low as possible.† The two measurements of time of flight at two such widely spaced frequencies will give,

† But not so low that the signal does not escape the terrestrial ionosphere. Critical frequencies of the F2 layer vary from about 2 to 15 Mcps. If the beam goes through the ionosphere at an angle  $\chi$  from the zenith, the current value of critical frequency must be multiplied by  $\sec \chi$  to give the minimum useful frequency.

by simultaneous solution of two equations like Eq. (19), both the true range  $R$  and the integrated electron density. (It is assumed that light velocity  $c$  and frequency  $f$  are known accurately.)

A more convenient procedure<sup>57</sup> is to send a modulated signal and then examine the relative delays of the various sidebands in the received signal, but the limited frequency spread renders this method less sensitive than two separate experiments at widely separated frequencies. Also, as we have seen in Secs. IV-D and IV-E, rapid target fluctuations (doppler spread  $B$ ) or long multipath duration  $L$ , or both, have their effect on the fading of the sideband components. Reference 57 presents a discussion of a number of single-station experiments of this type employing various forms of modulation.

In either class of experiments, the fraction of the integrated electron density due to the interplanetary and target regions is not known until the terrestrial component is subtracted out. The interplanetary component is likely to be much smaller than the terrestrial component. Usually the terrestrial component is estimated from HF ionograms, but this gives only an approximate figure because of the variations of electron density with time and place. Briscoe<sup>58</sup> has made the ingenious suggestion that during a planetary radar experiment, or immediately before it or after it, one can examine the Faraday rotation of incoherent electron scatter returns from a region well above the F2 maximum of our ionosphere exactly along the planetary radar line of sight. Knowledge of the earth's magnetic field then gives an accurate figure for the terrestrial component by using Eq. (20).

If radar equipment becomes available that will do accurate ranging over a wide tunable frequency range, planetary ionospheric densities can be studied by noting the critical frequency below which the reflection is from the ionosphere and above which the reflection is from underlying regions. The transition will evidence itself most easily by a discontinuity in range or in other parameters, such as effective surface roughness.

## H. Magnetic Field

Faraday rotation has been used to deduce the total electron content of the earth-moon region using Eq. (20).<sup>18</sup> Similarly, using a radar polarimeter for reception of a planetary echo, and subtracting this same near-the-earth component, it is possible to find the integrated field-electron density product  $F_g(s) N(s)$ . Then, if the integrated  $N(s)$  has been obtained by some alternative means (see the preceding section), one can say something about the magnetic field between the vicinity of the earth and the target. Unfortunately, it is the product that appears in Eq. (20), so it is not possible to localize the field contributions even if the location of the electron density contributions is known, unless collateral information of some sort is available. The depolarization (Sec. II-E) due to target surface roughness may impede the measurement of total Faraday rotation  $\phi$ .

Experiments with tunable radars to discover critical frequencies can provide very interesting information on the magnetic field. Specifically, if the ordinary and extraordinary modes can be separated either according to direction of circular polarization or propagation delay times,<sup>†</sup> then the critical frequencies for the two modes can be isolated. One can then set crude bounds on the value of the local gyro frequency, which is proportional to the magnetic field intensity.

<sup>†</sup> The indices of refraction are slightly different, as discussed in Ref. 19.

## VI. MEASUREMENT ERRORS

### A. Statistical Estimation

The final sections of this report will be devoted to various matters relating to errors in making the measurements discussed earlier. In planning and carrying out physical investigations, it is important not only to be able to conceive the sort of experiment that will place in evidence the variables to be measured but also to know what the sources of error are, the expected size of the errors, and whether the experiment conceived is apt to minimize them, relative to other possible alternative ways of conducting the experiment. In the radar astronomy experiments we have discussed, the noise added into the echo signal is the principal factor influencing measurement error. If the target itself produces fluctuations in the echo, this too is a source of error.

The abstract methodology of setting up experiments to minimize error in the presence of random influences, the calculation of what sorts of error behavior are achievable, and so forth—these are the domain of mathematical statistics.<sup>59</sup> Some of the particular theories developed by statisticians have proved to be extremely useful to the communications and radar engineer. An outstanding example is the theory of hypothesis testing, which treats the radar detection operation, for example, as a test between these two mutually exclusive hypotheses: "the received signal is noise plus a target echo," and "the received signal is noise alone." In the companion report,<sup>4</sup> this approach is applied to the class of targets of interest to the radar astronomer (those that are spread in  $\tau$  or  $f$  or both) in such a way as to derive the form of transmitted signal and receiver processing equipment that will minimize the probabilities of failing to detect the presence of the object and of falsely concluding that it is present. The theory also tells how good the system will be, that is, to what level these probabilities will be reduced in the actual system in use.

There is an analogous statistical theory, estimation theory (see, for example, Helstrom,<sup>60</sup>), which is applicable to experiments that are intended to measure something, for example, a radar target parameter. This theory, too, has proved useful to the radar experimenter since, in those cases which are mathematically tractable, it provides him with the form of transmitted signal and receiver processing equipment that will minimize the error with which the desired quantity is registered. The theory goes on to say how good the measurement is, that is, what the average spread (variance) in observation values would have been if the experiment could have been repeated a large number of times under statistically identical conditions (ensemble average). In this section we shall be interested in presenting expressions for error variance.<sup>†</sup>

The gist of the statistical estimation approach is as follows. The transmitted waveform  $x(t)$  is reflected from the target, one of whose properties  $\alpha$  we desire to measure. The property  $\alpha$  might be a single parameter like range  $r$ , it might be a parameter set like the pair  $\tau$  and  $f$ , or it might be a function like  $\sigma(r)$  or  $\sigma(\tau, f)$ . Suppose the true value of this quantity is the one denoted by  $\alpha_0$ . The reflected signal  $y(t)$  arrives at the receiver mixed with noise  $n(t)$ ; the received signal is  $w(t) = y(t) + n(t)$ . Call  $p(\alpha, \alpha_0)$  and  $x(\alpha)$  the probability that the actual observed receiver input waveform  $w(t)$  did arise from the transmission  $x(t)$  and a certain  $\alpha$  lying in the interval  $\alpha$  to  $\alpha + d\alpha$ . (Often this probability can actually be known to the receiver if the statistics of the

<sup>†</sup> In order to understand completely how the errors will actually be distributed, one must know their probability distribution, but for purposes of the present cursory treatment we will be content to discuss only the variance of the errors.

noise  $n(t)$  are known.) The function of the receiver is to produce an output or an estimate  $\alpha^*$  which we would like to have correspond to the actual  $\alpha_0$ , but which will not, of course, because of the noise. One logical procedure for the receiver to carry out is to produce as the output  $\alpha^*$  that value of  $\alpha$  for which  $p(w/\alpha \text{ and } x)$  is a maximum.<sup>†</sup> Such a receiver is called a maximum-likelihood estimator. In practice, the way it is designed is first to determine analytically what  $p(w/\alpha \text{ and } x)$  is. Then it often turns out that the expression for this probability can be interpreted in terms of simple signal processing operations on the received signal  $w(t)$  that produce an  $\alpha^*$  for which this probability is maximized, when the noise statistics and the form of the transmission  $x(t)$  are known. After this is done it is usually possible to go back and perform alterations on the transmission  $x(t)$  to still further improve the performance.

The maximum-likelihood procedure is not just heuristically plausible; when the  $\alpha$  to be estimated is a parameter or a parameter set, it has been shown that the  $\alpha^*$  based on  $n$  independent such observations approaches the true  $\alpha$  for all practical purposes as  $n \rightarrow \infty$  ("consistent" and "asymptotically unbiased" estimator), and the variance of  $\alpha^*$  approaches zero as fast as any other possible form of estimator ("asymptotically efficient" estimator). And, what is more important practically, for a finite  $n$  (e.g., unity), if the estimator exists giving the theoretical minimum achievable error variance (an "efficient" estimator) as calculated from the so-called Cramer-Rao lower bound (on error variance), then that method is a maximum-likelihood estimator. However, not all maximum-likelihood procedures achieve this lower limit. Indeed, in some cases, the Cramer-Rao lower bound is lower than that achievable by any realizable estimator; for example, sometimes it is zero.

Suffice it to say that a maximum-likelihood strategy is the most appropriate approach under most conditions, with an exception to be mentioned in the next paragraph. It is often mathematically tractable and gives estimators that have been found by experience to be useful and are often, in fact, minimum-variance estimators. In measuring the cross section of a point nonfluctuating target, for example, the minimum-variance estimator exists and is a maximum-likelihood estimator. For estimating the scattering function  $\sigma(\tau, l)$ , on the other hand, methods of getting the maximum-likelihood estimates have recently been found, but at present it is not known whether the variance of the estimate is as small as is theoretically achievable. For measurements of more involved quantities, estimation theory has been little used up to now. For example, no one has worked out a maximum-likelihood estimator of  $\vec{\Omega}$ , the vector target rotation rate.

The above discussion is appropriate to the often-encountered situation in which the receiver operations take place in ignorance of any prior knowledge of the relative probability that various values of  $\alpha$  will occur. Sometimes one does have such information in the form of an a priori probability distribution  $p(\alpha)$ . Then, instead of having the receiver produce as  $\alpha^*$  that value of  $\alpha$  for which  $p(w/\alpha \text{ and } x)$  is maximum, one uses instead  $p(\alpha) p(w/\alpha \text{ and } x)$ . Also, one may want to assign "costs" to estimation errors; for example, a 10-mile error in target range might be considered twice as undesirable in the vicinity of 2000 miles range as at 2500 miles range. A second modification can be made to take care of this. The form of estimation procedure that takes into account cost and/or a priori probabilities is called Bayes estimation. If the cost

<sup>†</sup>The asterisk is used here to represent an estimated value as distinct from our earlier usage in indicating the complex part of a complex quantity.

assignment and the a priori probability  $p(\alpha)$  are both spread broadly over values of  $\alpha$ , whereas the function  $p(w/\alpha \text{ and } x)$  is relatively sharply peaked, then the Bayes and maximum-likelihood procedures are equivalent. The reader is referred to Ref. 60 for a discussion of Bayes estimation; we shall assume here that the a priori probability and cost functions are too broad to be a factor in our measurement procedures. For example, if the reader will refer to Fig. 13, he will probably agree that previous measurements of the astronomical unit have been so widely spread as to discourage assigning a peak of a priori probability in a region of a. u. values any narrower than several times the probable error of a new measurement.

### B. Point Nonfluctuating Targets

When the target has a scattering function that is much narrower along both the  $\tau$ - and  $f$ -axes than is the ambiguity function of any signal we might be interested in using to observe it, then we can say that it is a point nonfluctuating target.

The effect of a point nonfluctuating target on the transmission  $x(t)$  is simply to change its amplitude in proportion to  $\sqrt{\sigma}$  where  $\sigma$  is the target's actual radar cross section, its delay by the actual round-trip delay  $\tau$ , and its frequency by  $f$ , the actual doppler offset. Maximum-likelihood estimators for all these quantities have been found and described in the literature. Helstrom,<sup>60</sup> among others, gives a reasonably complete treatment of this problem, and we shall reproduce his results here, stating first the signal processing operations implied by the expressions for the maximum-likelihood estimate, and then giving the variance of the estimate. White gaussian noise will be assumed.

When  $\tau$  and  $f$  are known, and one wants to obtain an estimate of received signal amplitude (which will be proportional to  $\sqrt{\sigma}$ ), one forms the quantity

$$(\sqrt{\sigma})^* = \int_{-\infty}^{\infty} w(t) x(t) dt / \int_{-\infty}^{\infty} x^2(t) dt \quad (47)$$

which, according to Sec. IV-B, can be interpreted as the suitably normalized output at time  $t_0$  of a filter matched to the transmission [i.e.,  $m(t) = x(t_0 - t)$  as in Eq. (26)]. As one might expect, the variance is the noise-to-signal power ratio times the amplitude squared:

$$\text{Var} [(\sqrt{\sigma})^*] = \overline{[(\sqrt{\sigma})^* - (\sqrt{\sigma})_0]^2} = \frac{N_0}{2E_s} (\sigma)_0 \quad (48)$$

where the subscript zero indicates the true value.

It can be shown that Eq. (48) is the minimum achievable variance of estimation of amplitude (by the Cramer-Rao inequality), so no other estimator of  $\sqrt{\sigma}$  can do any better than the matched filter.

Assuming that the echo is of unknown amplitude and buried in white gaussian noise, the maximum-likelihood estimate of the parameter pair  $\tau$  and  $f$  is the value of  $\tau$  and  $f$  that maximizes

$$Q(\tau, f) = \left| \int_{-\infty}^{\infty} x^*(t) w(t + \tau) \exp[2\pi jft] dt \right|^2 \quad (49)$$

which is the square of the envelope at time  $\tau + t_0$  of a filter matched to  $x(t)$ , except that the filter is offset by  $f$  cycles per second. As in Eq. (27),  $t_0$  is the time at which the filter would have maximum response if target delay  $\tau$  were zero. In practice, one implements Eq. (49) by building

a set of matched filters, each followed by an envelope squarer, and all having different frequency offsets with the total frequency span encompassing all reasonable values of  $f$ . One then examines all the outputs over an interval of time large enough to span all likely values of  $\tau$ , and selects the delay and frequency of the target peak as representing the estimated values  $\tau^*$  and  $f^*$ . Since  $\tau$  and  $f$  are continuous variables, strictly speaking there should be a continuum of stagger-tuned matched-filter-envelope-squarer combinations, and also the continuum of  $\tau$ -values should be examined. In practice, of course, the  $f$ -spacing and  $\tau$ -spacing would be set for some fraction of the expected rms error (square root of the variance) in  $f$  and  $\tau$ , respectively.

Formulas for the range and doppler error variances as a function of duration  $T_0$  and bandwidth  $W_0$  have been found to be

$$\text{Var}(\tau^*) = \overline{(\tau^* - \tau_0)^2} = \frac{N_0}{2E_s} \frac{1}{W_0^2} \quad (50)$$

and

$$\text{Var}(f^*) = \frac{N_0}{2E_s} \frac{1}{T_0^2} \quad (51)$$

where

$$T_0^2 = \frac{\int_{-\infty}^{\infty} (t - t_1)^2 |x(t)|^2 dt}{\int_{-\infty}^{\infty} |x(t)|^2 dt} \quad ; \quad t_1 = \frac{\int_{-\infty}^{\infty} t |x(t)|^2 dt}{\int_{-\infty}^{\infty} |x(t)|^2 dt}$$

and

$$W_0 = \frac{\int_{-\infty}^{\infty} (f - f_1)^2 |X(f)|^2 df}{\int_{-\infty}^{\infty} |X(f)|^2 df} \quad ; \quad f_1 = \frac{\int_{-\infty}^{\infty} f |X(f)|^2 df}{\int_{-\infty}^{\infty} |X(f)|^2 df}$$

That is,  $T_0$  and  $W_0$  are the "rms" duration and bandwidth, respectively. The variance expressions (50) and (51) are valid if three conditions are satisfied: (1) the ambiguity function of  $x(t)$ , the transmission, can be approximated near the origin by parabolas along the  $\tau$ - and  $f$ -axes; (2) the axes of symmetry of the ambiguity function lie along the  $\tau$ - and  $f$ -axis; (3) the signal-to-noise ratio is sufficiently large that the error arises from random shifts of the peak of the function  $Q$  near the true value of the parameter, and not from more remote peaks becoming sufficiently large. The first condition is usually met, except for such things as ideally square pulses. The second condition is met by all the functions of the sort typified in Fig. 10 except for the "chirp" (swept frequency) waveform of Fig. 10(c). For waveforms that obey condition (2), the range error is not a function of signal duration  $T_0$  and the doppler error is not a function of bandwidth  $W_0$ . Also, the range error is not increased by ignorance of the velocity, and vice versa.

Expressions (50) and (51) are seen to involve only the signal-to-noise ratio  $2E_s/N_0$  and the widths of the ambiguity surface. They express the way in which both the noise and the widths of the ambiguity function conspire to render the estimate of the true values of  $f$  and  $\tau$  imprecise by causing the maximum of  $Q$  in Eq. (49) to shift to the wrong place. Were it not for the noise, the smearing effect of finite signal bandwidth or duration would be reversible and the position of the peak could be located to arbitrarily high precision.

One may wonder whether the processor of Eq. (49) gives error variances [Eqs. (50) and (51)] that are the minimum achievable variances. Manasse<sup>61</sup> has shown that in a point target-gaussian

noise case like the present one, at large signal-to-noise ratios the estimates are jointly minimum-variance estimates (i.e., "jointly efficient") so long as the transmission  $x(t)$  is a well-behaved function of each parameter  $\alpha$ . An interesting situation in which the Cramer-Rao lower bound on error variance is not physically achievable is the case where the transmission is a single rectangular pulse of sinusoid having a duration  $T$ . Again, one would expect the range and doppler errors to depend on pulse width and signal-to-noise ratios and, if the noise is small enough, for range error to be considerably smaller than pulse width, as before. But when one computes the theoretical lower bound for range error it turns out to be zero for any finite noise level, and this does not make physical sense. The derivation leading to Eqs. (50) and (51) is not usable because Condition (1) is violated. However, Manasse<sup>62</sup> has developed a different, more heuristic approach to find the error variances from a matched filter processor and has found that the error variances in this square-pulse case are

$$\text{Var}(\tau^*) = (N_0/2E_s)^2 \sqrt{2} T^2 \quad (50a)$$

$$\text{Var}(f^*) = N_0/2E_s \ 3/\pi^2 T^2 \quad (51a)$$

When a number  $n$  of similar but statistically independent measurements are added together, the variance is decreased by a factor  $n$ . An example of this would be  $n$  pulses, each measuring range or doppler independently. However, in many practical circumstances the  $n$  measurements may not be independent. For example, the pulse train illustrated in Fig. 10(d) has the phase preserved from pulse to pulse, so the doppler resolution available is that appropriate to the duration of the train (as expressed by the frequency width of the ambiguity function), rather than only  $1/n$  times the variance to be obtained with one pulse. The computation of error variances of range and doppler becomes somewhat complicated when the target has an appreciable acceleration component, when we desire to measure this acceleration, or when skewed or curved ambiguity surfaces are allowed (as shown in Fig. 10(c)). These cases are particularly hard to handle when large-TW signals such as pulse trains are considered rather than single pulses. The best available treatment of these more complicated cases has been given by Kelly.<sup>63</sup>

### C. Targets Spread only in Delay or Doppler

After the point nonfluctuating target, the next class of radar targets in order of complexity is that for which there is a spread along either the  $\tau$ -axis or the  $f$ -axis (relative to the corresponding spread of the signal ambiguity function), but not both.

For example, with a point fluctuating target, there is a spread only along the  $f$ -axis, and the scattering function is  $\sigma(\tau, f) = \sigma(f) \delta(\tau - \tau')$  where  $\tau'$  is the range. With such a target there are at least four quantities one might be interested in estimating: (1) the range  $\tau'$ , (2) the curve  $\sigma(f)$  to whatever frequency resolution is interesting, (3) the bulk doppler shift of the target as a whole, given the shape  $\sigma(f)$  apart from the unknown translation, and (4) the width of the doppler spectrum, given both the center frequency and the spectral shape  $\sigma(f)$  apart from the unknown width factor.

With the classical nonfluctuating point target, the real source of error (other than such things as calibration errors) was the receiver noise, represented by the density  $N_0$ . For the fluctuating target, the echo fluctuations are an additional cause of error. As we shall see shortly, these fluctuations place a limit on the measurement accuracy even when additive received noise is zero. Such contributions to the random variation of the estimates will be designated as "self-noise" as

before, according to the convention employed here that any random variations in the output that remain after  $N_0$  goes to zero are to be so designated.

To estimate the range  $\tau'$ , it appears plausible to proceed as with the point nonfluctuating target, namely, to build a parallel set of signal-to-noise ratio-maximizing processors that are spaced in delay and to pick as the estimate  $\tau'^*$  the delay of the processor exhibiting the largest output. Since the target is fluctuating, the processors will now be weighted radiometers rather than the matched-filter-envelope-detector devices implied by Eq. (49). The  $\tau$ -spacing between adjacent processors will be a convenient fraction of the rms range error. For small input  $S/N$ , and large output  $S/N$ , R. Price<sup>64</sup> has found the error variance to be

$$\text{Var}(\tau'^*) = (S/N)_0^{-1} \frac{\int_{-\infty}^{\infty} \int_{-\infty}^{\infty} \psi^2(0, f) \sigma(f+f') \sigma(f) df df'}{-\frac{d^2}{d\tau^2} \bigg|_{\tau=0} \int_{-\infty}^{\infty} \int_{-\infty}^{\infty} \psi^2(\tau, f) \sigma(f+f') \sigma(f) df df'} \quad (52)$$

where  $\psi^2$  is the ambiguity function of the transmission, as before, and the output signal-to-noise ratio  $(S/N)_0$  is given by Eq. (34).†

The estimation of the function  $\sigma(f)$  is, of course, just the problem of spectral analysis; i.e., given a sample segment of a random process of unknown spectral density, one is to estimate the spectral density, which in our context is  $S(f) = \sigma(f) + N_0$ , where  $N_0$  is the noise density. Although there is a sizable literature on the subject of spectral analysis (e.g., Refs. 65 and 66), as matters now stand there is no well-formulated procedure leading to minimum-variance estimates of the spectrum  $S(f)$ . However, various recipes for estimation have been analyzed in detail and it is often possible to give approximate expressions for the error variance.

Suppose we have a sample of received signal  $T$  seconds long on which we desire to perform a spectral analysis. Such a sample might be obtained from a radar experiment in which the transmission is a sinusoid of duration  $T$ . If one either performs a Fourier series analysis of the sample or Fourier-transforms the autocorrelation of the sample (these are the two obvious ways of proceeding), the resulting estimated spectrum will have violent variations every  $1/T$  cps, no matter what the true spectrum of the random process from which the sample came. Clearly, if one insists on a frequency resolution  $\delta f$  that is as small as  $1/T$ , then this jagged picture is the only estimate possible, but is meaningless. In practice, the desired frequency resolution  $\delta f$  must be made larger than  $1/T$  so that a number of different samples (or "degrees of freedom" as we shall call them) will contribute to each point on the estimated spectrum.

Blackman and Tukey<sup>65</sup> suggest the following procedure which tends to give good estimates of smoothed values of the true spectral densities: (1) the autocorrelation of the sample is computed, (2) this even function  $\phi(\tau)$  is then multiplied by some suitably chosen even weighting function or window function  $D(\tau)$  which has a maximum at zero and is zero outside the interval  $(-1/\delta f, 1/\delta f)$  where  $\delta f$  represents the desired frequency resolution of the estimate, and finally (3) the product  $\phi(\tau) D(\tau)$  is Fourier-transformed to get the spectral estimate  $S^*(f)$ . This is equivalent to convolving the transform of  $D(\tau)$  with the transform of the specimen correlation

† This expression is valid only for targets having a nonzero doppler spread; it does not reduce to Eq. (50) as doppler width goes to zero.

function  $\varphi(\tau)$ . The proper choice of  $D(\tau)$  is a compromise between effectively throwing away some of the data by suppressing the extremities of  $\varphi(\tau)$  and retaining the violent variations of estimated spectrum with frequency. For gaussian processes, Blackman and Tukey give the following expression for error variance of the spectrum at a given frequency when the true  $S(f)$  varies slowly with frequency (relative to  $1/T$ ):

$$\text{Var } [S^*(f)] = \frac{\text{Ave } [S^*(f)]}{T\delta f} \quad (53)$$

The average of the estimate  $S^*(f)$  is essentially the true  $S_0(f)$ . Much the same result will be obtained if the spectral estimate is performed by making a Fourier analysis of the sample and then adding together the powers in the  $T \delta f$  frequency increments contained in  $\delta f$  cps.

Equation (53) places in evidence the well-known rule of thumb that the ratio of variance to squared mean is inversely proportional to the number of independent samples or degrees of freedom (roughly  $2T\delta f$  for a spectral interval  $\delta f$  wide observed for  $T$  seconds).<sup>†</sup> Thus, if one is measuring  $S(f)$  of a radar astronomy target he must try to make the total observation time  $T$  several times longer than the reciprocal of  $\delta f$  the desired frequency resolution, as to increase the number of degrees of freedom contributing.

For our radar astronomy purposes the usual recipe for spectral analysis (of which we have just presented one that has been elaborately studied for practical applicability) suffers from the defect that it provides an estimate of  $S(f) = \sigma(f) + N_0$  and not  $\sigma(f)$  itself. Without careful calibration it may be difficult to know just what baseline level to subtract out of the resulting plot  $S^*(f)$  in order to isolate the echo component  $\sigma(f)$ .

The problem of estimating the frequency shift  $f_d$  of a spectrum of known shape  $S(f)$  from a sample of duration  $T$  of a random gaussian function of true spectral density  $S(f - f_d)$  has been treated by Swerling<sup>67</sup> and Levin.<sup>68</sup> Swerling has suggested a procedure in which the estimate  $S^*(f)$  obtained by the Blackman-Tukey method just described is operated on by a frequency weighting factor  $\alpha(f)$  so that the estimate  $f_d^*$  is given by  $\int S^*(f) \alpha(f) df$ . The function  $\alpha(f)$  is chosen from prior knowledge of the  $S(f)$  shape to minimize the error variance of  $f_d^*$  in terms of error variances of  $S^*(f)$ . Since the latter quantity  $S^*(f)$  is obtained to begin with by a more or less ad hoc procedure, as we have seen, the use of  $S^*$  to get  $f_d^*$  is not guaranteed to produce minimum-variance estimates of  $f_d$ .

Levin<sup>68</sup> sought to find a maximum-likelihood estimator of  $f_d$  directly and has examined the Cramer-Rao lower bound on error variance. He finds that

$$\text{Var } (f_d^*) \geq \left\{ T \int_0^\infty \left[ \frac{\sigma'(f)}{\sigma(f) + N_0} \right]^2 df \right\}^{-1} \quad (54)$$

where  $\sigma'(f)$  is the derivative of  $\sigma$  with respect to frequency. Note that rapid variations of  $\sigma(f)$  with  $f$  tend to make estimates of frequency shift more reliable, as one would expect. The maximum-likelihood estimator of  $f_d$  is that which picks that value of  $f_d$  for which

$$\sum_n \frac{a_n^2 + b_n^2}{S(\frac{n}{T} - f_d)} = \sum_n \frac{a_n^2 + b_n^2}{\sigma(\frac{n}{T} - f_d) + N_0} \quad (55)$$

<sup>†</sup> The factor 2 occurs because at each frequency the signal is characterized by two quantities, e.g., an amplitude and a phase.

is a minimum, where  $a_n$  and  $b_n$  are the Fourier sine and cosine coefficients of a Fourier series expansion of the sample function. In other words, one processes the received sample to generate a jagged function representing the power in the successive Fourier components and then convolves this with the reciprocal of the known shape  $S(f) = N_0 + \sigma(f)$  to find the shift  $f_d$  for which a minimum output is observed. As the product of observation time  $T$  and  $B$  of  $S(f)$  becomes large, this maximum-likelihood estimate is a minimum-variance estimate and Eq. (54) converges to the equality condition.

The frequency width of a spectrum can be estimated by a related procedure also worked out by Levin.<sup>68</sup> (Recall that one method of determining the rotation vector of a planet is to measure the width of the echo power spectrum at various times during the synodic period.) Let the true spectral shape be  $S[h(f - f_d)] = \sigma[h(f - f_d)] + N_0$ , where  $f_d$  is the center frequency and  $h$  is a scale factor on width. If only  $h$  is unknown and is to be estimated, Levin finds that the Cramer-Rao lower bound is

$$\text{Var}[h^*] \geq \left\{ T \int_0^\infty (f - f_d)^2 \left[ \frac{\sigma'(f - f_d)}{\sigma(f - f_d) + N_0} \right]^2 df \right\}^{-1} \quad (56)$$

which is very similar to Eq. (54). Note again that rapid variations of target behavior  $\sigma$  with frequency facilitate measurement of the width factor  $h$ ; also that the quadratic factor means that such variations at frequencies distant from the band center are more helpful than those near the center. The maximum-likelihood estimator of  $h$  picks that value of  $h$  for which

$$\sum_n \frac{a_n^2 + b_n^2}{S[h(\frac{n}{T} - f_d)]} + \frac{K}{h} = \sum_n \frac{a_n^2 + b_n^2}{\sigma[h(\frac{n}{T} - f_d)] + N_0} + \frac{K}{h} \quad (57)$$

is a minimum,  $K$  being a certain constant. In other words, one processes the received sample to generate the power in the successive Fourier components (for example by using a narrow-band filter), and then computes the convolution for fixed shift of this jagged function with the reciprocal of the profile  $\sigma[h(f - f_d)]$ , choosing various values of  $h$  until the convolution is minimized. Again, the bound [Eq. (56)] applies with the equality sign when  $BT$  is large.

The other form of target spread in one domain only is the deep nonfluctuating target whose scattering function is  $\sigma(\tau, f) = \sigma(\tau) \delta(f - f')$ . All the notions just presented about errors of estimating  $\tau'$ ,  $\sigma(f)$ ,  $f_d$  and  $h$  apply through a certain duality relationship<sup>29</sup> to the estimation of  $f'$ ,  $\sigma(\tau)$ ,  $\tau_d$ , etc. for the deep nonfluctuating target. Instead of dealing with a sample function  $T$  seconds long, obtained perhaps by illuminating the target with a sine wave, the target is effectively illuminated with a single impulse and phase and amplitude of the echo components at various frequencies are measured over a bandwidth  $W$ . Instead of having a narrow-band received signal exhibiting fluctuations of amplitude and phase every  $1/B$  seconds in time throughout  $T$ , we have fluctuations of amplitude and phase every  $1/L$  cps. throughout  $W$ . In situations where previously we dealt with a Fourier series analysis of a time function  $T$  seconds long we deal with time samples of the echo waveform every  $1/2W$  seconds. The detailed application of this duality to get answers for the deep nonfluctuating target will not be pursued any further here. This duality has been developed in detail by Bello.<sup>69</sup>

#### D. Deep Fluctuating Targets

As the reader will see from comparing the material in the previous two sections the application of statistical estimation theory to the classical nonfluctuating point target is rather complete, but our present understanding of the more complicated singly spread target, although filling out rapidly, is still somewhat fragmentary. For the doubly spread or deep fluctuating target the situation is even worse. Only a few miscellaneous results are available.

In practice one might want to estimate the following attributes of the true scattering function  $\sigma(\tau, f)$ : (1) the center frequency and/or center delay, given the exact shape of  $\sigma(\tau, f)$ ; (2) the frequency width and/or delay width, given all other information on  $\sigma(\tau, f)$ ; (3) the function  $\sigma(\tau, f)$  itself, given no a priori data about it. Of these, only the first and last have received much attention.

The simplest method of measuring  $\sigma(\tau, f)$  is the rather direct one that was discussed in Table I, the use of a simple matched filter or correlation detector with preset  $\tau$  and  $f$  offsets to probe the scattering function at the point  $\tau, f$ . This is the method employed in Pettengill's moon-mapping work.<sup>8,9</sup> Suppose we desire to do such an experiment and achieve a frequency resolution of  $\delta f$  and a delay resolution  $\delta \tau$ ; that is, we wish to measure the average echo power in a cell of the  $\tau - f$  plane having the dimensions  $\delta f$  and  $\delta \tau$ . If we make the signal bandwidth  $1/\delta \tau$  and the duration  $1/\delta f$ , then we get in the output squared envelope just such an observation of the desired cell [Eqs. (31) and (32)], but the number of degrees of freedom of the observation is only two and the variance equals the mean, as with the simpler spectral analysis case described by Eq. (53). If, however, a bandwidth  $m/\delta \tau$  and/or a duration  $n/\delta f$  is used ( $m$  and  $n > 1$ ) and the  $mn$  separate received squared envelopes are added together and the square root taken, then the number of degrees of freedom is  $2mn$  and the variance of estimation of  $\sigma(\tau, f)$  is

$$\text{Var} [\sigma^*(\tau, f)] = \frac{\text{Ave} [\sigma^*(\tau, f)]}{mn} \quad (58)$$

as with Eq. (53).

One defect of this simple procedure is its behavior when the target approaches the over-spread condition, that is, when the product of total doppler spread  $B$  and total multipath spread  $L$  is near unity. As we have seen earlier, the operation of such a matched filter or correlation detection method can be visualized as overlaying onto the surface  $\sigma(\tau, f)$  the surface  $\psi^2(\tau, f)$  (with appropriate delay and frequency offsets) and then adding up all the volume under the product function. As long as the ambiguity function  $\psi^2$  has most of its volume in the central peak, very little output power comes from any place but in or very near the desired cell in the  $\tau, f$  plane, no matter how large the area  $BL$  covered by the function  $\sigma$ . However, as the invariance relation Eq. (30) assures us, such a concentration of the volume in  $\psi^2$  will occur only when the base of the central peak has an area of approximately unity, as with the waveforms of Figs. 10(a), (b) and (c). But suppose it is necessary to use one of the large-TW waveforms of Figs. 10(d) and (e). This would be the procedure if it is desired to resolve a cell in the  $\tau, f$  plane of size  $\delta \tau \delta f = 1/TW \ll 1$ . Because of the secondary peaks of Fig. 10(d) or the low-lying skirts of Fig. 10(e), if the area  $BL$  covered by the scattering function is great enough, then the processor output power due to the desired region of the  $\tau, f$  plane (the region of the central peak of  $\psi^2$ ) will have added to it self-noise power from undesired regions. (Once again we use the term self-noise to designate output components that do not go to zero even if the additive input noise does.) Clearly, whether such components will appear in the output depends on the scattering function area  $BL$  and on the type of ambiguity function chosen to probe it.

Let us illustrate these ideas by picking some numbers from a specific radar astronomy experiment. Suppose we wish to make a radar map of Mars using a pulse train [Fig. 10(d)]. The multipath depth  $L$  from nose to limb is 24 msec, which means that observations of the received signal made more frequently than once every 24 msec will be noisy due to time overlap of the echoes. The echo power near the limb is so small relative to that from the nose, that a periodic sampling of the echo from the nose would not be significantly corrupted with echoes from the limb until the sampling interval became much less than 24 msec, but the converse would not be true; samples of the echo from near the limb would be badly corrupted by strong self-noise from the nose as soon as the sampling period was reduced below 24 msec. Now the carrier frequency above which the total doppler spread of Mars is  $1/24$  kcps turns out to be 26.5 Mcps. In order to compute a clean echo spectrum  $1/24$  kcps wide, the ability to get a clean sample once every 24 msec must be preserved, and we see that this condition begins to be violated at a carrier frequency of 25.5 Mcps; i.e., this is the lowest frequency for which  $BL = 1$ , if by  $B$  we mean the total limb-to-limb doppler spread and by  $L$  we mean the total multipath duration. [The frequencies for which  $BL$  (so defined) equals unity are given in Table II for other radar astronomy targets.]

Now suppose we are operating at 440 Mcps so that  $BL$  is very high, actually 18,  $B$  being 750 cps. If we do not need more than about 18 cells in our radar map, we can send a simple  $TW = 1$  pulse [Figs. 10(a) and (b)] of duration, say, 6 msec, and by averaging the received power at the desired receiver  $\tau$ - and  $f$ -offsets get an observation of echo power in a cell of the  $\tau$ - $f$  plane that is  $\delta\tau = 6$  msec by  $\delta f = 1/6$  kcps in area.

We conclude that when  $BL$  is much smaller than unity, a large- $TW$  signal can be chosen such that the self-noise is negligible. For example, in Fig. 10(d), so long as the scattering function does not spread outside the area enclosed by the dotted lines, self-noise due to noncentral peaks

Target	Frequency (Mcps)
Moon (at maximum libration rate)	$f_s = 3150$
Mercury (assuming 88-day rotation period)	4280
Venus (assuming 225-day rotation period)	1880
Earth	39.7
Mars	26.5
Jupiter	1.58
Saturn	0.380
Uranus	2.08
Neptune	3.77
Pluto (assuming 16-hour rotation period)	2.25

will be negligible. We further conclude that when  $BL$  is much greater than unity, if one can be satisfied with a resolution cell of size  $\delta\tau \delta f = 1$ , then a  $TW = 1$  pulse [Fig. 10(a), (b) or (c)] can be used, and because of the central concentration of the volume in the ambiguity function, once again the self-noise will be negligible. It is the in-between values of  $BL$  of the order of unity that produce self-noise difficulties.<sup>†</sup> For illustration, we have plotted in Fig. 15 several curves

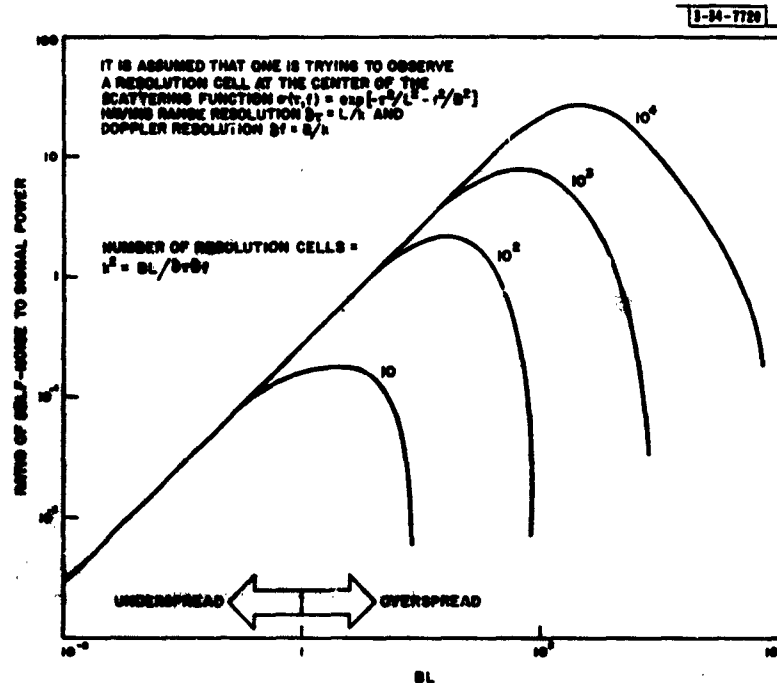


Fig. 15. The manner in which self-noise corrupts the estimate of the scattering function when the simple matched filter procedure is used and the target is moderately overspread.

of self-noise-to-signal ratio as a function of  $BL$ , assuming that the scattering function being observed has a gaussian shape in both  $f$  and  $\tau$  directions (i.e.,  $\sigma(\tau, f) = \exp - [\tau^2/L^2 + f^2/B^2]$ ), and that the size of the desired resolution cell  $\delta\tau \delta f$  is  $0.1 BL$  to  $10^{-4} BL$ . It is assumed that the waveform in use is the pseudonoise whose ambiguity function is idealized at the right of Fig. 10(e).

The two-frequency method of measuring the scattering function also encounters difficulties as the target becomes overspread, as is quite easily visualized. By referring to the fourth entry of Table I we are reminded that one first obtains  $\mathcal{A}(\Delta f, \Delta\tau)$  by cross-correlating the outputs

<sup>†</sup>We may conjecture that it is impossible to realize a physical waveform whose ambiguity function has less than a certain amount of volume in an area much larger than the order of unity surrounding the central peak. The volume may occur in the central peak, as in Fig. 10(a), (b) or (c); in separate peaks, as in Fig. 10(d), or in wide foothills as in 10(e). [Such an area with a low noncentral volume is the dotted region of Fig. 10(d).] This conjecture remains unproved to date.

of two filters tuned to separately receive two sinusoids transmitted  $\Delta f$  apart, and then Fourier-transforms  $\mathcal{G}(\Delta f, \Delta \tau)$  to get  $\sigma(\tau, f)$ . Now  $\mathcal{G}$  varies with  $\Delta f$  at roughly a rate  $1/L$ ; that is, we will want to measure  $\mathcal{G}$  for frequency spacings  $\Delta f$  as low as  $1/L$  cps. But each sinusoid is smeared by  $B$  cps, so a clean (self-noiseless) signal separation will be possible only if  $B > 1/L$ , i.e., if the target is underspread.

There is a class of methods of measuring the scattering function  $\sigma(\tau, f)$  that appears to be devoid of the problem of self-noise due to overspreading, and has other advantages over the matched filter (or correlator) method we have described, even though the latter is easier to implement. These methods are the fourth moment method,<sup>70,71</sup> the S/N-maximization method,<sup>72</sup> and the least-squares method.<sup>73</sup> Each requires elaborate receiving equipment and/or computer processing. These three approaches are worth taking a bit of space to describe here, because, although their advantages and usability are not completely understood at present, they are being actively investigated and are not ad hoc methods (as is the matched filter approach) but have optimum properties, as we shall now explain.

The fourth moment method proposed by Kailath involves a receiver which processes the received signal  $w(t)$  so as to compute the quantity

$$\langle w(t) w(t + \alpha) x(t - \beta) x(t + \alpha - \beta) \rangle$$

in which the transmission  $x(t)$  is a white noise. As before,  $\langle \rangle$  represents the infinite time average. Starting from such a measurement of this fourth moment, we can then calculate the estimated scattering function  $\sigma^*(\tau, f)$ .

Levin's least-squares method is a more general procedure of which the fourth moment method is the special case for very long integration time and for  $x(t)$  a white noise. In the least-squares procedure one processes the finite length sample  $w(t)$  to get the same fourth moment (except that the integration time is now finite). This fourth moment is then operated on by an explicit linear transformation involving the known transmission  $x(t)$  and the result<sup>†</sup> is a quantity which, when Fourier-transformed once, is the desired  $\sigma^*(\tau, f)$ .

Price's S/N-maximization method consists of building a rake radiometer [Fig. 11(d)] with adjustable filter characteristics  $|H_i(f)|$  at each tap. These characteristics are then adjusted by some trial-and-error procedure until the trial output signal-to-noise ratio is maximized. Recalling that the  $|H_i(f)|^2$ 's that maximize signal-to-noise ratio are a reproduction of the scattering function  $\sigma(\tau, f)$  [Eq. (35)], we have thus created an estimate  $\sigma^*(\tau, f)$  in the "best" settings of the filters. Price shows that at low input signal-to-noise ratios, this method produces a maximum-likelihood estimate. Levin has shown that the least-squares and S/N-maximization methods are equivalent, and therefore that at low input signal-to-noise ratios they are both maximum-likelihood estimators.

† It turns out that at all signal-to-noise ratios this procedure is equivalent to performing a least-squares fit between the covariance matrix of the sample waveform (call it  $W$ ) and a trial covariance matrix  $S$ . That is, the elements  $s_{ij}$  of  $S$  are adjusted to minimize

$$\sum (s_{ij} - w_{ij})^2$$

$S$  involves both the known and fixed transmission  $x(t)$  and the adjustable trial target scattering function.

At present, not much is known about the variance of estimates obtained by these methods. It seems plausible that some specification of the intended degree of range resolution  $\delta r$  and Doppler resolution  $\delta f$  must be made, and that then the variance of the estimates will go down as  $\delta r \delta f / W$ , the number of degrees of freedom per resolution cell, goes up ( $T$  being the sample duration and  $W$  being its bandwidth).

Price<sup>64</sup> has investigated the problem of estimating  $\tau_0$ , the center range of a deep fluctuating target whose scattering function is known apart from this range parameter. The result is a more general case of that given in Eq. (52), and amounts to the following. The estimator is an array of rake radiometers set for various delays. The estimate  $\tau_0^*$  is that corresponding to the processor exhibiting the largest output. Under the conditions of low input and high output signal-to-noise ratios, and assuming that the output in the absence of noise is parabolic in the neighborhood of the true  $\tau_0$ , Price finds that

$$\text{Var}(\tau_0^*) = (S/N)_0^{-4} \frac{\int_{-\infty}^{\infty} \int_{-\infty}^{\infty} \int_{-\infty}^{\infty} \int_{-\infty}^{\infty} \psi^2(\tau, f) \sigma(\tau' - \tau, f' + f) \sigma(\tau', f) d\tau df d\tau' df'}{-\frac{d^2}{d\lambda^2} \Big|_{\lambda=0} \int_{-\infty}^{\infty} \int_{-\infty}^{\infty} \int_{-\infty}^{\infty} \int_{-\infty}^{\infty} \psi^2(\tau, f) \sigma(\tau' - \tau, f' + f) \sigma(\tau' - \lambda, f') d\tau df d\tau' df'}} \quad (59)$$

## VI. SUMMARY AND CONCLUSIONS

In this report the author has attempted to summarize the techniques by which various astronomically interesting properties of remote objects may be studied by processing of received radar signals. In the case of "soft" targets such as ionized regions, clouds of small particles, and so forth, little that is unfamiliar was said here; conventional sounding techniques are available for estimating electron density and magnetic field.

Hard targets are quite interesting from the signal processing viewpoint, since by the choice of suitable transmitted signals and receiver operations a number of target properties may be determined. One of the most important of these is the statistical character of the rough target surface. In this report a number of procedures were discussed for determining the radar angular power spectrum  $\sigma_0(\varphi)$  of either a portion of the target or the whole surface (the latter under the assumption of statistical uniformity of the surface). The function  $\sigma_0$  expresses directly the second-order statistics of the random spatial irregularities in the echo wavefront, and it expresses indirectly the second-order statistics of the target terrain itself. The relation between statistical properties of wavefront and terrain was not dealt with here.

Measurement of  $\sigma_0(\varphi)$  of uniform objects can be made by short-pulse, long-pulse, spaced-frequency or interferometer experiments; also, the roughness can be inferred grossly from polarimetry measurements. This last type of procedure requires at this writing much further theoretical work before one can say just how the amount of signal depolarization depends on surface roughness (suitably defined).

For nonuniform objects one is interested in determining  $\sigma_0(\varphi)$  for various regions. Isolation of various target regions in antenna beamwidth is usually out of the question because of the great target ranges; also, it was found to be impossible to perform the isolation on the basis of different motions of the corresponding parts of the diffraction pattern observed at the earth. However, resolution of target regions can be effected by using large time-bandwidth signals such as pulse

trains or pseudonoise signals to isolate echo power returning at various points in a hypothetical range-vs-doppler plane (that is, to estimate the "scattering function" of the target). Moreover, there is a simple distortionless geometrical mapping between points on the target and points in this plane.

There are a number of unanswered questions about processing techniques for isolation of target regions. For example, the way in which one might apply in practice certain measurement procedures that are known to be statistically optimum is unclear. It is unclear to what extent one can avoid the added noise injected into the receiver output when examining an overspread target. The added complexities of processing and the added possibilities for sensitive mapping experiments using range-doppler trajectories have not been adequately studied.

The measurement of target rotation speed and axial orientation was discussed and various fairly straightforward methods were outlined for partially determining these quantities by processing of single station or interferometer echo signals.

The radar measurement of several other target attributes (e.g., target shape) was discussed briefly.

Explicit procedures for actually carrying out the observations were dealt with in Sec. IV-F, and particularly in Table I.

#### ACKNOWLEDGMENT

The author would like to express his grateful appreciation to Martin Balsler for his help at various points in this investigation, and to J.V. Evans, M.J. Levin, G.H. Pettengill, and R. Price, who likewise participated in educating the author in the matters reported here.

## REFERENCES

1. R. Price and P.E. Green, Jr., "Signal Processing in Radar Astronomy—Communication via Fluctuating Multipath Media," Technical Report No. 234 [U], Lincoln Laboratory, M.I.T. (6 October 1960), ASTIA 246782.
2. J.A. Ratcliffe, "Some Aspects of Diffraction Theory and Their Application to the Ionosphere," in *Reports on Progress in Physics* 19 (Phys. Soc. London, 1956), p. 188.
3. J.V. Evans, "Radar Methods of Studying Distant Planetary Surfaces," Bull. Virginia Polytechnic Institute 55, No. 9, 237 (July 1962).
4. H.G. Booker and P.C. Clemmow, "The Concept of an Angular Spectrum of Plane Waves and Its Relation to That of Polar Diagram and Aperture Distribution," Proc. IEE 97 III, 11 (1950).
5. G.H. Pettengill, "Radar Measurements of the Lunar Surface," in *The Moon*, Z. Kopal and Z. Mikhailov, Editors (Academic Press, New York, 1962).
6. P.E. Green, Jr., "A Summary of Detection Theory Notions in Radar Astronomy Terms," Group Report 34-84 [U], Lincoln Laboratory, M.I.T. (18 January 1960), ASTIA 245698, H-189.
7. B.H. Briggs, G.J. Phillips and D.H. Shinn, "Analysis of Observation on Spaced Receivers of the Fading of Radio Signals," Proc. Phys. Soc. (London) B63, 106 (1950).
8. G.H. Pettengill, "Measurements of Lunar Reflectivity Using the Millstone Radar," Proc. IRE 48, 933 (1960).
9. G.H. Pettengill and J.C. Henry, "Enhancement of Radar Reflectivity Associated with the Lunar Crater Tycho," *Astron. J.* 67, 4881 (1962).
10. M.H. Cohen, "Radio Astronomy Polarization Measurements," Proc. IRE 46, 172 (1958).
11. G.F. Pippert, "A Study of the Effect of Unpolarized Transmitted Radiation on Radar Reflectivity," Group Report 312-7 [U], Lincoln Laboratory, M.I.T. (10 October 1956).
12. P. Beckmann, "The Depolarization of Electromagnetic Waves Scattered From Rough Surfaces," Technical Report No. 12, Institute of Radio Engineering and Electronics, Czechoslovakian Academy of Sciences, Prague (1961).
13. B. Chytil, "The Depolarization of Electromagnetic Waves Scattered From Certain Bodies," Technical Report No. 17, Institute of Radio Engineering and Electronics, Czechoslovakian Academy of Sciences, Prague (1961).
14. L.N. Ridenour (Editor), *Radar System Engineering*, M.I.T. Radiation Laboratory Series Vol. I (McGraw-Hill, New York, 1947), p. 64.
15. J.P. Dougherty and D.T. Farley, "A Theory of Incoherent Scattering of Radio Waves by a Plasma," Parts I and II, Proc. Roy. Soc. (London) A256, 79 (1960); A263, 238 (1961).
16. J.F. Lee, private communication (14 June 1957), to be published.
17. N.G. Parke, III, *Statistical Optics and Related Topics*, Collected Reprints (Parke Mathematical Laboratories, Carlisle, Massachusetts, 1959).
18. E. J. Kerr, "On the Possibility of Obtaining Radar Echoes from the Sun and Planets," Proc. IRE 40, 660 (1952).
19. K. Rawer, *The Ionosphere* (Ungar, New York, 1952).
20. J.V. Evans, "The Electron Content of the Ionosphere," *J. Atmos. Terr. Phys.* 11, 259 (1957).

21. G.L. Turin, "An Introduction to Matched Filters," Trans. IRE, PGIT IT-6, 311 (1960).
22. P.M. Woodward, Probability and Information Theory, with Application to Radar (Pergamon-McGraw-Hill, 1953).
23. W.M. Siebert, "A Radar Detection Philosophy," Trans. IRE, PGIT IT-2, 204 (1956).
24. R.M. Lerner, "Signals with Uniform Ambiguity Functions," IRE Natl. Conv. Rec. (1958), part 4, 27.
25. E.C. Westerfield, R.H. Prager and J.L. Stewart, "Processing Gain Against Reverberation (Clutter) Using Matched Filters," Trans. IRE, PGIT IT-6, 342 (1960).
26. K.L. Jordan, Jr., "Time and Frequency Dependence of Fading from a Collection of Scatterers," private communication (30 November 1960).
27. C.A. Stutt, "A Note on Invariant Relations for Ambiguity and Distance Functions," Trans. IRE PGIT IT-5, 164 (1959).
28. J.H. Trexler, "Lunar Radio Echoes," Proc. IRE 46, 286 (1958).
29. T. Hagfors, "Some Properties of Radio Waves Reflected from the Moon and Their Relation to the Lunar Surface," J. Geophys. Res. 66, 777 (1961).
30. J.W. Craig, Jr., "Optimum Approximation to a Matched Filter Response," Trans. IRE, PGIT IT-6, 409 (1960).
31. R.M. Lerner, "A Matched Filter Detection System for Complicated Doppler Shifted Signals," Trans. IRE, PGIT IT-6, 373 (1960).
32. S.M. Susman, "A Matched Filter Communication System for Multipath Channels," Trans. IRE, PGIT IT-6, 367 (1960).
33. P.E. Green, Jr., "The Output Signal-to-Noise Ratio of Correlation Detectors," Trans. IRE, PGIT IT-3, 10 (1957).
34. D.G. Lampard, "The Minimum Detectable Change in the Mean Noise-Input Power to a Radio Receiver," Monograph No. 80, Proc. IEE 101 IV, 118 (1954).
35. H.G. Booker, J.A. Ratcliffe and D.H. Shinn, "Diffraction from an Irregular Screen with Applications to Ionospheric Problems," Phil. Trans. Roy. Soc. (London) 242A, 579 (1950).
36. W.B. Davenport, Jr., and W.L. Root, An Introduction to the Theory of Random Signals and Noise (McGraw-Hill, New York, 1958), Sec. 12.3.
37. R. Manasse, "The Use of Radar Interferometer Measurements to Study Planets," Group Report 312-24 [U], Lincoln Laboratory, M.I.T. (18 March 1959).
38. R.N. Bracewell, "Radio Interferometry of Discrete Sources," Proc. IRE 46, 97 (1958).
39. \_\_\_\_\_, "Radio Interferometry and the Spectral Island Diagram," Trans. IRE, PGAP AP-9, 59 (1961).
40. E. Gehrels and A. Parsons, "Interferometer Techniques Applied to Radar," Trans. IRE, PGMIL MIL-5, 139 (1961).
41. J.B. McGuire, E.R. Spangler and L. Wong, "The Size of the Solar System," Sci Am. 204, 64 (1961).
42. Millstone Hill Staff, "The Scale of the Solar System," Nature 190, 592 (1961).
43. V.A. Kotelnikov, "Radar Contact with Venus," J. Brit. IRE 22, 293 (1961).
44. J.H. Thompson, et al., "A New Determination of the Solar Parallax by Means of Radar Echoes from Venus," Nature 190, 519 (1961).

45. W.K. Victor and R. Stevens, "Exploration of Venus by Radar," *Science* 133, 46 (1961).
46. D.O. Muhleman, D. B. Holdridge and N. Block, "The A.U. Determined by Radar Reflections from Venus," *Astron. J.* 67, 191 (1962).
47. G.H. Pettengill, *et al.*, "A Radar Investigation of Venus," *Astron. J.* 67, 181 (1962).
48. W.B. Smith, "Radar Observations of Venus, 1961 and 1959," *Astron. J.* (in press).
49. R.N. Bracewell, "Strip Integration in Radio Astronomy," *Austral. J. Phys.* 9, 158 (1956).
50. G.S. Levy and D. Schuster, "Venusian and Lunar Radar Depolarization Experiments," *Astron. J.* 67, 320 (1962).
51. R.K. Moore, "Resolution of Vertical Incidence Radar Returns into Random and Specular Components," Eng. Station Report EE-6, Univ. of New Mexico (July 1957).
52. S.O. Rice, "Statistical Properties of a Sine-Wave Plus Random Noise," *BSTJ* 27, 109 (1948).
53. L.J. Cutrona, *et al.*, "A High-Resolution Radar Combat-Surveillance System," *Trans. IRE, PGML MIL-5*, 103 (1961); see also L.J. Cutrona, *et al.*, *Trans. IRE, PGIT IT-6*, 386 (1960).
54. T. Kailath, "Communication via Randomly Varying Channels," Sc. D. Thesis, M.I.T. (June 1961).
55. P.E. Green, Jr., "Some Future Experiments in Radar Astronomy," Group Report 34-81 [U], Lincoln Laboratory, M.I.T. (May 1959).
56. M.H. Cohen, "Radar Echoes from a Rough Rotating Planet," Report EE428, Cornell University (1 June 1959).
57. V.R. Ezhleman, P.B. Gallagher and R.C. Barthle, "Radar Methods of Measuring the Cis-lunar Electron Density," *J. Geophys. Res.* 65, 3079 (1960).
58. H.W. Briscoe, private communication (April 1961).
59. H. Cramer, *Mathematical Methods of Statistics* (Princeton Univ. Press, Princeton, 1945).
60. C.W. Helstrom, *Statistical Theory of Signal Detection* (Pergamon Press, New York, 1960), Chaps. 8 and 9.
61. R. Manasse, "Parameter Estimation Theory and Some Applications of the Theory to Radar Measurements," Technical Report No. 3, MITRE Corporation (April 1960).
62. \_\_\_\_\_, "Range and Velocity Accuracy from Radar Measurements," Group Report 312-26 [U], Lincoln Laboratory, M.I.T. (3 February 1955, Revised 2 May 1960).
63. E.J. Kelly, "The Radar Measurement of Range, Velocity, and Acceleration," *Trans. IRE, PGML MIL-5*, 51 (1961).
64. Division 3 Quarterly Progress Report [U], Lincoln Laboratory, M.I.T. (15 April 1962), ASTIA 275470, Group 34. Variance of the Maximum Likelihood Estimate of the Epoch of a Nonstationary Random Process, by R. Price.
65. R.B. Blackman and J.W. Tukey, *The Measurement of Power Spectra* (Dover, New York, 1959).
66. U. Grenander and M. Rosenblatt, *Statistical Analysis of Stationary Time Series* (Wiley, New York, 1957), Chap. 4.
67. P. Swerling, "Estimation of Doppler Shifts in Noise Spectra," *IRE Natl. Conv. Rec.* (1960), Part 4, 148.

68. M. J. Levin, "Estimation of Doppler Shift and Spectral Width of a Random Process," G-Report 34G-6 [U], Lincoln Laboratory, M. I. T. (12 June 1962), ASTIA 278686, H-409.
69. P. Bello, "Time-Frequency Duality," manuscript submitted to Trans. IRE, PGIT, October, 1962.
70. T. Kailath, "Measurement of Average Channel Parameters," private communication (July 1959).
71. \_\_\_\_\_, "Measurements on Time-Variant Communication Channels," Trans. IRE, PGIT-IT-8, 229 (1962).
72. R. Price, "Maximum-Likelihood Estimation of the Correlation Function of a Threshold Signal, and Its Application to the Measurement of the Target Scattering Function in Radar Astronomy," G-Report 34G-4 [U], Lincoln Laboratory, M. I. T. (25 May 1962), ASTIA 276903, H-403.
73. M. J. Levin, "Estimation of the Second-Order Statistics of Randomly Time-Varying Linear Systems," G-Report 34G-7 [U], Lincoln Laboratory, M. I. T. (2 November 1962), ASTIA 289607, H-445.
74. E. N. Bramley, "Diversity Effects in Spaced-Aerial Reception of Ionospheric Waves," Proc. IEE 98III, 19 (1951).

For convenience in ordering copies of Lincoln Laboratory reports cited in this document, each reference is followed by its ASTIA number. In addition, Unclassified (released) reports have also been assigned Hayden serials (designated H-), indicating that they are obtainable, at cost, as microfilm or photoprint copies from the Microreproduction Laboratory, Hayden Memorial Library, M. I. T., Cambridge 39, Massachusetts.

APPENDIX A  
A DISCUSSION OF CORRELATION FUNCTIONS AND ANGULAR SPECTRA  
OF INTEREST IN RADAR ASTRONOMY

by

Martin Balser

Consider, for simplicity, the one-dimensional problem of a component of the field  $\mathcal{E}(x, 0)$  given on the plane  $z = 0$  as a function of the coordinate  $x$  along the plane. Here,  $x$  and  $z$  are distances expressed in multiples of a wavelength. We assume  $\mathcal{E}$  and  $\mathcal{E}^2$  are integrable; i.e., the field is essentially limited to a given region or aperture in the plane. Thus  $\mathcal{E}$  has a Fourier transform, given by

$$\mathcal{W}(\ell) = \int_{-\infty}^{\infty} \mathcal{E}(x, 0) \exp[-j2\pi\ell x] dx \quad (\text{A-1})$$

and, inversely,

$$\mathcal{E}(x, 0) = \frac{1}{2\pi} \int_{-\infty}^{\infty} \mathcal{W}(\ell) \exp[j2\pi\ell x] d\ell \quad (\text{A-2})$$

It is easy to see that

$$\mathcal{E}(x, z) = \frac{1}{2\pi} \int_{-\infty}^{\infty} \mathcal{W}(\ell) \exp[j2\pi(\ell x + nz)] ds \quad (\text{A-3})$$

where  $n = \sqrt{1 - \ell^2}$ , is a solution to Maxwell's equations, being a superposition of plane waves, the one of amplitude  $\mathcal{W}(\ell) d\ell$  traveling in the direction  $\psi$ , where  $\ell = \sin \psi$  and  $n = \cos \psi$ . The well-known result that structure in the aperture field which is finer than the wavelength does not propagate is seen formally in the observation that such structure corresponds in Eq. (A-2) to values of  $|\ell| > 1$ , which results in Eq. (A-3) in imaginary values for  $n$  and hence in damped waves.

It can further be shown<sup>4</sup> that at great distances (compared to the size of the aperture) from the source plane, the field in Eq. (A-3) becomes  $\mathcal{E}(x, z) \sim \mathcal{W}(\ell)$ , where  $\ell = z/\sqrt{x^2 + z^2}$ ; i.e.,  $|\mathcal{W}(\ell)|^2$  is the angular spectrum, indicating the power radiated in the direction  $\psi = \sin^{-1} \ell$ . (The aperture distribution is assumed to be in the vicinity of the origin.) Also, the correlation in the angular pattern

$$\begin{aligned} \int_{-\infty}^{\infty} \mathcal{W}(p) \mathcal{W}^*(p + \ell) dp &= \iiint_{-\infty}^{\infty} \mathcal{E}(x, 0) \mathcal{E}^*(x', 0) \exp[-j2\pi p x + j2\pi(p + \ell) x'] dx dx' dp \\ &= 2\pi \int_{-\infty}^{\infty} |\mathcal{E}(x, 0)|^2 \exp[j2\pi\ell x] dx \quad (\text{A-4}) \end{aligned}$$

i.e., the Fourier transform of the aperture power distribution or illumination. Since the values of  $\ell$  can be immediately related to distances  $x$  along the observation plane  $z = z$  (denoted  $z_0$  in Fig. 2 of the text), this theorem relates a "distance correlation" to the aperture brightness.

A somewhat different concept of distance correlation along the observation plane is, however, usually considered in practical situations. First of all, the measurement is taken quite locally, not, as in Eq. (A-4), through all values of  $\ell$  (or  $x$  in the observation plane). Second,

the averaging (for most practical cases, in time) used to determine the correlation implies a statistical process, whereas the previously cited results are precisely correct for any individual distribution  $\mathcal{E}(x, 0)$ . Accordingly it may be asked whether the same, or a similar, result exists for a correlation function more nearly related to this practical concept. To see whether this is so,<sup>†</sup> consider the aperture field distribution to be a sample drawn from an ensemble of the form

$$\mathcal{E}(x, 0) = S(x) \mathcal{K}(x) \quad , \quad (\text{A-5})$$

where  $\mathcal{K}(x)$  is a stationary random process in  $x$ , and  $S(x)$  is a fixed envelope which determines the power distribution in the aperture plane ( $|S(x)|^2$  is the brightness distribution). The random function is assumed to have the ensemble averages (expected values)  $\langle \mathcal{K}(x) \rangle = 0$ ,  $\langle \mathcal{K}^2(x) \rangle = 1$ ,  $\langle \mathcal{K}(x) \mathcal{K}^*(x + \xi) \rangle = \rho(\xi)$ . If now we form the product

$$\begin{aligned} \mathcal{W}(p) \mathcal{W}^*(p + \ell) &= \iint_{-\infty}^{\infty} \mathcal{E}(x, 0) \mathcal{E}^*(x', 0) \exp[-j2\pi p x + j2\pi(p + \ell)x'] dx dx' \\ &= \iint_{-\infty}^{\infty} S(x) S^*(x') \mathcal{K}(x) \mathcal{K}^*(x') \exp[-j2\pi p(x - x')] \exp[j2\pi \ell x] dx dx' \quad (\text{A-6}) \end{aligned}$$

and take the ensemble average, we find

$$\langle \mathcal{W}(p) \mathcal{W}^*(p + \ell) \rangle = \iint_{-\infty}^{\infty} S(x) S^*(x') \rho(x - x') \exp[-j2\pi p(x - x')] \exp[j2\pi \ell x] dx dx' \quad . \quad (\text{A-7})$$

It is reasonable to assume that the over-all aperture power distribution  $|S(x)|^2$  changes very little over a correlation distance (i.e., the range of non-negligible values of  $\rho$ ), so that in Eq. (A-7) we can replace  $S(x') S^*(x) = |S(x)|^2$ . Changing the variable  $x' - x = u$ , we find

$$\langle \mathcal{W}(p) \mathcal{W}^*(p + \ell) \rangle = \int_{-\infty}^{\infty} \rho(u) \exp[j2\pi p u] du \int_{-\infty}^{\infty} |S(x)|^2 \exp[j2\pi \ell x] dx \quad . \quad (\text{A-8})$$

An incidental result of Eq. (A-8) is found by setting  $\ell = 0$ ; then

$$\langle |\mathcal{W}(p)|^2 \rangle = K \int_{-\infty}^{\infty} \rho(u) \exp[j2\pi p u] du \quad , \quad (\text{A-9})$$

(where  $K = \int_{-\infty}^{\infty} |S(x)|^2 dx$ ), which states that the angular spectrum radiated from the aperture is the Fourier transform of the correlation function of the field in the aperture. (This was also shown by Bramley<sup>74</sup>). The principal result is, however, the other integral, i.e.,

$$\langle \mathcal{W}(p) \mathcal{W}^*(p + \ell) \rangle = \langle |\mathcal{W}(p)|^2 \rangle \int_{-\infty}^{\infty} |S(x)|^2 \exp[j2\pi \ell x] dx \quad . \quad (\text{A-10})$$

This result is very similar to the one in Eq. (A-4) in that it relates the angular (or distance) correlation to the Fourier transform of the aperture illumination, but in Eq. (A-10) the statement is made for each value of direction cosine  $p$  separately, rather than integrated over all values of  $p$ .

<sup>†</sup> This is essentially the approach used by Ratcliffe (Ref. 2, p. 223).

For different values of  $p$ , the angular correlation function has the same form and differs only by the constant of proportionality, the angular spectrum.

At this point the effect of the assumption that  $S(x) S^*(x') \sim |S(x)|^2$  can be seen. [It was this assumption that allowed the separation into a product of the double integral in Eq. (A-7).] To negate this assumption, i.e., to state that the correlation distance of the aperture field is comparable to the total size of the aperture, would mean that the angular correlation distance is comparable to the width of the angular spectrum. Thus [from Eq. (A-10)], the received power level in the observation plane would change over distances comparable to the space correlation distance, destroying the normal assumption of "local stationarity" used in measuring correlation functions.

Note that all the previous analysis has based the angular coordinate system at the origin, located at the aperture. Actually, by defining a new set of angles from the point of observation as origin, it can be seen that Eq. (A-10) is the same as Eq. (A-9), which states that at a given plane the angular spectrum and space correlation function are a Fourier transform pair. It has already been mentioned that the ground pattern  $\mathcal{C}(x, z)$  at the observation plane is simple related to  $\mathcal{W}(s)$ , the angular spectrum based at the aperture. Thus the left side of Eq. (A-10) is essentially the space correlation function at the observation plane. Also, it is easily seen that the (received) angular spectrum is proportional to the illumination distribution in the aperture (clearly, the radiation is limited to the angle subtended at the receiver by the source). This duality between angle at one terminal and distance along the plane at the other terminal thus allows the inference of either Eq. (A-9) or Eq. (A-10) from the other.

It might also be mentioned, finally, that most experimental measurements consist of time, rather than ensemble, averages. This is essentially an assumption of ergodicity, or an assumption that the fields being observed are being replaced in time by other members of the ensemble, so that the one average is equivalent to the other. We can thus regard the abbreviation  $\langle \rangle$  used in this Appendix as representing a time average.

**APPENDIX B**  
**SCATTERING FUNCTION FOR UNIFORM ROUGH SPHERE<sup>6</sup>**

The problem treated here is the determination of the distribution in range and doppler of the radar return from a uniform rough rotating sphere. This quantity (defined as  $\sigma$ ) will depend on the diameter of the body, its rotation velocity, axial tilt relative to the line of sight, and the carrier frequency in use. It will also be a function of the radar reflecting characteristic  $\sigma_0(\varphi)$  (to be defined) of the material of which the surface is composed, and we will be interested in seeing the relationship between the radar return and this quantity  $\sigma_0$  describing the surface properties.

We define

$\alpha$  = tilt of axis from perpendicularity with line of sight,

$\vec{\Omega}$  = rotation velocity in radians per second,

$f_0$  = carrier frequency,

$\sigma_0(\varphi)$  = reflecting cross section per unit area of surface as a function of tilt of the radar line of sight from normal (radar angular power spectrum.)

We seek to find the expression showing how these quantities affect the scattering function

$\sigma(\tau, f)$  = time average radar energy returned in a hypothetical element of time delay (range)  $d\tau$  wide at delay  $\tau$  and  $df$  wide at doppler frequency  $f$ .

We shall assume that the position of the center of the sphere corresponds to the  $\tau$ -origin and that the velocity of the center of the sphere (assumed in straight-line motion) corresponds to the  $f$ -origin.

Figure B-1 depicts the rotating body cut by a plane Q containing both line of sight and axis. An arbitrary point P on the surface is shown having coordinates  $(\theta, \gamma)$ . Also shown is the angle  $\varphi$  between line of sight and radius vector from the center of the sphere to the point P.

The first step is to find the projection on the line of sight of  $\vec{V}$ , the velocity of P. First,

$$\text{magnitude of } \vec{V}, V = \Omega a \sin \theta \quad . \quad (\text{B-1})$$

The projection of  $\vec{V}$  on the plane Q is

$$\Omega a \sin \theta \sin \gamma \quad ; \quad (\text{B-2})$$

the projection of this quantity in turn along the line of sight is

$$\Omega a \sin \theta \sin \gamma \cos \alpha \quad , \quad (\text{B-3})$$

and the doppler frequency offset of the echo from P is

$$f = \frac{2f_0}{c} \Omega a \sin \theta \sin \gamma \cos \alpha \quad . \quad (\text{B-4})$$

But the perpendicular distance  $x$  from point P to plane Q is

$$x = a \sin \gamma \sin \theta \quad , \quad (\text{B-5})$$

so

$$f = \frac{2f_0}{c} \Omega x \cos \alpha \quad (-a \leq x \leq a) \quad . \quad (\text{B-6})$$

The range (delay) of point P is clearly given by

$$\tau' = \frac{2a}{c} \cos \varphi = -\tau \quad , \quad (\text{B-7})$$

8-84-7721

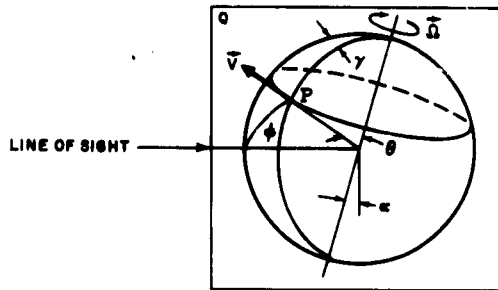
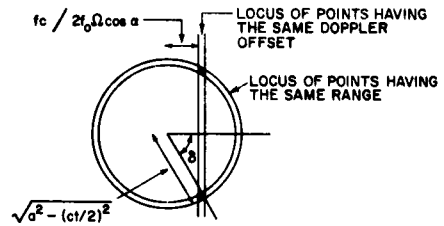


Fig. B-1. A rotating body cut by a plane Q containing both line of sight and axis.

3-34-7722

Fig. B-2. Head-on view of an annular range strip and a straight doppler strip on the target.



3-34-7723

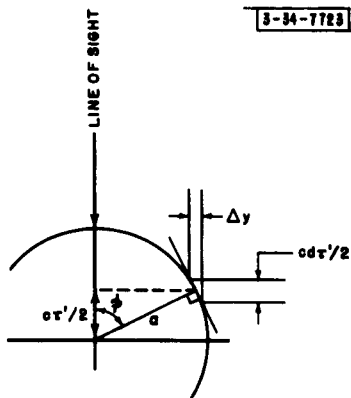


Fig. B-3. Plan view of plane containing line of sight and radius from target center to one of the shaded regions in Fig. B-2.

where for present purposes  $\tau'$  reads in a positive direction toward the observer.

Now we have defined  $\sigma_o(\varphi)$  to be the cross section per unit area of target surface (not per unit area of incident wavefront);  $\varphi$  is as shown in the figure. If we assume unit power flux density throughout the incident wavefront, the total power returned with delay  $\tau$  and doppler  $f$  in a range of delay  $d\tau$  and doppler  $df$  is

$$\sigma(\tau, f) = (\text{number of square meters of wavefront corresponding to the element } df d\tau) \times (\text{cross section per unit area of wavefront}). \quad (\text{B-8})$$

The second factor is  $\sigma_o(\varphi)/\cos \varphi$ .

Call the first factor A. Figure B-2 shows a head-on view of the target (looking along the line of sight with the line corresponding to plane Q in the up-down direction). The two regions making up area A are shown shaded. The width  $\Delta x$  (in meters) of the strip containing all the energy lying in unit bandwidth at frequency  $f$  is [from Eq. (B-6)]

$$\Delta x = c/(2f_o \Omega \cos \alpha) \quad (\text{B-9})$$

The width of the annular strip containing all the energy lying in unit spread of delays at delay  $\tau'$  we will call  $\Delta y$ . From Fig. B-3,

$$\Delta y = \frac{c}{2} \cos \varphi \quad (\text{B-10})$$

The area A is given by

$$A = 2\Delta x \Delta y / \cos \delta \quad (\text{B-11})$$

where  $\delta$  is indicated in Fig. B-2, and

$$\sin \delta = \frac{fc}{2f_o \Omega \cos \alpha} / \sqrt{a^2 - (c\tau'/2)^2} \quad (\text{B-12})$$

Combining (B-12) with (B-11) and (B-7) with (B-10) and then substituting (B-9), (B-10) and (B-11) in (B-8) we have finally

$$\sigma(\tau', f) = \begin{cases} \frac{c^2 \sigma_o [\cos^{-1}(c\tau'/2a)]}{2f_o \Omega \cos \alpha} [1 - (c\tau'/2a)^2 - (fc/2f_o a \Omega \cos \alpha)^2]^{-1/2} & \text{for real values} \\ 0 & \text{for imaginary values} \end{cases} \quad (\text{B-13})$$

From Eqs. (37) and (39), respectively, power as a function of delay only is

$$\sigma(\tau) = \pi a c \sigma_o (\cos^{-1}(c\tau'/2a)) \quad (\text{B-14})$$

and power as a function of doppler offset alone is

$$\sigma(f) = \int_{-\infty}^{\infty} (\text{B-13}) df \quad (\text{B-15})$$